IRON-SULFUR BASED MOLECULAR WIRES FOR ENHANCING CHARGE TRANSPORT IN ENZYMATIC BIO-ELECTRODES

A Dissertation

by

AISHWARYA MAHADEVAN

Submitted to the Office of Graduate and Professional Studies of
Texas A&M University
in partial fulfillment of the requirements for the degree of

DOCTOR OF PHILOSOPHY

Chair of Committee,	Sandun D. Fernando
Committee Members,	Maria King
	Girish Agarwal
	Mike McShane
	Carmen Gomes
Head of Department,	Stephen W. Searcy

August 2019

Major Subject: Biological and Agricultural Engineering

Copyright 2019 Aishwarya Mahadevan

ABSTRACT

Iron-sulfur complexes, the first link between proteins and mediating molecules in the biological electron transport chain(s), possess intrinsic electron transport capabilities. In this work, the application of inorganic iron-sulfur clusters ([Fe-S]) viz. FeS, FeS_2, Fe_2S_3, and Fe_3S_4, as molecular wires to mediate electron transport between a glucose-selective redox enzyme and the gold electrode is studied using voltammetry methods. It is shown that [Fe-S] can emulate the functionality of the natural electron transport chain. Voltammetry studies indicate a significant improvement in electron transport, surface coverage, and resilience achieved by the [Fe-S]-based glucose anodes when compared to a conventional pyrroloquinoline quinone (PQQ)-based glucose anode. Next, the ability of [Fe-S] to perform electron transport ex vivo once wired to redox coenzymes (NAD/NADP, FAD, PQQ, and CoQ_{10}) is studied using electrochemical methods. The formation of layer-by-layer self-assembled monolayers of the [Fe-S] and the coenzymes on Au surface was confirmed using cyclic voltammetry. Results indicated that [Fe-S] effectively anchors the redox coenzymes to gold electrodes and shuttles electrons between the two. Fourier-transform infrared spectroscopy (FTIR) and secondary ion mass spectrometry (SIMS) on FeS-NAD complex showed the FeS and NAD interacted via iron carbonyl bond formation. Reductive desorption studies revealed that, among the inorganic [Fe-S], Fe_3S_4-functionalized electrodes had the highest surface coverage, the lowest resistance and highest power requirements for monolayer desorption. Upon testing for a biosensing application, a 77% increase in sensitivity and a 53% improvement in detection limit was observed for a FeS-based glycerol biosensor when

compared to the conventional PQQ-based counterpart, for glycerol concentrations ranging from 1–25 mM. When tested to construct glucose-selective bioanode, a combination of FeS and Fe_3S_4 combined with BDT (an aromatic thiol linker) gave promising performances when used as a glucose sensor and a fuel cell. Thus, using multiple forms of inorganic iron-sulfur clusters, the ability of direct and robust wiring of the enzyme active site to an electrode while eliminating the issue of constrained charge transport endemic to bioelectronic systems is demonstrated. These discoveries are expected to create archetypes for wiring biological molecules where charge transport is critical – especially in bioelectronics systems.

DEDICATION

To my teacher and mentor, Dr. Sandun Fernando. As a teacher you inspired me and as a mentor you motivated and invested in me. I can never repay you for everything I've gained from your instruction. I hope to inspire others as you have inspired me during this journey.

ACKNOWLEDGEMENTS

I would like to thank my advisor, Dr. Sandun Fernando, who expertly guided me through my graduate education and who shared the excitement of seven years of research and discovery. It was a great learning experience writing manuscripts and discussing experiments with him. His meticulous approach to mentoring and encouragement to voice my opinions has been a huge influence, in this dissertation and in my life. I would also like to thank my dissertation committee – Dr. Maria King, Dr. Girish Agarwal, Dr. Mike McShane, and Dr. Carmen Gomes, for their guidance, encouragement and support throughout the course of this research. I also thank Dr. Sreeram Vaddiraju for expertly guiding me on the FTIR experiments, and Dr. Stanislav Verkhoturov for his contributions on the SIMS experiments.

I am grateful to my wonderful team of undergraduate student researchers – David Martinez, Audrey Nelson, Mathew Pietz, and Ikechukwu Anyakee, for all the hard work, enthusiasm and positivity they put into this research. They took the meaning of teamwork to a whole new level. Thank you!

I also thank my friends in the Nanoscale Biological Engineering Laboratory for their support throughout the years. I extend my gratitude to my fellow graduate students, the BAEN faculty and staff for making my time at Texas A&M University a great experience.

Lastly, this dissertation is impossible without the support from my friends and family that kept me sane, grounded, and laughing throughout everything. My gratitude to them is beyond what I can express in words. Thank you, everyone!

CONTRIBUTORS AND FUNDING SOURCES

Contributors

This work was supervised by a dissertation committee consisting of Dr. Sandun D. Fernando (chair), Dr. Maria King, and Dr. Girish Agarwal of the Department of Biological and Agricultural Engineering, and Dr. Mike McShane of the Department of Biomedical Engineering, and Dr. Carmen Gomes of the Department of Mechanical Engineering at Iowa State University.

The SIMS data analyzed in Section 3 was provided by Dr. Stanislav Verkhoturov of the Department of Chemistry. The FTIR study in Section 3 was performed in Dr. Sreeram Vaddiraju's laboratory in Department of Chemical Engineering under his guidance and supervision. The aromatic thiol linker used in Section 5 were also suggested by Dr. Sreeram Vaddiraju. Undergraduate student researchers – David Martinez, Audrey Nelson, Mathew Pietz, Ikechukwu Anyakee, and Peter Di Carlo contributed to parts of data collection for Section 3 and Section 5.

All other work conducted for the dissertation was completed by the student independently.

Funding Sources

This work was supported by National Science Foundation (NSF) under Grant Number CBET-1511303 and in part by CBET 1243311. Its contents are solely the responsibility of the authors and do not necessarily represent the official views of NSF.

Graduate study was supported by NSF grant CBET-1511303, TEXAS A&M College of Agriculture and Life Sciences (TAMU-COALS), and Department of Biological & Agricultural Engineering - TAMU.

TABLE OF CONTENTS

Page

ABSTRACT ii

DEDICATION iv

ACKNOWLEDGEMENTS v

CONTRIBUTORS AND FUNDING SOURCES vii

TABLE OF CONTENTS ix

LIST OF FIGURES xii

LIST OF TABLES xvii

1. INTRODUCTION 1

1.1. Dissertation organization 1
1.2. Objective and hypothesis 1
1.3. Problem statement 3
1.4. Literature review 4
1.4.1. Enzyme-based bioelectronics 4
1.4.2. Molecular wiring of enzymes 5
1.4.3. Fe-S based molecular wires 7
1.4.4. Origin of iron-sulfur clusters 10
1.4.5. Iron-sulfur complexes found in nature 13
1.4.6. How the presence of oxygen affects the Fe-S complex and why Fe-S complexes are unstable in water 15

2. ASSESSMENT OF THE EFFECTIVENESS OF USING INORGANIC IRON-SULFUR CLUSTERS TO WIRE NAD-GLUCOSE DEHYDROGENASE ONTO GOLD ELECTRODES 18

2.1. Introduction 18
2.2. Experimental 20
2.2.1. Reagents and apparatus 20
2.2.2. NAD-GDH anode(s) fabrication 21
2.2.3. Electrochemical measurements 22

2.2.4. Ferricyanide/ferrocyanide-voltammetry to confirm multi-layer SAM formation 23
2.2.5. Potentiometric analysis of glucose anodes 23
2.2.6. Voltammetry analysis of glucose anodes 23
2.2.7. Surface coverage of the Fe-S monolayers on gold 24
2.2.8. Statistical Analysis 24
2.3. Results and discussion 24
2.3.1. Ferricyanide/ferrocyanide-voltammetry confirmed multi-layer SAM formation 24
2.3.2. Potentiometric analysis of glucose anodes 27
2.3.3. Voltammetry analysis of glucose anodes 28
2.3.4. Surface coverage of the Fe-S monolayers on gold 33
2.4. Conclusions 36

3. EVALUATION OF THE EFFECTIVENESS OF USING INORGANIC AND ORGANIC IRON-SULFUR CLUSTERS TO WIRE SELECT COENZYMES ONTO GOLD ELECTRODES 38

3.1. Introduction 38
3.2. Materials and methods 40
3.2.1. Reagents and apparatus 40
3.2.2. Au-[Fe-S]-[Coenzyme] electrode preparation 40
3.2.3. Secondary ion mass spectrometry (SIMS) 41
3.2.4. Fourier-transform infrared spectroscopy (FTIR) 43
3.2.5. Docking simulations 43
3.2.6. Electrochemical analyses 43
3.2.7. Statistical analysis 44
3.3. Results and discussion 45
3.3.1. Verifying the self-assembly of [Fe-S] and coenzymes on Au 45
3.3.2. Electrochemical performance 56
3.4. Conclusions 60

4. IDENTIFYING AND TESTING METHODS TO STUDY BIOSENSOR PERFORMANCE OF ENZYME ELECTRODES USING AN ESTABLISHED [FE-S]-COENZYME-ENZYME SYSTEM (I.E. AU-FES-NAD-GLYCEROL-DEHYDROGENASE ANODE) 62

4.1. Introduction 62
4.2. Materials and methods 66
4.2.1. Reagents and apparatus 66
4.2.2. Glycerol dehydrogenase electrode(s) fabrication 67
4.2.3. Electrochemical measurements 68
4.2.4. Statistical analysis 69
4.3. Results and discussion 70

4.3.1. Glycerol biosensor performance 70
4.3.2. Electrochemical behavior of a FeS-based biosensor 72
4.3.3. Effect of enzyme stimulants 75
4.3.4. The effects of buffers and the pH 77
4.3.5. Interference study 80
4.4. Conclusions 81

5. OPTIMIZATION OF IRON-SULFUR-BASED MOLECULAR WIRES AND COMPARISON OF THEIR PERFORMANCE WITH THE CONVENTIONAL PQQ-BASED MOLECULAR WIRE FOR BIOSENSING AND BIOFUEL CELL APPLICATIONS 83

5.1. Introduction 83
5.2. Materials and methods 86
5.2.1. Reagents and apparatus 86
5.2.2. Electrode preparation 88
5.2.3. Glucose biosensor analysis 89
5.2.4. Glucose fuel cell analysis 89
5.2.5. Statistical analysis 90
5.3. Results and discussion 90
5.3.1. Optimization studies of glucose biosensor 90
5.3.2. Storage stability 95
5.3.3. Interference study 96
5.3.4. Glucose biofuel cell 97
5.4. Conclusions 101

6. CONCLUSIONS 102

7. RECOMMENDATIONS FOR FUTURE WORK 104

REFERENCES 105

APPENDIX A SECTION III SUPPLEMENTARY INFORMATION 123

APPENDIX B SECTION IV SUPPLEMENTARY INFORMATION 140

LIST OF FIGURES

Page

Figure 2.1 Ferricyanide/ferrocyanide-voltammetry to verify multi-layer SAM formation: Cyclic voltammograms (CVs) of (A) FeS, (B) FeS_2, (C) Fe_2S_3, (D) Fe_3S_4, and (E) PQQ functionalized gold surfaces were conducted in 0.01 M potassium ferricyanide with 0.1 M KNO_3 at a scan rate of 0.05 V/s vs. Ag/AgCl reference electrode to confirm self-assembly of successive monolayers of molecular wires on gold surfaces. 26

Figure 2.2 Potentiometric analysis of glucose anodes: Instantaneous open circuit voltages obtained by Fe-S-based and PQQ-based glucose anodes between 0.1-100 mM glucose solutions with 0.1 M Tris-HCl buffer (pH 8) acting as carrier. The analysis shows that all Fe-S-based anodes generated higher open circuit voltages as compared to PQQ-based counterpart but were negatively correlated with glucose concentrations. Different letters indicate significant difference among the sample response means. 27

Figure 2.3 Voltammetric analysis of glucose anodes: Excerpts of cyclic voltammograms scanned between −1.5 V and +1.5 V display anodic and cathodic peaks of (A) FeS, (B) FeS_2, (C) Fe_2S_3, (D) Fe_3S_4, and (E) PQQ based glucose anodes confirm a positive correlation between anodic and cathodic peak current densities with glucose concentrations 0-100 mM in Tris-HCl buffer (pH 8), at a scan rate of 0.05 V/s vs. Ag/AgCl reference electrode. 29

Figure 2.4 (A) Calibration plot of glucose anodes: Calibration plot of anodic peak current densities measured by glucose anodes between glucose concentrations 0.1-100 mM at working potential 0.5 V vs. Ag/AgCl reference electrode, derived from the CV scans between −1.5 V and +1.5 V at a sweep rate of 0.05 V/s; (B) Sensitivity and Limit of Detection: Sensitivity and limit of detection of the glucose anodes calculated from the calibration plots indicate FeS-based glucose anode to possess greater suitability for sensing applications with highest sensitivity (25.21 µA mM^{-1} cm^{-2}) and lowest detection limit (0.77 mM). Different letters indicate significant difference among the sample response means. 31

Figure 2.5 Linear sweep voltammetry to analyze surface coverage: (A) Reductive desorption of Fe-S in 50 mM KOH, at a sweep rate of 50 mV/s; (B) Comparison of the surface coverage observed for the Fe-S with the reductive desorption voltage for each molecule depicted on top of the corresponding bars; (C) Resistance ($V_{at\ Ip}/I_p$) for all molecules with and without NAD; (D) Power ($V_{at\ Ip} * I_p$) for all molecules with and without

NAD. $V_{at\ Ip}$ is the anodic peak potential and I_p is the anodic peak current. Fe_3S_4 shows the highest surface coverage, lowest resistance, and highest binding affinity to the electrode surface. Different letters indicate significant difference among the sample response means. 35

Figure 3.1 CV scans of Au-[Fe-S] / Au-[Fe-S]-[coenzyme] electrodes conducted in 0.01 M potassium ferricyanide with 0.1 M KNO_3 at a scan rate of 50 mV/s vs. Ag/AgCl reference electrode. Formation of each layer was verified via reduction of I_p after addition of each layer. 46

Figure 3.2 Mass spectra of the samples SAM FeS on Au (top, blue) and NAD deposited at SAM FeS (red, bottom). (A) Mass spectra for mass range 0-100 amu, and (B) Mass spectra for mass range 100-300 amu. Presence of additional ions: CN^-, $(Ade\text{-}H)^-$, $(Ade\text{-}CNH)^-$, PO_2^-, PO_3^-, $AuCN^-$, and AuSCN on the 'FeS+NAD on Au' confirms the presence of NAD and FeS on Au. 48

Figure 3.3 Mass spectra of SAM FeS+NAD on Au used for determining surface coverage. Total mass spectrum of sample SAM FeS+NAD on Au (bottom, red) and mass spectrum of NAD surface (top, green). Mass spectrum of NAD surface is the sum of individual spectra containing PO_3^- ions. (A) Mass spectra for mass range 0-100 amu, and (B) Mass spectra for mass range 100-300 amu. 50

Figure 3.4 Fourier transform infrared (FTIR) spectra of NAD (control 1), FeS (control 2), and FeS-NAD complex in the regions (A) 2,200 to 1,300 cm^{-1} and, (B) 3,800 to 2,600 cm^{-1}, confirms the formation of iron carbonyl bond. 53

Figure 3.5 (A) Three-dimensional interactions between FeS and NAD using Autodock Vina. It can be seen that the Fe (orange) primarily interacting with oxygen atoms of NAD; (B-F) Binding affinities of [Fe-S]-{coenzyme] predicted by simulations, shows Fe_3S_4 having the highest binding affinity on Au. 55

Figure 3.6 Reductive desorption using linear sweep voltammetry: (A) Surface coverage, and (B) Resistance of the [Fe-S] and [Fe-S]-[coenzymes] modified Au electrodes; and (C) Power required to desorb the [Fe-S] and [Fe-S]-[coenzymes] monolayers from Au surface. Fe_3S_4 showed the highest surface coverage, lowest resistance, and highest desorption power requirement when used to wire the coenzymes onto the Au surface. Different letters indicate significant difference among the sample response means. 58

Figure 3.7 I_{pa} derived from the CV scans of Au-[Fe-S] / Au-[Fe-S]-[coenzyme] electrodes conducted in 0.01 M potassium ferricyanide with 0.1 M KNO_3 at

a scan rate of 50 mV/s vs. Ag/AgCl reference electrode shows that all inorganic [Fe-S] forms allowed higher I_{pa} values as compared to organic FDx while Fe_3S_4 displaying the highest I_{pa} values. Different letters indicate significant difference among the sample response means. 60

Figure 4.1 (A) A schematic of wiring systems. (a) Complex conventional wiring of the coenzyme NAD to a gold electrode using a series of molecules, including a cystamine linker, a PQQ mediator, and a phenyl boronic acid linker; (b) Simplified wiring of a NAD coenzyme directly onto the gold electrode by a multi-functional mediator, FeS. Reprinted with permission from ref (Mahadevan et al., 2016). Copyright 2015 Elsevier B.V; Surface morphology of (B) bare Au surface and (C) an enzyme immobilized Au surface examined via FE-SEM. 64

Figure 4.2 (A) Amperometry responses to increments of 0.001 M glycerol at E = 1.3 V; (B) Calibration plots for current responses generated by the FeS-based biosensor and PQQ-based biosensor as a function of glycerol concentration; (C) Summary of the biosensor performance obtained from a dynamic CPA test. 71

Figure 4.3 (A) Cyclic voltammograms for FeS-based biosensor in increasing concentrations of glycerol (a – 0 M, b – 0.001 M, c - 0.01 M, d - 0.1 M and e - 1 M) diluted with water containing enzyme stimulants at benchmark concentrations. Scan rate is 50 mV/s; (B) Effect of applied potential, ranging from 0 to 1.5 V on the current response of the FeS-based biosensor in the presence of 1 M glycerol; (C) Effect of scan rates (10, 30, 50, 70, 90, 110, 130, and 150) mVs^{-1} on the current response of the FeS-based biosensor in the presence of 1 M glycerol where the color intensity of the CV scan increases with an increasing scan rate in the figure; (D) Anodic and cathodic peak currents plotted with respect to the square root of the scan rate ($v^{1/2}$). 74

Figure 4.4 (A) Cyclic voltammograms of FeS-based biosensor in (0, 0.003, 0.01, 0.03, 0.05, 0.07, 0.09, 0.15 and 0.3) M of $(NH_4)_2SO_4$ diluted with water containing 1 M glycerol, scan rate is 50 mV/s. Color intensity of the CV scans increases with increasing concentrations of $(NH_4)_2SO_4$; (B) Equilibrated (60 s) constant potential amperometry measurements of anodic currents in increasing concentrations of $(NH_4)_2SO_4$ diluted with water containing 1 M glycerol, at E = 1.3 V; (C) Cyclic voltammograms of FeS-based biosensor in (0, 0.03, 0.1, 0.3, 0.5, 0.7, 0.9, 3, 30, 300 and 1000) µM of $MnCl_2.4H_2O$ diluted with water containing 1 M glycerol, scan rate is 50 mV/s. Color intensity of the CV scans increases with increasing concentrations of $MnCl_2.4H_2O$; (D) Equilibrated (60 s) constant potential

amperometry measurements of anodic currents in increasing concentrations of $MnCl_2.4H_2O$ diluted with water containing 1 M glycerol, at E = 1.3 V. 76

Figure 4.5 (A) Effect of pH/buffers on anodic currents at E=1.3 V, generated by FeS-based biosensor in 5 mM glycerol solution containing benchmark concentrations of enzyme stimulants; (B) Peak currents at 1.3 V vs. glycerol concentrations measured by FeS-based biosensor derived from CV scans between 0 and 1.5 V, scan rate 50 mV/s. A fitting equation for FeS-based biosensor @ 1.3 V under buffered conditions (Tris buffer/pH10, 0.03 M $(NH_4)_2SO_4$ and 30 µM $MnCl_2.4H_2O$) is $y = 2.7\ln(x) + 119.2$, $R^2 = 0.99$, and non-buffered conditions (pH~6, 0.03 M $(NH_4)_2SO_4$ and 0.3 µM $MnCl_2.4H_2O$) is $y = 1.5\ln(x) + 28.6$, $R^2 = 0.99$. Error bars depict ±1 standard deviation. Different letters indicate significant difference among the sample response means. 78

Figure 4.6 Effect of the interferents on the current responses generated by the FeS-based biosensor. Current responses were derived from cyclic voltammograms performed from 0 to 1.5 V. Grey color bars depict peak current derived at 1.3 V under No buffer/pH~6, 0.03 M $(NH_4)_2SO_4$ and 0.3 µM $MnCl_2.4H_2O$ conditions. Black color bars depict the peak current derived at 0.6 V under the Tris buffer/pH10, 0.03 M $(NH_4)_2SO_4$ and 30 µM $MnCl_2.4H_2O$ conditions. Different letters indicate significant difference among the sample response means. 80

Figure 5.1 (A) Voltammetry analysis of anodes: Excerpts of cyclic voltammograms scanned at a sweep rate of 0.05 V/s vs. Ag/AgCl reference electrode within potential window −1 V and + 1 V display anodic and cathodic peaks of BDT-FeS, BDT-Fe_3S_4, ATP-FeS, ATP-Fe_3S_4, FeS, Fe_3S_4, and PQQ based glucose anodes in 100 mM glucose prepared with 100 mM Tris-HCl buffer (pH 8); (B) Calibration plot: Logarithmic calibration plots for the glucose concentration 0.1 – 100 mM using the voltammetry analysis at 0.5 V. Different letters indicate significant difference among the sample response means. 92

Figure 5.2 Sensitivity and lower detection limits: Sensitivity (A) and detection limits (B) of the glucose biosensors based on different wiring types obtained through cyclic voltammetry indicate BDT-FeS-based glucose anode being more suitable for sensing applications with the highest sensitivity (14.4 µA mM^{-1} cm^{-2}) and lowest detection limits (0.4 mM). Different letters indicate significant difference among the sample response means. 94

Figure 5.3 Storage stability – Sensitivity of the electrodes measured by cyclic voltammetry for 30 days indicate BDT-Fe_3S_4 and Fe_3S_4 based electrodes to

be more stable as biosensors compared to other wiring types. Different letters indicate significant difference among the sample response means. 96

Figure 5.4 The effect of interference on biosensor response at 0.5 V in the presence of 5mM glucose. Different letters indicate significant difference among the sample response means (black letters – response means of interferants; colored letters – response means of glucose biosensors with different wiring types).....97

Figure 5.5 (A) Schematic of a membraneless enzymatic glucose biofuel cell; (B) Open circuit voltages generated by glucose biofuel cells based on different wiring types vs. platinum cathode. Different letters indicate significant difference among the sample response means.....99

Figure 5.6 (A) Polarization curves and (B) power density curves of membraneless glucose biofuel cells based on different wiring types at room temperature under steady-state conditions. Note that power values pertinent to very low resistance values for select electrodes were excluded due to practical insignificance.....100

LIST OF TABLES

Page

Table 2.1 Comparison of performances of various enzymatic glucose anodes 31

Table 2.1 Continued 32

Table 3.1 Degree of coverage, $\boldsymbol{\alpha}$, measured for the sample "FeS SAM +NAD on Au". The standard deviation is better than ±5% for the experimental $\boldsymbol{\alpha}$.....52

Table 5.1 Recent glucose biofuel cells based on direct electron transfer.....84

1. INTRODUCTION

1.1. Dissertation organization

This dissertation consists of six sections. Each specific objective is presented as an individual section. At the beginning of each section, an introduction comprising of literature review associated with the specific objective is presented. Section 1 (this section) consists of the problem statement, objective and hypothesis, a literature review, and rationale. The ability of an array of iron-sulfur clusters ([Fe-S]) to wire different coenzymes and redox enzyme systems onto an electrode surface directly while maintaining excellent charge transport properties, i.e. specific objective 1, is presented in Section 2. Section 3 reports how inorganic [Fe-S] perform electron transport ex vivo once wired to redox coenzymes pertaining to electron transport, i.e. specific objective 2. Section 4 presents the findings of specific objective 3, i.e. construction and testing of a known [Fe-S]-coenzyme-enzyme system (i.e. FeS-NAD-GlDH) to identify methods to test biosensor performance. In Section 5, optimization studies and application of the optimized electrodes to biosensors and biological fuel cells is reported. Section 6 states the summary of conclusions and the recommendations for future work.

1.2. Objective and hypothesis

The overarching objective of this study is to evaluate if common inorganic [Fe-S] could be used to anchor coenzyme(s)-laden enzyme systems to metal electrode supports and the implications of enzyme attachment via [Fe-S] on electron transport kinetics. In

doing so, the possibility of fabricating highly effective molecular wires for transporting electrons ex vivo (i.e., between enzymes and supporting electrodes) was evaluated.

This study is based on the central hypothesis that redox enzymes will transfer electrons at a higher rate (generate higher currents under load) when the coenzymes are directly attached to electrodes using inorganic [Fe-S] as compared to a conventional wiring scheme (control) that consists of cystamine, PQQ, and boronic acid.

The hypothesis was tested, and the overall objective of this study was achieved through the following specific objectives:

1. Assess the effectiveness of using several forms of inorganic [Fe-S] to wire nicotinamide adenine dinucleotide-dependent glucose dehydrogenase (NAD-GDH) coenzyme-apoenzyme complexes onto gold (Au) electrodes.
2. Evaluate the effectiveness of using inorganic [Fe-S] (FeS, FeS_2, Fe_2S_3 and Fe_3S_4) and organic [Fe-S] (ferredoxin), as molecular wires to tether select coenzymes nicotinamide adenine dinucleotide phosphate (NADP), flavin adenine dinucleotide (FAD), PQQ, coenzyme Q10 (CoQ_{10}) and nicotinamide adenine dinucleotide (NAD) (control) on Au electrode.
3. Identify and test methods to study biosensor performance of enzyme electrodes using an established [Fe-S]-coenzyme-enzyme system (i.e. NAD-glycerol dehydrogenase, FeS-NAD-GlDH).
4. Optimize the [Fe-S]-based molecular wires and compare their performance with the conventional PQQ-based molecular wire for biosensing and biofuel cell applications.

1.3. Problem statement

An approach to improving electron transport in enzymatic electrodes ex vivo was established previously using iron (II) sulfide (FeS) molecular wires to directly attach the coenzyme-dependent redox enzyme systems on to the electrode support so that activation, transfer, and resistance overpotentials are significantly reduced. While the ability of FeS to anchor and enhance electron transport in an enzymatic model system (based on NAD-glycerol dehydrogenase) was elucidated previously (Mahadevan, Fernando, & Fernando, 2016), there are still key gaps in knowledge that need to be filled before such a wiring system could be used for practical applications: 1) the form of inorganic iron-sulfur complexes that works best for abiotic electron transport when used as a synthetic redox mediator was not identified; 2) it was unknown whether other common coenzymes will also respond positively to iron-sulfur mediation. It is important to test this ability since there are four identified coenzymes (FAD, PQQ, and coenzyme-Q10) that participate in biological electron transfer reactions; 3) the stability of the iron-sulfur complexes under working conditions was not known; and 4) the performance of iron-sulfur complexes based enzymatic electrodes under load remained unestablished. The only way to fill these critical gaps in knowledge is through a carefully designed series of studies. This dissertation comprises a series of studies geared toward developing this fundamental knowledge.

1.4. Literature review

1.4.1. Enzyme-based bioelectronics

There is a growing interest in developing enzyme-based bioelectronics for biosensing and bio-power generation due to the ever-rising demand for detection, diagnostics, and clean energy generation. The key component of enzyme-based bioelectronics is an enzyme electrode that comprises of an electronic transducer electrically connected to a redox enzyme as the active element. The redox enzyme catalyzes an electrochemical process of interest to produce a stream of electrons which is transmitted to the electronic transducer to produce a transducer signal. While the redox enzyme introduces analytical selectivity due to its specificity for the electron-generating interaction with the substrate/analyte, it is the responsibility of the electronic transducer to effectively engage the electrons by offering a highly conductive platform. (Updike & Hicks, 1967) Clearly, the fundamental requirement of any enzyme-based bioelectronic system is the existence of effective electrical contact between the enzymes, and the electrode supports to foster the transmission of electrical signals efficiently. However, the electrical contact and communication is difficult to accomplish, as enzymes and electrode surfaces are foreign components with respect to one another.(Göpel & Heiduschka, 1995; Schuhmann, 1995; I. Willner, Katz, & Willner, 1997) Therefore, due to the lack of efficient electrical contact and communication between enzymes and electrode supports, the full potential of redox enzymes for the development of self-powering bioelectronics devices such as sensors and fuel cells is yet to be harnessed.

During electron transfer, electrons move from specific electronically localized donors to acceptors, which can be the active site of the enzyme, redox mediators/relays, or simply an electrode in contact with the enzyme. When the electrons flow directly from the active site of the enzyme to the electrode, a direct electron transfer (DET) is established. DET between the electrode surface and the enzyme is often difficult due to the insulation of enzyme active site from the electrode support by the protein matrix (Heller, 1992), and thus special methods such as "molecular wiring" of enzymes are required to realize a direct electrical contact.

1.4.2. Molecular wiring of enzymes

The method of attaching the active site of an enzyme directly with the solid electrode surface using a wiring scheme comprising of electron-mediators and linker molecules is known as molecular wiring of enzyme (Katz, Heleg-Shabtai, Willner, Willner, & Bückmann, 1997). Wired enzyme electrodes have been established for many redox enzymes, which incorporate redox mediators such as PQQ, ferrocene derivatives, ferredoxins, Au nanoparticles, rotaxane structures, and single-wire-carbon-nanotubes, between the enzyme active site and the supporting electrode. The redox mediators help extract electrons from the coenzyme-enzyme complex and transfer them to the electrode supports. (Katz, Sheeney-Haj-Ichia, & Willner, 2004; Patolsky, Weizmann, & Willner, 2004; I. Willner et al., 1996; Xiao, Patolsky, Katz, Hainfeld, & Willner, 2003)

Molecular wires rely on covalent bonding to form intermolecular unions and during the process of making the molecules chemically and redox compatible. Since

known redox mediators do not have the correct combination of prosthetic groups to anchor the coenzyme from one end and the base electrode from the other, molecules with appropriate functional groups are introduced to a wiring scheme to fulfill the anchoring function. This way the wires often becomes lengthy giving rise to kinetic and thermodynamic limitations, therefore, impeding charge transport. For example, the conventional PQQ-redox-mediator-based wiring scheme for tethering enzymes onto a metal electrode is lengthy because PQQ does not have the correct combination of prosthetic groups to anchor the enzyme system (i.e., the apoenzyme-coenzyme complex) from one end and the base electrode from the other. Hence linker molecules, such as cystamine, aminophenyl boronic, and EDC/NHS, with appropriate functional groups are introduced into the wiring scheme to fulfill the anchoring function. The outcome of such a long wiring scheme is high ohmic resistance, resulting in constrained electron transport (Johnston, Strachan, & Johnson, 2007; Park, Lim, Alivisatos, Park, & McEuen, 1999; Reed, Zhou, Muller, Burgin, & Tour, 1997) and producing fuel cells with low power density and sensors with low sensitivity (Minteer, Liaw, & Cooney, 2007; Reed et al., 1997; Riklin, Katz, Willner, Stocker, & Buckmann, 1995).

While redox mediators increase ohmic overpotential, coenzymes, on the other hand, cause activation overpotential. Coenzymes (also known as cofactors), which are non-protein chemical compounds required for the enzyme's catalytic activity, are typically resistant to switching between oxidation and reduction reactions (generally referred to as activation overpotential), further contributing to constrained charge transport.

It should be noted that redox enzymes are naturally occurring bioelectronic entities that can act as power plants or self-powering sensors due to their ability to generate an electron stream in the presence of an enzyme-specific substrate (fuel or analyte). In a living cell, enzymes and coenzymes are held in the cell membranes. Although, it is exciting to wire the coenzyme-enzyme system onto the electrodes ex vivo (i.e., outside a living), their charge transport ability diminishes significantly due to the kinetic and thermodynamic limitations associated with coenzymes and the need of redox mediators. (Akkerman, Blom, De Leeuw, & De Boer, 2006; Holmlin et al., 2001; Mahadevan, Gunawardena, & Fernando, 2014) Thus, the lack of an effective molecular wiring system that can allow unimpeded charge transport is a significant problem that hinders the ability to harness the full potential of enzymes-based self-powering bioelectronic devices. So, there is a need for a method that can immobilize enzymes onto the supporting electrodes while efficiently shuttling the electrons between the enzyme active site and combating/preventing the charge dissipation occurring as a result of overpotentials. If accomplished, such a method can revolutionize bioelectronics systems that depend on enzyme catalysis.

1.4.3. Fe-S based molecular wires

An important characteristic to facilitate DET is to ensure controlled binding and orientation of the enzyme molecules. Iron-sulfur groups are ideal for the controlled binding and orientation of the enzyme to metal electrode supports (and thus, wiring the enzyme) because they: 1) can mediate electron transport; 2) have correct prosthetic

groups to anchor the metal electrode at one end and coenzyme-enzyme complex at the other; and, quite importantly, 3) are short enough to alleviate charge transport limitations. The concept was inspired from the electron-mediating role of iron-sulfur complexes in biological electron transport chains (Berk, Zipursky, & Lodish, 2000; Lill et al., 1999), and the reported performance of iron-sulfur protein derivatives in bio-electrochemical applications. (Beinert, Holm, & Münck, 1997; Beinert & Kiley, 1999; Fontecave, 2006; Lill, 2009)

Although many linker molecules have been attempted thus far to anchor redox enzymes to supporting electrode surfaces, none have been effective enough to emulate the functionality of biological electron transport chains. This is because there are no known entities (other than iron-sulfur complexes) that have the required (multi-functional) capabilities embedded in a single molecule, i.e., the ability to anchor the enzyme from one end and to the electrode support from the other, facilitate electron mediation, and enhance charge transport.

Sulfur atom in the iron-sulfur complex coordinates with metal centers (Graham & Dingman, 2006; Love, Estroff, Kriebel, Nuzzo, & Whitesides, 2005; Mrksich et al., 1996; Tour et al., 1995; Zhong & Porter, 1994) and onto proteins with cysteinyl residues (Meyer, 2008), while the iron atom likely coordinates with the heterocyclic nitrogen atoms (Cline et al., 1985; Lavrenova, Ikorskii, Varnek, Oglezneva, & Larionov, 1986; Marlin, Olmstead, & Mascharak, 1999) or amine linkages (Bedford, Bruce, Frost, & Hird, 2005; T. Liu, DuBois, & Bullock, 2013; Zuo, Lough, Li, & Morris, 2013) or carbon groups that are present in the coenzymes and redox enzymes. Apart from the

presence of synergistic functional groups, the low cost, natural abundance, and outstanding redox properties of iron-sulfur complexes make them potentially an excellent electron-mediator capable of wiring redox active sites to an electrode surface. The obstacle that prevented the replication of the core of the natural electron transport chain was the inability to duplicate the functionality of iron-sulfur molecules ex vivo. Iron-sulfur complexes such as iron sulfides, although abundantly available, are quite unstable in an aqueous environment. However, the breakthrough came as a result of performing the iron (ii) sulfide (FeS) dissolution and attachment on to a metal electrode in a 100% ethanol environment. These studies proved that FeS attaches to the metal electrode via metal-sulfur coordination and once the initial monolayer (of FeS) is formed, the coenzyme could be anchored to Fe-S complex in an aqueous medium with remarkable efficacy. The resulting FeS-based enzyme electrode was able to amplify a current signal 11-fold compared to the conventional PQQ-based enzyme electrode (an enzyme attached to a gold electrode via the cystamine, PQQ, boronic acid, coenzyme wiring scheme). (Mahadevan et al., 2016) Although the simple FeS-based wires fared well in the electron transport realm, there may be other iron-sulfur compounds that are superior, i.e., having the optimal reduction potential, length, chemical configuration, and resiliency. The truly promising performance of the FeS-based molecular wires warrants further investigations, specifically on the performance and resiliency of these wires under load and in the presence of the other coenzymes that are critical for the proper functioning of several redox enzymes that are of interest in bioelectronic applications.

The crux of the study associated with this dissertation is to investigate the effectiveness of easily available inorganic iron-sulfur complexes to tether different coenzymes to supporting electrodes and in doing so, investigate the implications on electron transport.

1.4.4. Origin of iron-sulfur clusters

Iron-sulfur cluster ([Fe-S]) formed the redox centers and coenzymes of several proteins during the first billion anaerobic years of life on the Earth. They were important for several functional processes including respiration, regulation of gene expression, amino acid and nucleotide metabolism, DNA modification and repair, tRNA modification and determination of protein folding. (Andreini, Rosato, & Banci, 2017) These [Fe-S] may have formed inside the cells of the organisms involving complex biogenesis (Outten, 2015) or outside the cell where the apo-proteins are exposed to inorganic iron and sulfur (Qi & Cowan, 2011). Naturally, the processes involving iron (Fe) (and thus, [Fe-S]) were affected during the oxygenation event of the Earth's atmosphere. For instance, O_2 radically reduced the bioavailability of Fe present in the environment by oxidizing it to Fe^{3+}, which forms precipitates and indissoluble complexes with other ions. Also, massive conversion of [Fe-S] to spontaneously decomposing inorganic species took place due to the oxidative stress, causing the [Fe-S] to fall out of the enzyme and making them inactive. For example, superoxide ion or hydrogen peroxide impair the enzyme activity of [Fe-S]-coenzyme containing enzyme hydroxyacid dehydratase by losing a Fe^{2+} ion (see reaction 1, 2, and 3).(Andrade et al., 2014) Besides, O_2 itself oxidizes the Fe-S cluster (Fe_4S_4) and produces superoxide

radical species which cause additional oxidative stress (see reaction 4).(Andrade et al., 2014; Imlay, 2006)

$$Fe_4S_4]^{2+} + O_2^{\bullet-} + 2\ H^+ \rightarrow Fe_4S_4]^{3+} + H_2O_2 \quad (1)$$

$$Fe_4S_4]^{2+} + H_2O_2 + H^+ \rightarrow Fe_4S_4]^{3+} + H_2O + HO^{\bullet} \quad (2)$$

$$Fe_4S_4]^{3+} \rightarrow Fe_4S_4]^{+} + Fe^{2+} \quad (3)$$

$$Fe_4S_4]^{2+} + O_2 \rightarrow Fe_4S_4]^{3+} + O_2^{\bullet-} \quad (4)$$

The result of reaction (1) may vary according to the different kinds of [Fe-S] pertaining to the number and nature of their ligands. Some enzymes such as aconitase and lysine 2,3-aminomutase coordinate only with clusters containing 3 protein ligands and hence, the 4th Fe atom is available for linking with substrates or coenzymes. Other redox active [Fe-S] do not keep the 4th Fe atom open for association with substrates and coenzymes. One such example is the Fe-S cluster in ferredoxin which may have 4 ligands buried in the protein matrix. Similarly, the interaction between reactive oxygen species (ROS) differs with ever different Fe-S cluster, as seen in reaction (4) where the buried Fe_4S_4 clusters with 4 protein ligands are less sensitive to H_2O_2 and superoxide, but are readily oxidized by O_2.(Andrade et al., 2014)

Despite the drastic effect of oxygenation on iron-sulfur clusters, due to their importance to all forms of life, microbes have developed unique strategies and mechanisms for Fe uptake and Fe-S biogenesis, to tackle oxidative stress. The strategies and mechanisms included: 1) colonization in anoxic environments such as the bottom of the lakes and the ocean; 2) rapid reduction of O_2 and the reactive oxygen species; 3) Fe-S cluster repair mechanisms; 4) replacement of the O_2-sensitive Fe-S cluster with O_2-

resistant coenzymes or redox centers such as Fe_3S_3 cluster of O_2-tolerant hydrogenases; 5) some organisms evolved to switch between anaerobic and aerobic metabolisms.(Andrade et al., 2014)

Oxyphotobacteria – members of bacteria phylum Cyanobacteria were the first living organisms to encounter and sustain the oxidative stress due to the great oxygen event. Although developing the capability of oxygenic photosynthesis after the oxygen event, these organisms lived innately through anoxygenic photosynthesis at first, possibly with only sporadic generation of O_2 in rather small amounts. (Fischer, Hemp, & Valentine, 2016)

Bacteria certainly did not have the defenses essential to deal with significant oxidative stress at this point. In bacteria, the oxygenation of the Earth's atmosphere led to the development of defense mechanisms to regulate the concentration of the O_2-derived radicals for maintaining the free iron levels or fixed oxidative stress and damages. Iron is required by the bacteria at ~millimolar concentrations to carryout Fe-S assembly and for heme synthesis. The phototrophic oxyphotobacteria perhaps required larger amounts of iron and sulfur. At the time, iron and sulfur were abundantly available in the form of Fe^{2+} and sulfides and thiols forming ferrous-thiolate ferrous-sulfide complexes using ligand-free cysteine, cystines attached to proteins, etc. At the oxygenation of the Earth's atmosphere, the ferrous-thiolate ferrous-sulfide complexes probably got oxidized to Fe^{3+}, the sulfides into elemental sulfur, polysulfides, sulfite, thiosulfate and sulfate, thiolates into disulfides, and cysteines to cystines. (Ayala-Castro, Saini, & Outten, 2008; Touati, 2000)

Small amounts of O_2 and ROS were not a threat to the bacteria as long as Fe^{2+}, thiols, and sulfides were available in non-limiting amounts to scavenge the oxidants. However, with higher levels of O_2, accumulation of Fe^{3+} could have led to the cytotoxicity of the anaerobic cells. (Sessions, Doughty, Welander, Summons, & Newman, 2009)

There are theories that the oxyphotobacteria survived great amounts of O_2 with the help of catalytic antioxidant systems, e.g., Fe(II)–sulfide and Fe(II)–thiolate which helped recycle sulfite and sulfate using reductase enzymes, and the Fe^{3+} formed reduced by the excess sulfide. There were several such biochemical systems and inorganic reactions (such as Manganese, glutathione, alpha-tocopherol in oxyphotobacteria) with antioxidant chemistry, which with high oxidative stress evolved into more complex enzymatic antioxidant systems. (Fischer et al., 2016)

Microbes such as bacteria and fungi overcame this obstacle by secreting siderophores which are soluble organic molecules with high affinity to oxidized iron from mineral phases such as iron oxides and hydroxides. The Fe^{3+}-siderophore was taken up by the organisms by active transport mechanisms, and once in the cytoplasm, they were reduced to Fe^{2+} to release the iron from the complex which is then used in several metabolic pathways.(Chu et al., 2010)

1.4.5. Iron-sulfur complexes found in nature

Iron-sulfur complexes found in nature are proteins that comprise iron-sulfur clusters or centers containing sulfide-linked di-, tri-, and tetra-iron centers in variable

oxidation states. Iron-sulfur clusters are found in nature in three distinct forms ([2Fe-2S], [4Fe–4S] and [3Fe–4S]) in a variety of metalloproteins, such as the ferredoxins, as well as NADH dehydrogenase, hydrogenases, coenzyme Q – cytochrome c reductase, succinate-coenzyme Q reductase, and nitrogenase. (Lippard & Berg, 1994) Iron-sulfur complexes are best known for their role in the redox reactions of mitochondrial electron transport. The iron-sulfur complexes circumvent the electron transport issues associated with redox enzymes in the biological systems by acting as their active redox centers. This is possible because: 1) While the organic portions of the electron transfer protein are not capable of shuttling electrons, the Fe metal center readily undergo redox reaction to shuttle electrons; 2) The potential of the iron-sulfur complexes can be regulated over a wide range by their coordination environment (This is helpful because electron transfer is faster when the free energy difference between the donor and the acceptor is somewhat negative but not too much, and the reduction potential must be finetuned to be in between those of the donor and the acceptor when the same protein donates and accepts electrons); 3) Due to their size, the conductive metal centers enhance electron transport in pathways by shortening the electron transfer distance; and 4) Metals have special coordinating geometries that favor both the redox states of the metal, also during electron transport they can distribute electrons over several metal ions, hence the reorganization energy on passing from one redox state to another is minimized. (Gray & Winkler, 1996, 2005, 2010) $Fe(Cys)_4$, [2Fe-2S], [4Fe-4S] and [3Fe-4S] are particularly known for their electron transfer function in redox-active proteins such as rubredoxin, desulforedoxin, ferredoxins, Fe only hydrogenase, fumarate reductase, high potential

iron protein, nitrogenase Fe-protein, and trimethylamine dehydrogenase.(Beinert et al., 1997; Kondo, Okamoto, Hashimoto, & Nakamura, 2015; Rees & Howard, 2003) Given below are the reaction schemes for the iron-sulfur clusters mentioned above (Guo, Sulc, Ribbe, Farmer, & Burgess, 2002; Hans, Buckel, & Bill, 2008):

$$Fe^{II}(SCys)_4 \rightleftharpoons Fe^{III}(SCys)_4$$

$$[Fe_2S_2]^{+} \rightleftharpoons [Fe_2S_2]^{2+}$$

$$[Fe_3S_4]^{0} \rightleftharpoons [Fe_3S_4]^{1+}$$

$$[Fe_4S_4]^{0} \rightleftharpoons [Fe_4S_4]^{1+} \rightleftharpoons [Fe_4S_4]^{2+} \rightleftharpoons [Fe_4S_4]^{3+}$$

1.4.6. How the presence of oxygen affects the Fe-S complex and why Fe-S complexes are unstable in water

The primary reason for not being able to use iron-sulfur complexes as electron mediators for practical applications is their instability in an aqueous environment. So, a discussion on how the presence of oxygen impacts the stability of iron-sulfur complexes and their fate in the presence of water warrants a discussion.

Oxygen being an oxidizing agent oxidizes Fe-S complexes. Let's first take the example of iron (II) sulfide (FeS). FeS can dissolve both in oxidative and in non-oxidative solutions. The interaction between FeS and aqueous solutions containing dissolved oxygen creates acidic and rusty solutions that can have a seriously negative impact on the environment. It has been reported that the rate of aqueous oxidation of FeS increases when initial acidity (H^+) and temperature increase. (Chiriţă, 2009; Chiriță, 2016)

$$4FeS + 3O_2 \rightarrow 2Fe_2O_3 + 4S \text{ (reaction 1)}$$

$$4FeS + 4H_2O + 9O_2 \rightarrow 2Fe_2O_3 + 4H_2SO_4 \text{ (reaction 2)}$$

Reaction 1 of FeS oxidation is exothermic with enthalpy, ΔH, values of -635 kJ/mol. Upon allowing the oxidation reaction to advance quickly with little or no dissipation of heat can cause high temperatures leading to glowing and sparking of FeS. The product Fe_2O_3 or iron (III) oxide, often called rust, precipitates on the FeS surface, and can affect further oxidation of FeS. Aqueous oxidation of FeS by oxygen is controlled by a mixed regime of diffusion and surface reaction control. (Chiriță, 2016; Roling et al., 2001)

Another example is that of, pyrite (FeS_2) oxidation which results in the formation of water-soluble sulfate ions (SO_4^{2-}), ferrous ions (Fe^{2+}) and acid (H^+; reaction 3). Fe^{3+} is nearly insoluble and in the presence of oxygen, the relatively reduced Fe^{2+} is readily oxidized (reaction 4), except under acidic conditions (pH 2-3) as the kinetics of this reaction is pH dependent and slows down with the increase in H^+. The ferric iron (Fe^{3+}) formation in water results in the hydrolysis of iron to form ferric hydroxide [$Fe(OH)_3$] and acid (H^+) (reaction 5). (Campaner, Luiz-Silva, & Machado, 2014) (Roling et al., 2001)

$$FeS_2 + 3½\ O_2 + H_2O \Leftrightarrow Fe^{2+} + 2\ SO_4^{2-} + 2H^+$$
(Reaction 3)

$$Fe^{2+} + ¼\ O_2 + H^+ \Leftrightarrow Fe^{3+} + ½\ H_2O \quad \text{(Reaction 4)}$$

$$Fe^{3+} + 3H_2O \Leftrightarrow Fe(OH)_3 + 3H^+ \quad \text{(Reaction 5)}$$

Similarly, iron-sulfur protein complexes can be unstable in the presence of oxidizing agents. Although many iron-sulfur clusters are unstable to oxidation, these

clusters are commonly found in both anaerobic organisms and in aerobic organisms to perform key functions. Not all protein-bound iron-sulfur clusters are unstable to oxidation. Proteins that contain stable iron-sulfur clusters have the cluster bound in a region of the protein that is unreachable to solvent and oxidants. (Rouault & Klausner, 1996)

Aforementioned origins of iron-sulfur complexes were the key inspiration to select and test the effectiveness of commonly found inorganic [Fe-S] for studies associated with this dissertation.

2. ASSESSMENT OF THE EFFECTIVENESS OF USING INORGANIC IRON-SULFUR CLUSTERS TO WIRE NAD-GLUCOSE DEHYDROGENASE ONTO GOLD ELECTRODES[*]

2.1. Introduction

The restricted electrical contact and communication between the active site(s) of a redox enzyme and the supporting electrode is a major factor limiting the performance of enzyme-based bioelectronic devices.(Göpel & Heiduschka, 1995; Luong, Glennon, Gedanken, & Vashist, 2017; Schuhmann, 1995; I. Willner et al., 1997) Active sites of the redox enzymes are generally buried deep inside the protein matrices(Heller, 1992) requiring redox relays for shuttling electrons between the enzyme and the electrode surface.(B. Willner, Katz, & Willner, 2006) Many relays such as PQQ, ferrocene derivatives, ferredoxins, gold (Au) nanoparticles, rotaxane structures and single-wire-carbon-nanotubes) have been attempted.(Katz et al., 2004; Patolsky et al., 2004; J. Wang, 2008; I. Willner et al., 1996; Xiao et al., 2003) However, during the process of making the molecules chemically and redox compatible, the wires often become lengthy giving rise to kinetic and thermodynamic limitations, which in turn, impedes charge transport.(Akkerman et al., 2006; Holmlin et al., 2001; Mahadevan et al., 2014) Having a relay system that can anchor the supporting electrode and the enzyme system while

[*] Reprinted with permission from "Inorganic iron-sulfur clusters enhance electron transport when used for wiring the NAD-glucose dehydrogenase based redox system." by Mahadevan, A., & Fernando, S., 2018, Microchimica Acta, 185(7), 337, Copyright [2018] by Springer Nature.

efficiently shuttling the electrons between the active site and the electrode can revolutionize bioelectronics systems such as sensors and fuel cells that depend on enzyme catalysis.

Previously, the ability of inorganic iron(II) sulfide (FeS) to anchor nicotinamide adenine dinucleotide-dependent glycerol dehydrogenase (NAD-GlDH) to the gold electrode surface was reported (Mahadevan et al., 2016). This work was inspired due to the electron mediating role of iron-sulfur clusters in the biological electron transport chain(s)(Lill et al., 1999) and the reported performance of iron-sulfur protein derivatives for bioelectrochemical applications.(Beinert et al., 1997; Beinert & Kiley, 1999; Fontecave, 2006; Lill, 2009) The FeS-based electrode assembled during the previous work displayed promising electrical charge transport properties, likely, as a result of reduced internal resistance of the enzymatic electrode caused by the shorter FeS single-molecular-wires; and the ability of FeS to be a single-molecular anchor as well as an electron shuttling agent between nicotinamide adenine dinucleotide (NAD) coenzyme and the solid electrode support.(Mahadevan & Fernando, 2017; Mahadevan et al., 2016) Although the ability of FeS to anchor and enhance electron transport in the NAD-GlDH model system was elucidated previously, there is still a gap in knowledge with regards to the utility and performance of other inorganic iron-sulfur compounds for anchoring biomedically relevant redox enzymes such as glucose dehydrogenase.

For the first time, the functionalization of gold surface with nicotinamide adenine dinucleotide-dependent glucose dehydrogenase (NAD-GDH) using inorganic Fe-S, i.e. FeS, FeS_2, Fe_2S_3 and Fe_3S_4, via molecular self-assembly and the notable ability of the

Fe-S to efficiently mediate electron transport between the GDH active site and the supporting electrode is reported. By voltammetry analyses, the forms of Fe-S that may work best for abiotic electron transport when used as a synthetic redox mediator was determined.

2.2. Experimental

2.2.1. Reagents and apparatus

NAD-GDH from Bacillus sp. (EC.1.1.1. 47) was purchased from Sekisui Diagnostics. ß-NAD, glutaraldehyde, iron (II) sulfide (FeS), iron disulfide (FeS_2), pyrroloquinoline quinone (PQQ), cystamine dihydrochloride, 3-aminophenyl boronic acid monohydrate (3APB) and D-glucose were purchased from Sigma-Aldrich, USA (www.sigmaaldrich.com). Iron (III) sulfide (Fe_2S_3) and greigite (Fe_3S_4) were obtained from 1717 CheMall Corporation (www.1717chem.com). 1-Ethyl-3-(3-dimethylaminopropyl) carbodiimide (EDC) and N-Hydroxysuccinimide (NHS) were purchased from Thermo Fisher Scientific (www.thermofisher.com/us). Fe-S were suspended in ≥99.5% ethanol, and cystamine dihydro chloride was dissolved in pure water; ß-NAD, GDH, and glutaraldehyde solutions were prepared in a 0.1 M phosphate buffer (pH = 7); PQQ and 3-aminophenylboronic acid solutions were prepared using a 0.1 M HEPES buffer (pH 7.2) in the presence of 5 mM EDC and 2.5 mM NHS. (Mahadevan & Fernando, 2017) Glucose solutions of different concentrations were prepared in 0.1 M Tris-HCl buffer (pH 8) and stored at 4°C for 36±1 hrs to allow

mutarotation. Tris-HCl buffer (pH 8) was selected to enable optimal performance of the NAD-GDH without affecting the pH stability of the other molecular wire components.

Molecular-biology-grade water obtained from Sigma-Aldrich was used to prepare all the aqueous-based solutions and for rinsing/cleaning purposes throughout this study. Two-millimeter gold-disk working electrodes, Ag/AgCl (1M KCl) reference electrodes, Pt auxiliary electrodes and a gold electrode polishing kit were purchased from CH Instruments Inc. All experiments were carried out in an electrochemical cell set up using a C3 cell stand from BASi (www.basinc.com). A CHI8003D potentiostat from CH Instruments, Inc (www.chinstruments.com) was used for electrochemical methods.

2.2.2. NAD-GDH anode(s) fabrication

Five different glucose anodes were fabricated, based on Fe-S-based and PQQ-based molecular wiring systems used to tether the GDH enzyme system onto the gold electrode, using a layer-by-layer self-assembly method by dip-coating. The gold working electrodes were cleaned by first polishing the electrodes with 0.05 micron alumina for 3 minutes followed by sonication for 5 minutes to remove alumina particles; then, dipping the polished gold electrodes in a 50 mM KOH solution made in 30 wt% H_2O_2 for 30 minutes, followed by rinsing with pure water, and finally, implementing 5 cyclic voltammetry sweeps in the 50 mM aqueous KOH solution followed by a thorough rinsing with water.

For fabrication of Fe-S-based glucose anodes, the clean gold electrodes were first dipped into 0.3 M $FeS/FeS_2/Fe_2S_3/Fe_3S_4$-in-ethanol solution for 2 hrs. The Fe-S-tethered gold electrodes were immersed in 1 mM of ß-NAD for 2 hrs after which; the gold-Fe-S-NAD electrodes were dipped in 1mg mL^{-1} of GDH for 2 hrs. The resulting gold-Fe-S-NAD-GDH electrodes were lastly treated with 10% (v/v) glutaraldehyde for 20 min to crosslink and secure the GDH enzyme layer. Similarly, a PQQ-based glucose anode was constructed by successively dipping the clean gold electrode in 0.1 M cystamine dihydrochloride solution for 1 hr, a 3 mM solution of PQQ for 2 hrs, a 1 mM 3aminophenylboronic acid solution for 2 hrs, a 1 mM of ß-NAD solution for 2 hrs, a 1 $mg.mL^{-1}$ GDH for 2 hrs, and a final 20 min treatment with 10% (v/v) glutaraldehyde. After every successive dipping step, the monolayer-functionalized gold electrode was thoroughly rinsed with water.

2.2.3. Electrochemical measurements

All electrochemical studies were performed using the conventional three-electrode system (i.e., an enzymatic working electrode, a Pt counter electrode, and an Ag/AgCl reference electrode) placed in an electrochemical cell containing 10 mL of the corresponding substrates. Gold electrodes with a constant surface area of 0.031 cm^2 were used for all the experiments. All the studies were conducted at ambient temperature.

2.2.4. Ferricyanide/ferrocyanide-voltammetry to confirm multi-layer SAM formation

Cyclic voltammetry of the ferrocyanide/ferricyanide redox couple was used to verify the formation of multiple layers of SAMs on the gold electrode surface. After the tethering of every SAM in the molecular wiring systems, the electrode was scanned two times in 0.01 M potassium ferricyanide with 0.1 M KNO_3 from − 0.8 V to + 0.8 V, at a scan rate of 0.05 V/s. Bare gold electrodes were used as control electrodes.

2.2.5. Potentiometric analysis of glucose anodes

Instantaneous open circuit voltages (OCVs) were recorded for Fe-S-based and PQQ-based (control) glucose anodes in 0.1-100 mM glucose concentrations. OCVs were measured by a potentiostat using the conventional three-electrode system in a 10 mL total volume of glucose solutions.

2.2.6. Voltammetry analysis of glucose anodes

The Fe-S-based and PQQ-based (control) glucose anodes were tested for glucose detection using cyclic voltammetry with glucose concentrations ranging between 0-100 mM. The glucose anodes were scanned from −1.5 V to +1.5 V, at a scan rate of 0.05 V/s, to obtain the anodic peak current densities resulting from glucose oxidation.

2.2.7. Surface coverage of the Fe-S monolayers on gold

Linear sweep voltammetry (LSV) was used to measure the surface coverage of Fe-S on the gold electrode. SAMs of FeS, FeS_2, Fe_2S_3, Fe_3S_4, and cystamine (control) were formed on a clean gold electrode (Figure 2.5 A-D), followed by formation of NAD layers (Figure 2.5 C-D), using the same method as described in "NAD-GDH anode(s) fabrication." The modified electrodes were subjected to a potential sweep between 0 V and −1.2 V in 10 mL of 50 mM KOH solution, i.e., starting at a potential where no reaction occurs to a range of potentials where the reductive desorption of the SAMs are expected to occur.

2.2.8. Statistical analysis

All the studies were conducted in three replications. Analysis was done using JMP pro 14 (Version 14.0.1, SAS Institute Inc., Cary, NC) with Analysis of Variance (ANOVA). Post Hoc test (Student's t test or Tukey-Kramer HSD) was used to compare treatments means. Significance levels were defined using $p < 0.05$.

2.3. Results and discussion

2.3.1. Ferricyanide/ferrocyanide-voltammetry confirmed multi-layer SAM formation

Cyclic voltammetry of ferricyanide/ferrocyanide redox couple ($Fe(CN)_6^{3-/4-}$) has been previously utilized to verify the formation of self-assembled monolayers (SAMs) on electrode surfaces.(Mahadevan et al., 2016; Mahadevan, Gunawardena, Karthikeyan,

& Fernando, 2015) In this study, the formation of individual SAMs on gold electrodes was verified using cyclic voltammograms (CVs) obtained by applying a potential sweep on the electrodes placed in potassium ferricyanide solution.

Consecutive drops in peak current density and growing of peak width can be observed in the $Fe(CN)_6^{3-/4-}$ voltammograms (Fig. 1a-e), after immersing the electrodes in successive monolayer-containing solutions. A drop in current density was observed with the addition of each layer as a result of impedance to electron transport kinetics at the electrode caused by the formation of closely packed assemblages on the conductive gold surface.(Dowdy & Leopold, 2010) Thus, the stepwise drop in peak current density after each immersion and widening of peaks as shown in Figure 2.1 (A-E) can be attributed to the formation of successive SAMs on gold surfaces.

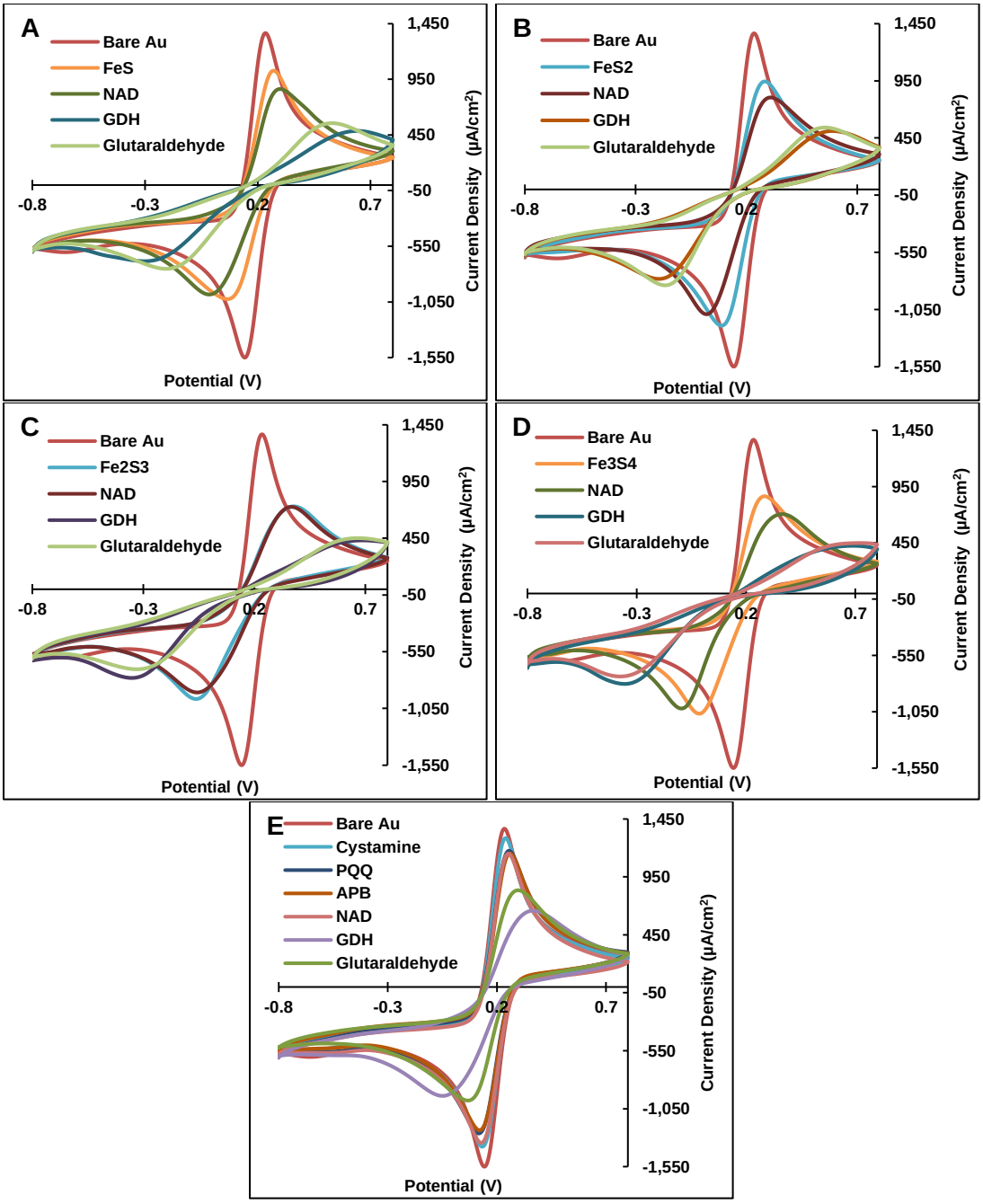

Figure 2.1 Ferricyanide/ferrocyanide-voltammetry to verify multi-layer SAM formation: Cyclic voltammograms (CVs) of (A) FeS, (B) FeS_2, (C) Fe_2S_3, (D) Fe_3S_4, and (E) PQQ functionalized gold surfaces were conducted in 0.01 M potassium ferricyanide with 0.1 M KNO_3 at a scan rate of 0.05 V/s vs. Ag/AgCl reference electrode to confirm self-assembly of successive monolayers of molecular wires on gold surfaces.

2.3.2. Potentiometric analysis of glucose anodes

Potentiometric analyses of the Fe-S and PQQ-based glucose anodes were done by measuring their instantaneous open circuit voltages (OCVs) in 0.1-100 mM glucose. All Fe-S based glucose anodes produced significantly greater OCVs than their PQQ-based counterpart (Figure 2.2). The higher OCVs suggest more favorable thermodynamics when using Fe-S as relays as compared to PQQ-based wiring systems. The reduction of OCV with increasing glucose concentrations indicate that the thermodynamics favor low glucose concentrations.

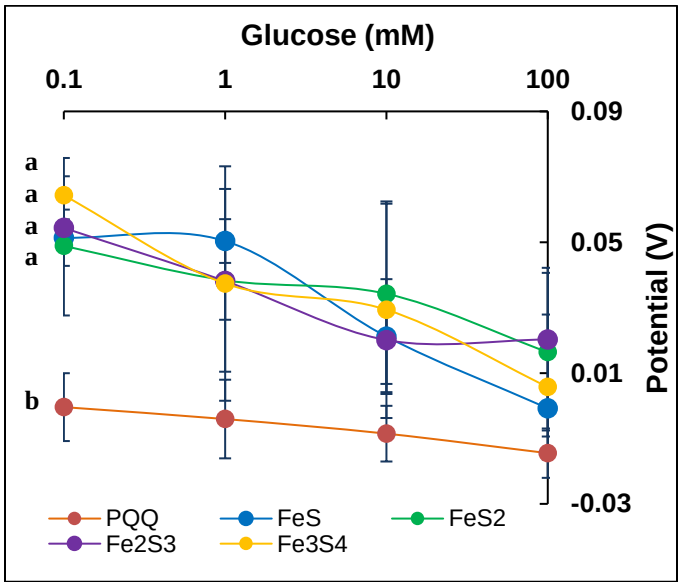

Figure 2.2 Potentiometric analysis of glucose anodes: Instantaneous open circuit voltages obtained by Fe-S-based and PQQ-based glucose anodes between 0.1-100 mM glucose solutions with 0.1 M Tris-HCl buffer (pH 8) acting as carrier. The analysis shows that all Fe-S-based anodes generated higher open circuit voltages as compared to PQQ-based counterpart but were negatively correlated with glucose concentrations. Different letters indicate significant difference among the sample response means.

2.3.3. Voltammetry analysis of glucose anodes

Voltammetry responses of the Fe-S and PQQ-based GDH glucose anodes obtained using cyclic voltammetry in 0-100 mM glucose are shown in Figure 2.3 A-E. The anodic and cathodic peak current densities ($|J_a|$ and $|J_c|$) observed at 0.5 V and 0.37 V correspond to the enzymatic oxidation/reduction of glucose/gluconic acid by GDH. Figure 2.3 A-E show that both $|J_a|$ and $|J_c|$ increase with increasing glucose concentrations.

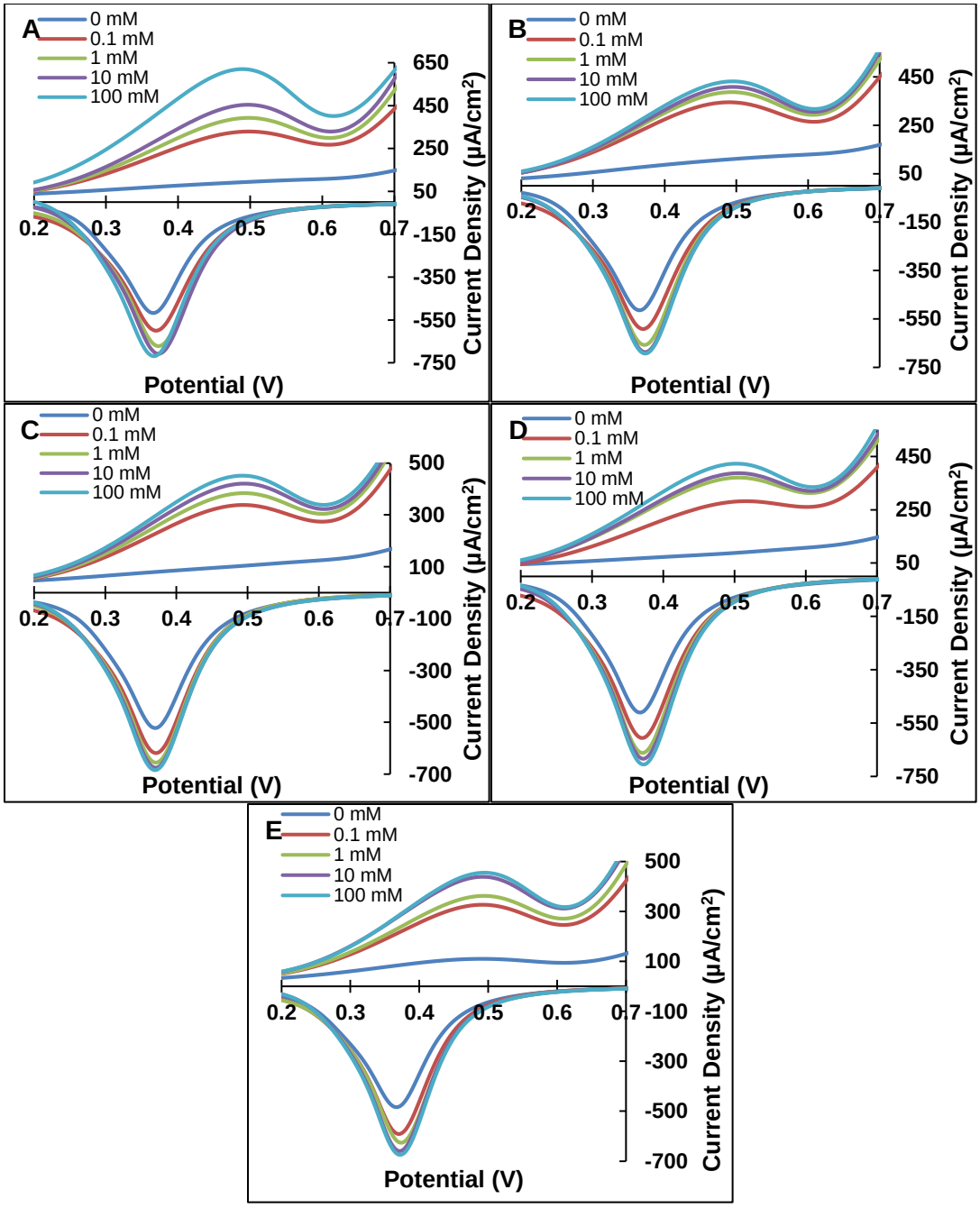

Figure 2.3 Voltammetric analysis of glucose anodes: Excerpts of cyclic voltammograms scanned between −1.5 V and +1.5 V display anodic and cathodic peaks of (A) FeS, (B) FeS_2, (C) Fe_2S_3, (D) Fe_3S_4, and (E) PQQ based glucose anodes confirm a positive correlation between anodic and cathodic peak current densities with glucose concentrations 0-100 mM in Tris-HCl buffer (pH 8), at a scan rate of 0.05 V/s vs. Ag/AgCl reference electrode.

A comparison of $|J_a|$ of Fe-S and PQQ-based glucose anodes (see Figure 2.4 A) shows that Fe-S-based glucose anodes consistently generated significantly higher anodic current densities than the PQQ-based glucose anode. A strong logarithmic correlation was observed between $|J_a|$ and glucose concentrations for all the anodes. Fe_2S_3 resulted in the highest $|J_a|$ values indicating its superior charge transportability as compared to all of the other forms of relays tested. However, by comparing the sensitivity and detection limits of the glucose anodes (Figure 2.4 B) FeS clearly displays greater suitability for sensing applications with highest sensitivity (25.21 $\mu A\ mM^{-1}\ cm^{-2}$) and lowest detection limit (0.77 mM). The performance of Fe-S and PQQ glucose anodes is compared with glucose anodes with other electrode compositions reported in the past (Table 2.1). The sensitivity and limit of detection values of Fe-S and PQQ glucose anodes are low compared to other electrode compositions, likely because of the relatively wide linear range of glucose concentrations used in this study.

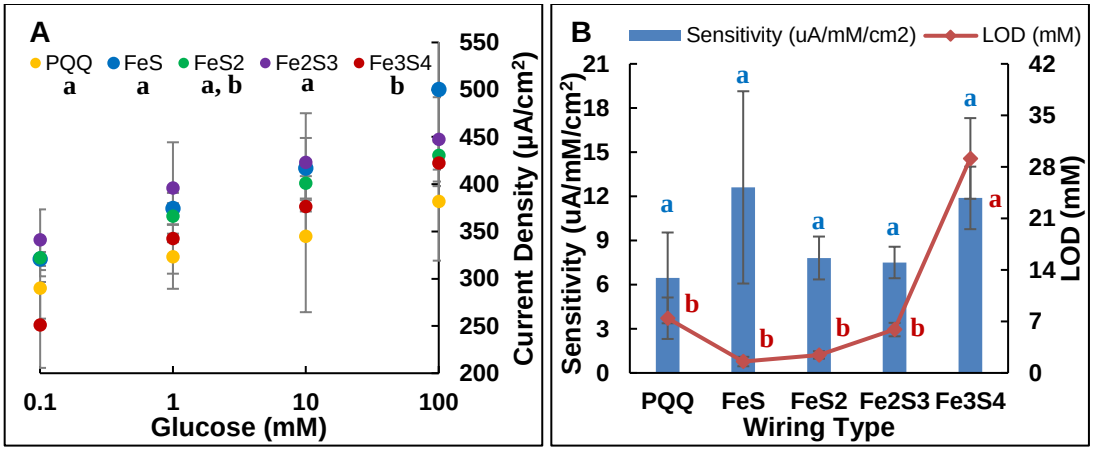

Figure 2.4 (A) Calibration plot of glucose anodes: Calibration plot of anodic peak current densities measured by glucose anodes between glucose concentrations 0.1-100 mM at working potential 0.5 V vs. Ag/AgCl reference electrode, derived from the CV scans between −1.5 V and +1.5 V at a sweep rate of 0.05 V/s; (B) Sensitivity and Limit of Detection: Sensitivity and limit of detection of the glucose anodes calculated from the calibration plots indicate FeS-based glucose anode to possess greater suitability for sensing applications with highest sensitivity (25.21 µA mM^{-1} cm^{-2}) and lowest detection limit (0.77 mM). Different letters indicate significant difference among the sample response means.

Table 2.1 Comparison of performances of various enzymatic glucose anodes

Electrode Composition	Applied Voltage (vs. Ag/AgCl)	Sensitivity	LOD	Linear Range	Reference
Au/FeS/GDH/ GA	+0.50 V	25.21 µA mM^{-1} cm^{-2}	0.77 mM	0.1–100 mM	This work
Au/FeS_2/ GDH/GA	+0.50 V	15.62 µA mM^{-1} cm^{-2}	1.22 mM	0.1–100 mM	This work
Au/Fe_2S_3/ GDH/GA	+0.50 V	15.01 µA mM^{-1} cm^{-2}	2.95 mM	0.1–100 mM	This work
Au/Fe_3S_4/ GDH/GA	+0.50 V	23.79 µA mM^{-1} cm^{-2}	14.57 mM	0.1–100 mM	This work
Au/Cys/APB/P QQ/ GDH/GA	+0.50 V	12.92 µA mM^{-1} cm^{-2}	3.72 mM	0.1–100 mM	This work

Table 2.2 Continued

Electrode Composition	Applied Voltage (vs. Ag/AgCl)	Sensitivity	LOD	Linear Range	Reference
SPCE/GN/GOx/Nafion	+0.475 V	-	20 mg·L^{-1}	50–2000 mg L^{-1}	(Mehmeti et al., 2017)
GCE/MWCNT/PyBA/GOx/GA	−0.440 V	28 µA mM^{-1} cm^{-2}	72 mM	0.5–3.5 mM	(Kowalewska & Jakubow, 2017)
GCE/MWCNT/PyBA/GOx/EDC	−0.438 V	20 µA mM^{-1} cm^{-2}	36 mM	0.25–3.25 mM	(Kowalewska & Jakubow, 2017)
RGO-Fe3O4/MSPE/GOx	− 0.45 V	5.9 µA/mM	13.78 mM	0.05–1 mM	(Pakapongpan & Poo-Arporn, 2017)
CdS–ZnS/MAA/PGE/GDH	+0.8 V	-	0.05 mM	0.2–8.0 mM	(Ertek, Akgül, & Dilgin, 2016)
GCE/MWCNTs/G-AuNPs/GOx	-0.45 V	29.72 mA $M^{-1}cm^{-2}$	4.8 mM	5–175 mM	(Yu et al., 2014)
Modified Carbon/FePhenTPy/GDH	+0.55 V	-	12.02 ±0.6 mg dL^{-1}	30–600 mg dL^{-1}	(Kim et al., 2013)
GCE/MWCNT/GDH	+0.30 V	0.474 nA μM^{-1}	4.81 µM	10–300 µM	(Zhou et al., 2010)

Abbreviations Au: gold; Cys: Cystamine; FeS: iron(II) sulfide; FeS2: iron disulfide; Fe2S3: Iron(III) sulfide; Fe3S4; greigite; AuNPs: gold nanoparticles; MWCNT: multi-walled carbon nanotubes; RGO: reduced graphene oxide; GCE: glassy carbon electrode; PyBA: 4-(pyrrole-1-yl) benzoic acid; GA: glutaraldehyde; EDC: 1-ethyl-3-(3-dimethylaminopropyl) carbodiimide; MSPE: magnetic screen-printed electrode; FePhenTPy: 5-[2,5-di (thiophen-2-yl)-1H-pyrrol-1-yl]-1,10-phenanthroline iron(III) chloride; LOD: limit of detection; GDH: Glucose dehydrogenase; GOx: glucose oxidase

2.3.4. Surface coverage of the Fe-S monolayers on gold

To correlate how the molecular size and structure of Fe-S affect the packing density of the SAMs and in turn how these parameters affect differences in the charge transport, surface coverage of FeS, FeS_2, Fe_2S_3 Fe_2S_3, Fe_3S_4 and cystamine (control) on the gold surface were examined. Reductive desorption of the Fe-S from the gold surface achieved by linear sweep voltammetry (LSV) is shown in Figure 2.5A.

The reduction of the Au-[S-Fe] bond that holds the sulfur atom of the Fe-S bonded to gold forms the reductive peak. Multiple peaks may occur as a result of desorption of monolayers from different adsorption sites (Arihara et al., 2003; Tudos & Johnson, 1995); this is possible due to surface irregularities. In this case, however, the different potentials may depict the energy required for the desorption of clusters bonded via distinct bonding mechanisms (e.g., Au-Fe vs. Au-S)(Kakiuchi, Usui, Hobara, & Yamamoto, 2002; Sagiv, 1980). The reductive desorption peaks occur at different potentials depending upon the ease of desorbing SAMs from gold. The ease of desorption of SAMs can depend on the size/length(Lavrich, Wetterer, Bernasek, & Scoles, 1998), structure(Ito, Noh, & Hara, 2008; Lavrich et al., 1998) and molecular density(Kondoh, Kodama, & Nozoye, 1998) of the molecules that create the SAM. The reductive desorption of Fe-S monolayer from the gold surface may be shown as:

$$\mathrm{Au{-}[S-Fe]} + \mathrm{e^-} \rightarrow \mathrm{Au} + \mathrm{[Fe-S]^-} \qquad \textbf{(Eq.1)}$$

The desorption potential of Fe_3S_4 is more negative than those of FeS, FeS_2, and Fe_2S_3, possibly due to the difficulty in cleaving the Au-S bond resulting from the cubic close-packed structure of Fe_3S_4. Using the experimentally determined charge of the

reductive desorption peaks at their corresponding desorption potentials, surface coverage (Γ) of Fe-S on gold surface were calculated using the equation $\Gamma = Q/nFA$, where Q is the charge passed to break the gold-S bond, which was determined by integrating the reductive desorption peak in the LSV scan and is the average from three replicates of each SAM, n is the number of electrons in the electron-transfer process (n=1), F is Faraday's constant, and A is the area of the bare gold electrode (0.031 cm^2) (see Figure 2.5 B).

It was observed that Fe_3S_4 has the highest surface coverage on gold (Fig. 5b) while also imparting the lowest resistance ($V_{at\ Ip}/I_p$, where $V_{at\ Ip}$ is the anodic peak potential and I_p is the anodic peak current; Figure 2.5 C) and the highest power required to desorb; thus, the highest affinity to the gold electrode ($V_{at\ Ip} * I_{p,}$ Figure 2.5 D). It is likely that the higher number of Fe atoms per S (Fe being the more conductive of the two) among many other variables played a role for the superior conductivity of Fe_2S_3 and FeS as compared to the other relays tested. The other variables include molecular orientations, packing density, molecular density, and intermolecular & intramolecular bonding. It was interesting to note that the cystamine-PQQ couple, despite showing a high coverage and affinity to the gold electrode, displayed the highest resistance to electron transport due to the insulating effect like many other biomolecules(Braun, Eichen, Sivan, & Ben-Yoseph, 1998; Scheibel et al., 2003). The cystamine and PQQ combination is a widely used relay in wiring enzymes on metallic bioelectrodes. In contrast, all forms of [FeS] performed better, yielding lesser resistance. It was encouraging to observe that the addition of the subsequent NAD coenzyme did not

impact charge transport significantly when [FeS] were used as relays. Nevertheless, the addition of the NAD layer further increased the resistance of the system when the conventional cystamine-PQQ couple was used to anchor the coenzyme. Figure 2.5 D also presents the low power required for the desorption of the cystamine-PQQ couple when compared with the Fe-S-based wiring systems. These observations prove that the inorganic Fe-S strongly bind to the coenzyme NAD making the bioelectrodes more robust.

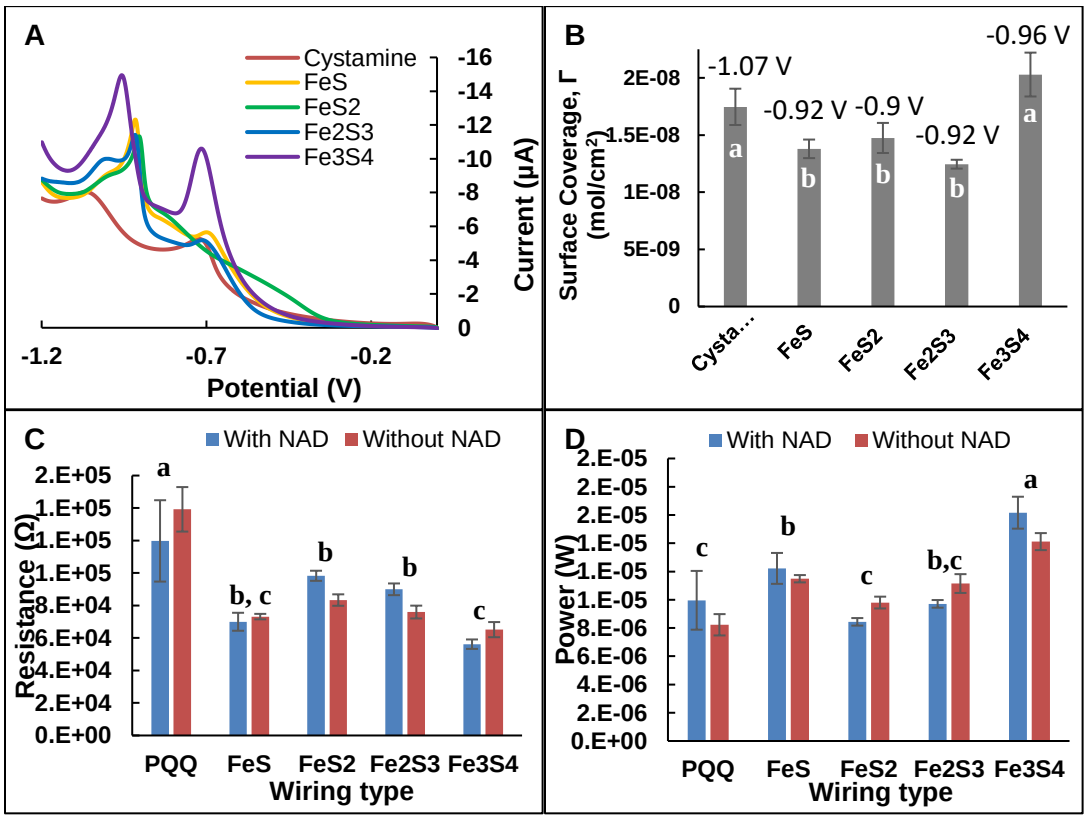

Figure 2.5 Linear sweep voltammetry to analyze surface coverage: (A) Reductive desorption of Fe-S in 50 mM KOH, at a sweep rate of 50 mV/s; (B) Comparison of the surface coverage observed for the Fe-S with the reductive desorption voltage for each molecule depicted on top of the corresponding bars; (C) Resistance ($V_{at\ Ip}/I_p$) for all molecules with and without NAD; (D) Power ($V_{at\ Ip} * I_p$) for all molecules with and without NAD. $V_{at\ Ip}$ is the anodic peak potential and I_p is the anodic peak current. Fe_3S_4 shows the highest surface coverage, lowest resistance, and highest binding affinity to the electrode surface. Different letters indicate significant difference among the sample response means.

2.4. Conclusions

In summary, the capability of simple inorganic iron-sulfur clusters viz. FeS, FeS_2, Fe_2S_3, and Fe_3S_4 to enable direct electrical communication between NAD-GDH and a gold surface was established. Iron-sulfur based molecular wires showed enhanced electron transfer between the enzyme active site and the base electrode as compared to the complex conventional PQQ-based wiring system that capitalizes on the formation of covalent bonds between molecules. The Fe_2S_3-based glucose anode consistently generated higher current densities at all glucose concentrations compared to other tested relays. When compared for performance, Fe-S-based glucose anodes were more sensitive with lower limit of detection (with the exception of Fe_3S_4-based anode) when compared with the PQQ-based glucose anode. FeS-based glucose anode showed highest sensitivity and lowest limit of detection surpassing the other iron-sulfur based anodes for sensing applications. The remarkable improvement in electron transfer and performance is likely a result of the ability of iron-sulfur clusters to strongly coordinate the enzyme system while aligning the active site with the supporting electrodes, providing a shorter unfettered electron travel path, thereby facilitating reduced resistance (direct electron transfer). It should also be noted that Fe_3S_4 had the highest surface coverage, lowest resistance, and highest binding affinity to the electrode surface along with next best sensitivity indicating to be an equally robust relay. Despite the advantages, the iron-sulfur based molecular wires are limited by the inability of the clusters to be uniformly dispersed in the solvent for optimal self-assembly. This work essentially demonstrates the possibility of using different iron sulfur clusters for electronically wiring redox

enzymes to electrode surfaces, thereby laying the foundation for the next step which is to optimize the iron-sulfur based wired enzyme electrodes and show their application in bioelectronic systems such as biosensors and biofuel cells. Thus, by studying the possibility of using inorganic iron-sulfur clusters to immobilize redox enzymes onto electrode surfaces, we move a step closer to mimic the biological electron transport chain ex-vivo and in turn, use such clusters to improve the charge transport in bioelectronic devices.

3. EVALUATION OF THE EFFECTIVENESS OF USING INORGANIC AND ORGANIC IRON-SULFUR CLUSTERS TO WIRE SELECT COENZYMES ONTO GOLD ELECTRODES

3.1. Introduction

There is a growing interest in developing redox enzyme-based bioelectronics for biosensing and bio-power generation due to the ever-rising demand for detection, diagnostics, and clean energy. A fundamental requirement of any redox enzyme-based bioelectronic system is the existence of molecular coupling that allows electrical communication between the enzymes and the electrode support. Direct electrical communication between the electrode surface and the active site is often inhibited due to the insulation effect of the protein matrix(Heller, 1992), and thus special techniques are required to realize proper electrical contact.

Electron transfer theory describes the dependence of all living organisms on electron transport to facilitate molecular transformations and fundamental biological processes. The electron transport by proteins is usually facilitated by redox coenzymes, such as NADP/NAD, PQQ, FAD, and CoQ_{10}, which are molecules bound to enzymes. (Gray & Ellis Jr, 1994; Munro & McLean, 2013)

The redox coenzymes at the enzyme active site(s) display a natural resistance to switching between oxidation and reduction reactions (generally referred to as activation overpotential) further hindering the use of enzymes for self-powered bioelectronics

applications like biosensors and bio-fuel cells. (Chenault & Whitesides, 1987; Mahadevan et al., 2014)

Several methods to electrically connect enzymes with electrode supports have been developed, including inventive approaches to align and orient the enzymes on the electrode surface to facilitate direct electrical communication. (Katz et al., 2004; Patolsky et al., 2004; I. Willner et al., 1996; Xiao et al., 2003) The ability of inorganic iron-sulfur clusters to anchor NAD-dependent oxidoreductases to an Au electrode surface was recently reported (Mahadevan & Fernando, 2017, 2018; Mahadevan et al., 2016). This work was inspired due to the electron mediating role of iron-sulfur complexes in biological electron transport chain(s) (Lill et al., 1999) and the reported performance of iron-sulfur protein derivatives in bio-electrochemical applications.(Beinert et al., 1997; Beinert & Kiley, 1999; Fontecave, 2006; Lill, 2009)

Although it was confirmed that a link can be formed between the NAD coenzyme and the Au surface ex vivo using the [Fe-S] precursors, it is unknown whether other coenzymes will respond positively to iron-sulfur mediation. (Mahadevan & Fernando, 2018) It is important to test this ability since there are four identified coenzymes (NADP, FAD, PQQ, and CoQ_{10}) that participate in biological electron transfer reactions that are of interest for ex vivo bioelectronics applications. The possibility of attaching the above coenzymes to a metal support using select inorganic and organic iron sulfur complexes and once attached, the resulting molecular interactions and electron transport properties is described.

3.2. Materials and methods

3.2.1. Reagents and apparatus

NAD, NADP, FAD, PQQ, CoQ_{10}, FeS, FeS_2, ferredoxin, 11-Mercaptoundecanoic acid (MUA) were purchased from Sigma-Aldrich, USA. Fe_2S_3 and Fe_3S_4 were obtained from 3B Scientific Corporation. 1-Ethyl-3-(3-dimethylaminopropyl) carbodiimide (EDC) and N-Hydroxysuccinimide (NHS) were purchased from Thermo Fisher Scientific. NAD, NADP, and FAD were prepared in a 0.1 M phosphate buffer (pH = 7). PQQ was prepared using a 0.1 M HEPES buffer (pH 7.2), and CoQ_{10} was prepared in acetone. Molecular-biology-grade water obtained from Sigma-Aldrich were used to prepare all the aqueous-based solutions and for rinsing/cleaning purposes throughout this study. Two-millimeter Au-disk working electrodes, Ag/AgCl reference electrodes, Pt auxiliary electrodes and an Au electrode polishing kit were purchased from CH Instruments Inc. All electrochemical experiments were carried out in an electrochemical cell set up using a C3 cell stand from BASi. A CHI8003D potentiostat from CH Instruments, Inc. was used for electrochemical measurements. 1 cm x 1 cm 100 nm Au-coated silicon wafer chips, obtained from Platypus Technologies, were used for SIMS analysis.

3.2.2. Au-[Fe-S]-[Coenzyme] electrode preparation

First, the Au working electrodes of 0.031 cm^2 were polished according to previously described methods and rinsed thoroughly with pure water. (Mahadevan & Fernando, 2018) Five different coenzymes were immobilized on the Au surface via

inorganic and organic [Fe-S] molecular wires by layer-by-layer self-assembly using the dip-coating method. For fabrication of the inorganic [Fe-S]-[coenzyme] electrodes, the clean Au electrodes were first dipped into 0.3 M FeS/FeS_2/Fe_2S_3/Fe_3S_4 prepared in ethanol for 4 hrs. The [Fe-S]-tethered Au electrodes will then be immersed in 1 mM of the coenzyme (NADP, FAD, PQQ, CoQ_{10}, and NAD) solution for 4 hrs. Similarly, for the organic [Fe-S]-[coenzyme] electrodes, the clean Au electrode was first immersed in the 30 mM MUA in ethanol for 1 hr, followed by rinsing off the residual MUA molecules with ethanol. Then MUA-functionalized Au electrode was dipped in 0.1 M HEPES buffer (pH 7.2) containing 5 mM EDC and 2.5 mM NHS for 1 hr to activate the COOH-terminated group of MUA. Subsequently, 0.1 mg/mL Fdx in Tris-HCl buffer (pH 7.3) was added onto the activated MUA monolayer for 2 hrs; it was then rinsed with distilled water. The Fdx-functionalized Au electrodes were then immersed in 1 mM of coenzyme solutions for 4 Hrs. (Note - After every successive dipping step, the monolayer-functionalized Au electrodes were thoroughly rinsed with water unless mentioned otherwise.)

3.2.3. Secondary ion mass spectrometry (SIMS)

SIMS was used to verify the presence of FeS and FeS-NAD on the surface of Au, and compute the coverage of the SAMs of FeS and NAD and explore the bonding between NAD and FeS. The experiments were run with a custom-built cluster-SIMS instrument consisting of C_{60} effusion source. C_{60} source is used for impacts on the front side of the bulk target at an angle of incidence of 25° from normal. The secondary ions

are emitted/detected in the reflection direction. The SIMS instrument is equipped with a 1.2 m linear time-of-flight, ToF, mass spectrometer, and an electron emission microscope, EEM (Eller, Verkhoturov, Della-Negra, & Schweikert, 2013; S. Verkhoturov, Eller, Rickman, Della-Negra, & Schweikert, 2009). The EEM was used to detect secondary electrons for the ToF start signal. The secondary electrons being detected as a magnified electron image are used for "electron collimator" of the bombarded area.

The data were acquired at the level of individual 50 keV C_{60} impacts with a repetition rate of 1000 impacts/s. This event-by-event bombardment-detection mode allows the selection of specific impacts, in the present case those involving FeS SAM or NAD (S. V. Verkhoturov et al., 2015) at the exclusion of signals from the uncoated Au support. A detailed description of the components and data acquisition processing scheme can be found elsewhere (Eller et al., 2013).

Secondary ions emitted/detected via a single projectile impact are collected as an individual mass spectrum. The number of individual mass spectra is ~10^7. They are collected from the area of Ø200 μm. The sum of all mass spectra, (called total mass spectrum) corresponds to the regular mass spectrum measured in the case of regular analysis by commercial SIMS. This technique has previously been used for analysis of self-assembled or self-organized organic molecules (S. Verkhoturov et al., 2001).

3.2.4. Fourier-transform infrared spectroscopy (FTIR)

FeS powder was mixed with 1 mM NAD and left undisturbed for 4 hours. The NAD was discarded and the mixture was dried in a vacuum dryer for a week prior to testing. A 5 % w/w sample was made by grinding the dried FeS-NAD mixture with KBr, and compressed into a thin pellet. Thermo Scientific NICOLET IR100 FTIR spectrophotometer was used to record spectra over a wavenumber region between 3,800 to 2,600 cm^{-1} and, 2,200 to 1,300 cm^{-1}.

3.2.5. Docking simulations

Autodock VINA which is a molecular docking tool was used to find binding modes of the coenzymes with the [Fe-S].

3.2.6. Electrochemical analyses

The electrochemical studies were conducted using the conventional three-electrode system (i.e., enzymatic working electrode, Pt counter electrode, and Ag/AgCl reference electrode) placed in an electrochemical cell containing 10 mL of the carrier electrolyte at room temperature.

3.2.6.1. Ferricyanide/ferrocyanide-voltammetry

Cyclic voltammetry was performed in the presence of ferricyanide/ferrocyanide ($Fe(CN)_6^{3-/4-}$) redox couple to confirm multi-layer SAM formation on the Au electrode surface. After functionalizing with molecular wires, the Au electrodes were scanned in

0.01 M potassium ferricyanide with 0.1 M KNO_3 from − 0.8 V to + 0.8 V, at a scan rate of 50 mVs^{-1}. Bare Au electrode was used as the control electrode in this study.

3.2.6.2. Electrode kinetics

The kinetics of [Fe-S]-coenzyme-functionalized Au electrodes were investigated using the same electrochemical setup and potential window as above, but varying the scan rates from 10 mVs^{-1} to 150 mVs^{-1}**.**

3.2.6.3. Reductive desorption

Linear sweep voltammetry (LSV) was used to measure surface coverage of the [Fe-S] and the coenzymes on Au electrode. The [Fe-S] and [Fe-S]-[coenzyme]-functionalized Au electrodes were subjected to a potential sweep in a 10 mL 50 mM KOH solution from 0 V to −1.2 V, i.e., from potentials at which no reactions happen to potentials where reductive-desorption of the monolayers occur.

3.2.7. Statistical analysis

All the studies were conducted in three replications. Analysis was done using JMP pro 14 (Version 14.0.1, SAS Institute Inc., Cary, NC) with Analysis of Variance (ANOVA). Post Hoc test (Student's t test or Tukey-Kramer HSD) was used to compare treatments means. Significance levels were defined using $p < 0.05$.

3.3. Results and discussion

3.3.1. Verifying the self-assembly of [Fe-S] and coenzymes on Au

The formation of individual SAMs of [Fe-S] and coenzymes on Au electrodes was verified using cyclic voltammograms (CVs) obtained by applying a potential sweep on the modified electrodes placed in potassium ferricyanide solution, see Figure 3.1. Consecutive drops in peak currents (I_p) and growing of peak widths were observed in the $Fe(CN)_6^{3-/4-}$ CVs, after functionalizing the Au electrodes with [Fe-S] and coenzymes. The drop in I_p with the addition of consecutive monolayers was a result of resistance to electron transport kinetics caused by the formation of closely packed assemblages on the conductive Au surface. (Dowdy & Leopold, 2010) The monolayers of coenzymes have the lower currents and wider peaks when compared with that of the [Fe-S] due to their relatively larger structures and lower conductivity. Thus, the stepwise drop in I_p after each immersion and widening of peaks confirms the formation of successive SAMs of [Fe-S] and coenzymes on the Au electrodes. (Mahadevan et al., 2016; Mahadevan et al., 2015)

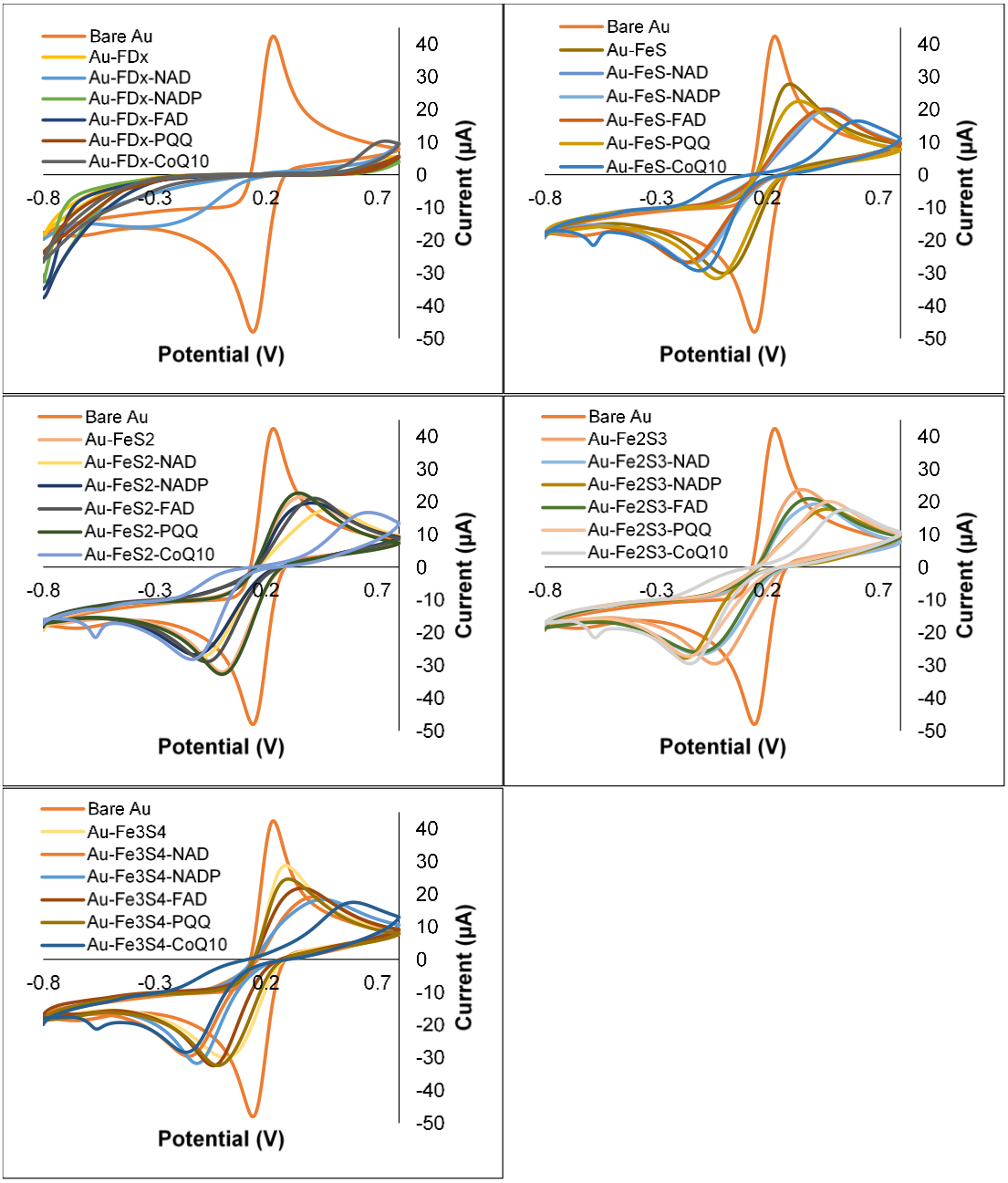

Figure 3.1 CV scans of Au-[Fe-S] / Au-[Fe-S]-[coenzyme] electrodes conducted in 0.01 M potassium ferricyanide with 0.1 M KNO_3 at a scan rate of 50 mV/s vs. Ag/AgCl reference electrode. Formation of each layer was verified via reduction of I_p after addition of each layer.

3.3.1.1. Surface characterization of Au-FeS-NAD interaction via SIMS

To get a general idea of how the [Fe-S] interact with the coenzymes and the Au surface, a SIMS analysis was performed to obtain the total mass spectra of FeS and FeS+NAD on Au, see Figure 3.2 A&B. The mass spectra of the "FeS on Au" sample (blue) contain characteristic peaks of FeS fragments: S^-, SH^-, FH^-, AuS^-, AuSH-, AuS_2H^-, $AuFeS^-$. The mass spectra of "NAD + FeS on Au" sample (red) show additional ions from NAD: CN^-, $(Ade\text{-}H)^-$, $(Ade\text{-}CNH)^-$, PO_2^-, PO_3^-, $AuCN^-$, AuSCN. It should be noted that the NAD molecule undergoes fragmentation via impact, thus the intact molecular ion of NAD is not present in the mass spectrum. However, the mass spectrum consists of the fragmentation pattern of NAD.

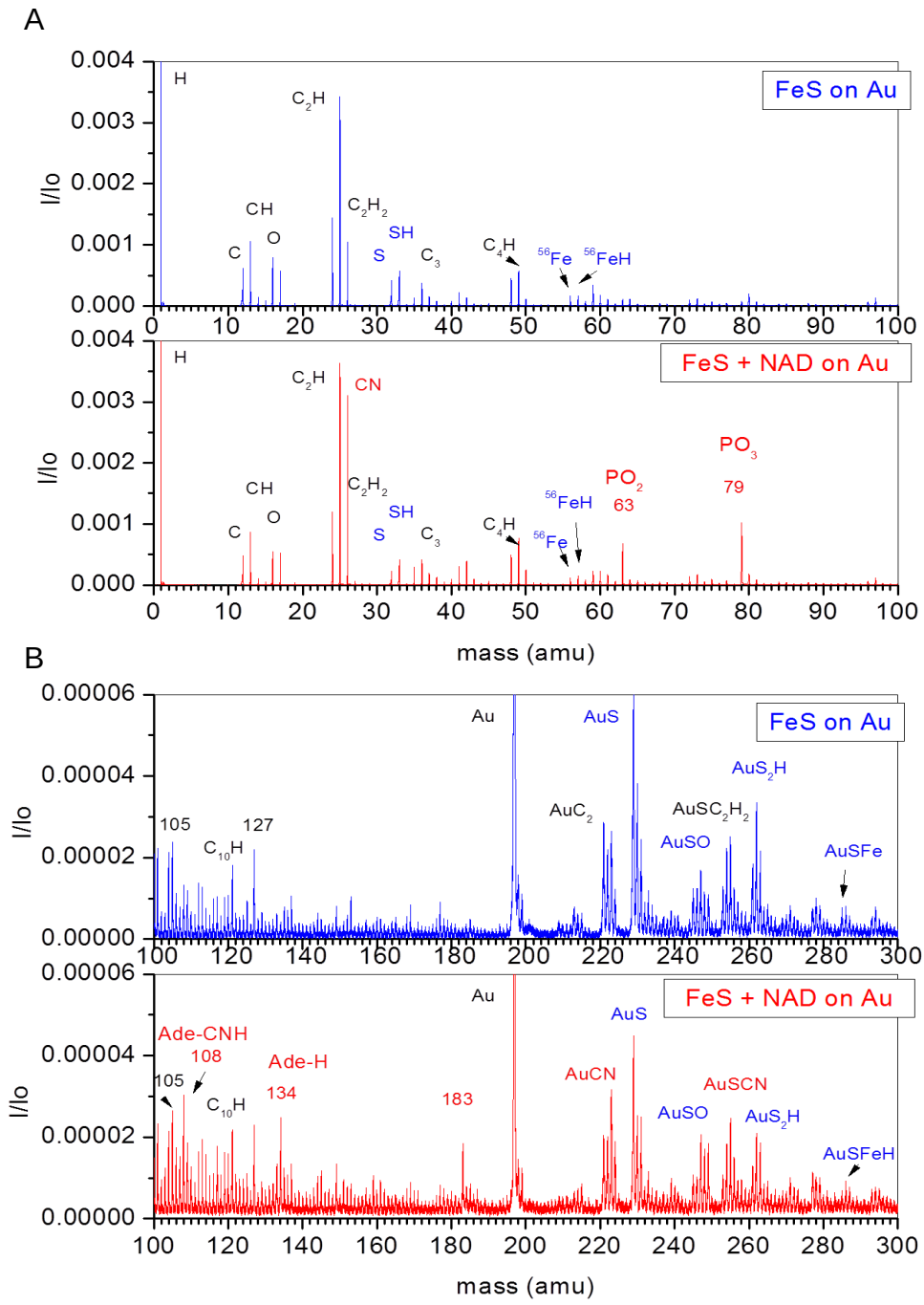

Figure 3.2 Mass spectra of the samples SAM FeS on Au (top, blue) and NAD deposited at SAM FeS (red, bottom). (A) Mass spectra for mass range 0-100 amu, and (B) Mass spectra for mass range 100-300 amu. Presence of additional ions: CN^-, $(Ade\text{-}H)^-$, $(Ade\text{-}CNH)^-$, PO_2^-, PO_3^-, $AuCN^-$, and AuSCN on the 'FeS+NAD on Au' confirms the presence of NAD and FeS on Au.

Cluster SIMS works well for organic molecular samples; usually mass spectra contain intact molecular ions. Unfortunately, the nucleotides, or similar molecules are easily fragmented via projectile impacts, by breaking of the bonds between phosphate group, ribose and nitrogenous base.(D. S. Verkhoturov, Geng, Verkhoturov, Kim, & Schweikert, 2016) The mass spectrum contains ions related to phosphate groups and adenine. Ribose and nicotinamide have low ionization probability to form negative ions, thus the peaks of their ions are insufficient in the spectrum. Important evidence is the presence of deprotonated intact molecular ion of adenine, $(Ade\text{-}H)^-$. It indicates, that adenine does not participate in NAD binding to FeS (discussion below).

As was mentioned above, the method of event-by-event bombardment-detection allows the selection of specific impacts, in the present case those involving NAD. The method is illustrated in Figure 3.S1.

The SIMS method used allows the selection of individual mass spectra. For instance, the selected individual mass spectra containing PO_3^- are attributed to the impacts on NAD surface, solely. The sum of these mass spectra represents the mass spectrum of the NAD surface. This spectrum is shown in Figure 3.3A&B. The spectrum of NAD consists of ions of NAD fragments, the intensities of which dominate when compared to the intensities of Au and FeS related ions. This spectrum contains information about the surface coverage of NAD (discussion below).

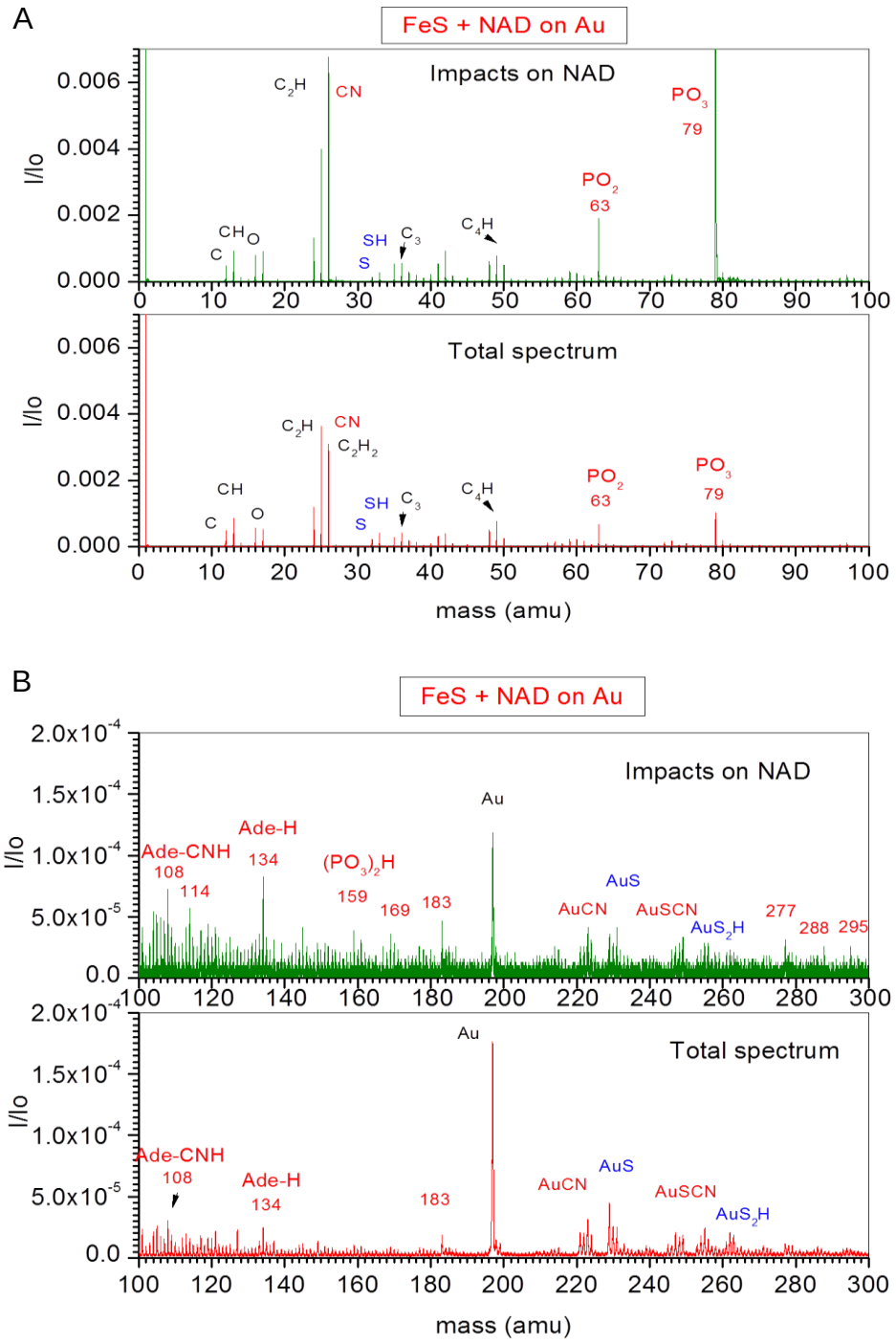

Figure 3.3 Mass spectra of SAM FeS+NAD on Au used for determining surface coverage. Total mass spectrum of sample SAM FeS+NAD on Au (bottom, red) and mass spectrum of NAD surface (top, green). Mass spectrum of NAD surface is the sum of individual spectra containing PO_3^- ions. (A) Mass spectra for mass range 0-100 amu, and (B) Mass spectra for mass range 100-300 amu.

3.3.1.2. Coverage test

The coverage of the NAD layer was tested using the event-by-event bombardment-detection mode. (S. Verkhoturov et al., 2009) The method allows the detection of co-emitted ions (e.g. PO_3^- and $(Ade\text{-}H)^-$) and calculation of the correlation coefficients of co-emission (Rickman, Verkhoturov, Parilis, & Schweikert, 2004):

$$K_n = \frac{Y_{PO3,,Ade}}{Y_{PO3}Y_{Ade}} \quad 3.1$$

where Y_{PO3} and Y_{Ade} are the yields (number of emitted ions which are detected per projectile impact) of $(Ade\text{-}H)^-$ ions and PO_3^- ions, $Y_{PO3,Ade}$ is the yield of co-emitted $(Ade\text{-}H)^-$ and PO_3^- ions.

For a homogeneous surface, the ions are emitted independently from any point of the impacting area [6]. Thus, for a homogeneous surface, $K_n = 1$.

The measured yields are given by:

$$Y_{Ade} = I_{Ade}/N_{eff} \quad 3.2$$

$$Y_{PO3} = I_{PO3}/N_{eff} \quad 3.3$$

$$Y_{PO3,Ade} = I_{PO3,Ade}/N_{eff} \quad 3.4$$

where I_{Ade} is the number of detected $(Ade\text{-}H)^-$, I_{PO3} is the number of detected PO_3^-, $I_{PO3,Ade,}$ is the number of detected co-emitted ions, and N_{eff} is the effective number of impacts on the area of the target, which is covered by the molecular layer.

Using the expressions (1-4), one can obtain N_{eff}:

$$N_{eff} = \frac{I_{PO3}I_{Ade}}{I_{PO3,Ade}} \quad 3.5$$

If the molecular coverage of the surface is incomplete, the effective number of impacts is less than the total number of impacts, N_0:

$$N_{eff} < N_0, \quad 3.6$$

To validate the quality of the NAD layer, the degree of coverage can be written in the form as:

$$\alpha\ (100\%) = \frac{N_{eff}}{N_0} 100\% \quad 3.7$$

For the case of "FeS SAM + NAD on Au" sample, the degree of coverage, α, of NAD, measured for the different pair of detected ions is presented in the Table 3.1.

Table 3.1 Degree of coverage, α, measured for the sample "FeS SAM +NAD on Au". The standard deviation is better than ±5% for the experimental α.

	PO_3, PO_2	**PO_3, Ade-H**	**PO_3, CN**	**Average**
α (degree of coverage) of NAD	46.6%	49.3%	45.3%	47%

The NAD degree of coverage was calculated to be 47% while for FeS, it was 96% (co-emitted ions of S and AuS). Important evidence is the presence of deprotonated intact molecular ion of adenine, $(Ade\text{-}H)^-$. It indicates that adenine does not participate in NAD binding to FeS. The same conclusion can be extrapolated on nicotinamide, which has a similar active NH_2 group. However, nicotinamide has a carbonyl group, which can be a binding site. The presence in the spectrum of $AuSCN^-$ ion may support this hypothesis. The absence of ions consisting of S, P and O (e.g. $(PSO_2)_n$) may indicate that the phosphate group does not participate as a binding site. Generally, the bonding between FeS and NAD should be a subject of further discussion.

3.3.1.3. FTIR characterization of FeS-NAD interaction

The FTIR spectra of FeS (control 1), NAD (control 2), and FeS-NAD complex (Figure 3.4 A&B) were obtained to further examine the nature of the association between the FeS and the NAD.

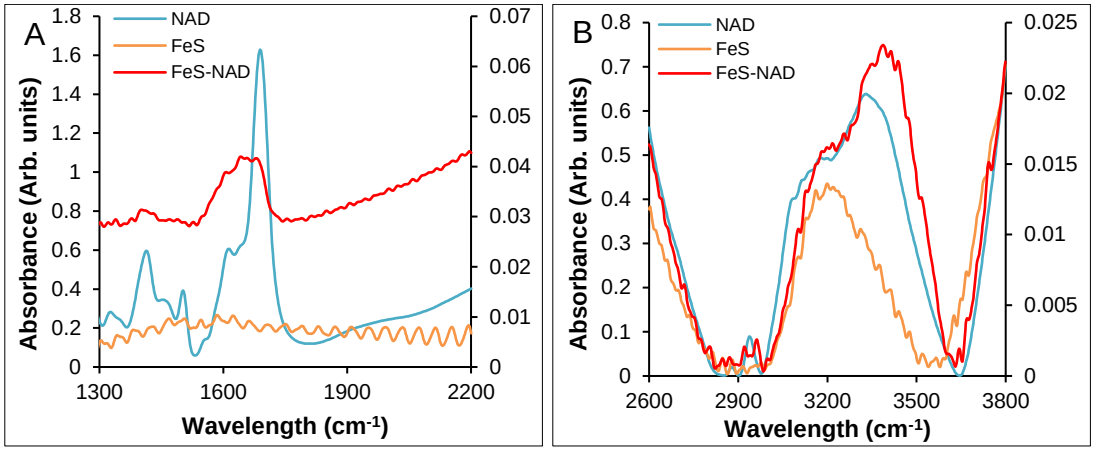

Figure 3.4 Fourier transform infrared (FTIR) spectra of NAD (control 1), FeS (control 2), and FeS-NAD complex in the regions (A) 2,200 to 1,300 cm^{-1} and, (B) 3,800 to 2,600 cm^{-1}, confirms the formation of iron carbonyl bond.

The 9H-adenine (mode description – dC_2H, $n(C_4C_5)$, $n(C_6N_6)$, $n(C_4N_9)$, dN_6H, dC_8H, dN_9H) stretch appears at 1,413 cm^{-1} (Figure 3.4 A) on both NAD and FeS-NAD spectra. (van Zundert et al., 2011) The appearance of the C=O stretch band (1,690 – 1,640 cm^{-1}) and the NH_2 scissors deformation band (1,616 cm^{-1}) of the unsubstituted amide (-CO-NH_2) can be seen on both, NAD and FeS-NAD spectra (Figure 4A).(Lin-Vien, Colthup, Fateley, & Grasselli, 1991) The relatively weakened intensity of C=O stretch on the FeS-NAD spectrum likely indicates C=O of NAD binding with the Fe of FeS.

Similarly, the asymmetric and symmetric NH_2 stretch of the unsubstituted amide appear near 3350 cm^{-1} and 3180 cm^{-1} on the NAD and the FeS-NAD spectra (Figure 3.4

B). (Lin-Vien et al., 1991) Above observations confirm the presence of NAD on the FeS-NAD sample and supports the formation of iron carbonyl bonds as indicated in the SIMS results.

3.3.1.4. Elucidating Fe-S and coenzyme interactions via docking simulations

To obtain better insights on binding interactions between [Fe-S] and coenzymes (NADP, FAD, PQQ, CoQ10 and NAD), to predict the strength of association or binding affinity and the nature of association between the two systems, in-silico docking simulations were performed. Docking was performed using the virtual screening program Autodock vina. Top binding conformation, binding energy and interaction information of FeS-NAD are presented in Figure 3.5 A. It is evident that Fe interacted with oxygen atoms of NAD. Also, it was noted that simulations predicted the binding affinities to change in the order of Fe_3S_4>Fe_2S_3>FeS_2>FeS regardless of the coenzyme (Figure 3.5 B-F). Further information on all the other coenzymes and iron-sulfur complexes are presented under supplementary information in Appendix A.

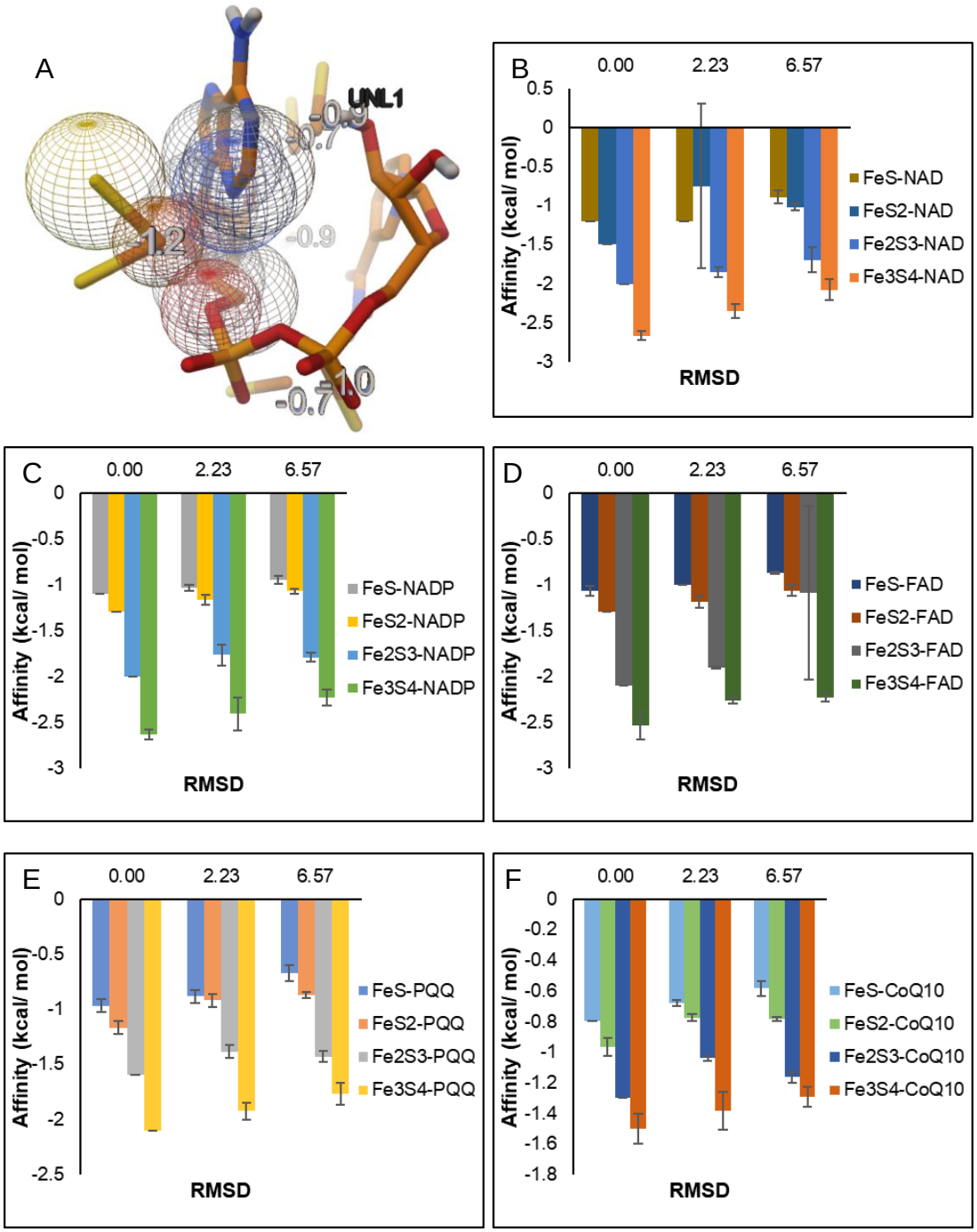

Figure 3.5 (A) Three-dimensional interactions between FeS and NAD using Autodock Vina. It can be seen that the Fe (orange) primarily interacting with oxygen atoms of NAD; (B-F) Binding affinities of [Fe-S]-{coenzyme] predicted by simulations, shows Fe_3S_4 having the highest binding affinity on Au.

3.3.2. Electrochemical performance

3.3.2.1. Surface coverage, resistance and power of the Fe-S and Fe-S-Coenzyme electrodes

Reductive desorption by LSV was used to determine the surface coverage, resistance and desorption power of the [Fe-S]/[Fe-S]-[coenzymes] from Au surface (see Figure 3.6 A-C). The concept and details of the method and relevant calculations are described elsewhere. (Mahadevan & Fernando, 2018)

Figure 3.6 A shows that FDx had the highest surface coverage on Au, which is expected due to its macromolecular structure covering a larger surface area. FDx imparted the highest resistance, likely due to the relatively low conductivity of the long wiring (comprising of MUA, EDC and NHS) it requires to attach onto the Au surface (Braun et al., 1998; Scheibel et al., 2003). The lowest power required to desorb from Au surface was also by FDx. FDx is a widely studied relay for wiring enzymes on bioelectrodes. (Léger & Bertrand, 2008; Madoz-Gurpide et al., 2000) This study indicated the shortcoming of using such large organic structures as redox relays to wire redox coenzymes for electron transport.

Among the inorganic [Fe-S], Fe_3S_4 and FeS displayed the ideal combination of characteristics for a redox relay (or a molecular wire to transfer electrons to and from the redox coenzyme) – a high surface coverage, a low resistance, and a high power requirement for desorption. Fe_3S_4 which had the next highest surface coverage on Au, also imparted the lowest resistance, and required the highest power to desorb from the Au surface. FeS despite showing a low surface coverage, exhibited the next lowest

resistance and next highest desorption power requirement. The low surface coverage of FeS is likely due to is simpler molecular structure.

Overall, the addition of a coenzyme monolayer on the [Fe-S] monolayers did not significantly impact the surface coverage, resistance, or the desorption power significantly. The observations made in this study proved that the inorganic Fe_3S_4 and FeS strongly bind to the coenzymes, anchoring strongly on the Au surface while improving charge transfer properties of the bioelectrodes.

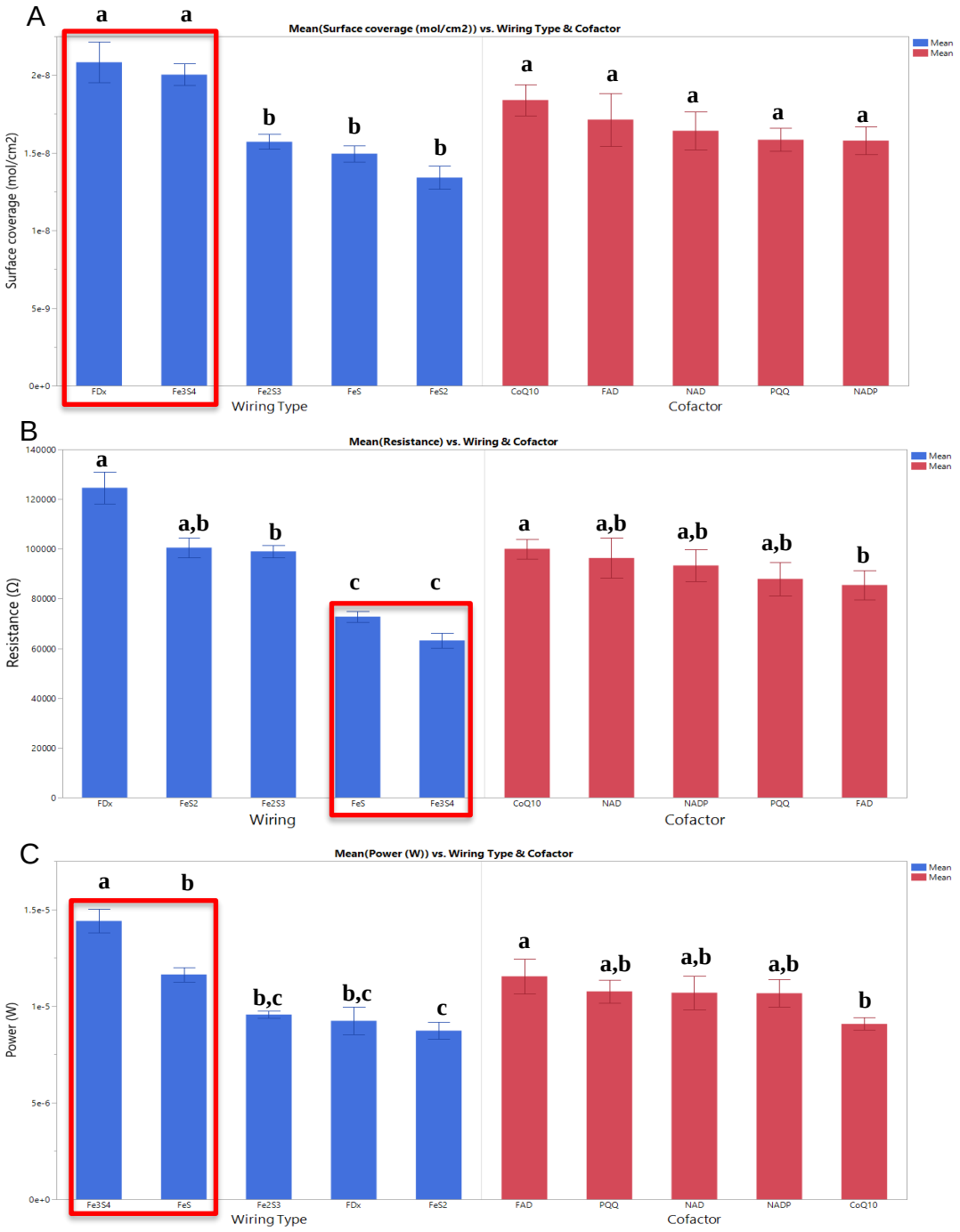

Figure 3.6 Reductive desorption using linear sweep voltammetry: (A) Surface coverage, and (B) Resistance of the [Fe-S] and [Fe-S]-[coenzymes] modified Au electrodes; and (C) Power required to desorb the [Fe-S] and [Fe-S]-[coenzymes] monolayers from Au surface. Fe_3S_4 showed the highest surface coverage, lowest resistance, and highest desorption power requirement when used to wire the coenzymes onto the Au surface. Different letters indicate significant difference among the sample response means.

3.3.2.2. Charge transfer and kinetics

The anodic peak current (I_{pa}) variation of different bioelectrodes with each of the monolayers are presented in Figure 3.7. It clear that the I_{pa} observed on all the inorganic [Fe-S]-based electrodes were higher as compared to the FDx based electrodes. It also evident that Fe_3S_4 and FeS displayed the highest peak currents among all the [Fe-S]-based electrodes.

The type of controlled processes that occur at the modified Au electrode was elucidated by studying the effects of the scan rate (10 mVs^{-1} to 150 mVs^{-1}) on the ferricyanide peak current, as shown in Figure 3.S2. The CVs show the changes in the anodic and cathodic peak currents of the $Fe(CN)_6^{3-/4-}$ redox peaks. The anodic and cathodic peak currents for $Fe(CN)_6^{3-/4-}$ increased linearly with increasing scan rate, indicating that the electrode reaction of ferricyanide was diffusion-controlled. Reactions under diffusion-controlled (or diffusion-limited) conditions occur so quickly that the reaction rate is determined by the rate of transport of the reactants through the reaction solution (Atkins, 1998; Bagotsky, 2005). This study thus further proves the redox mediation ability of the inorganic and organic [Fe-S] to efficiently shuttle electrons between the coenzymes and the Au electrode; and it proves that the layer of coenzyme-immobilized molecular wires is permeable to ferricyanide for a redox reaction.

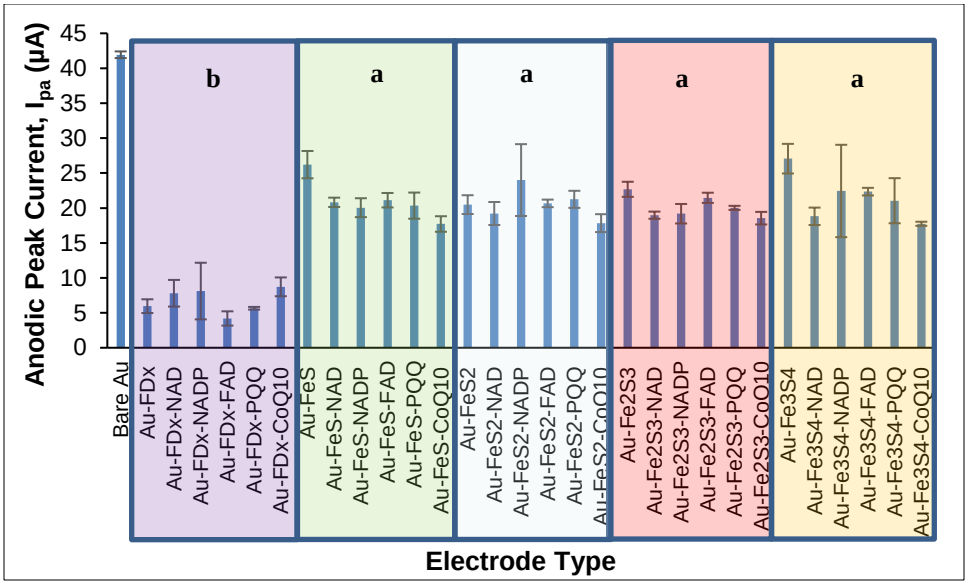

Figure 3.7 I_{pa} derived from the CV scans of Au-[Fe-S] / Au-[Fe-S]-[coenzyme] electrodes conducted in 0.01 M potassium ferricyanide with 0.1 M KNO_3 at a scan rate of 50 mV/s vs. Ag/AgCl reference electrode shows that all inorganic [Fe-S] forms allowed higher I_{pa} values as compared to organic FDx while Fe_3S_4 displaying the highest I_{pa} values. Different letters indicate significant difference among the sample response means.

3.4. Conclusions

Electrochemical experiments confirmed the effectiveness of using select inorganic (FeS, FeS_2, Fe_2S_3, and Fe_3S_4) and organic (ferredoxin) iron-sulfur complexes, as molecular wires to tether coenzymes NADP, FAD, PQQ, CoQ10 and NAD (control) on Au electrodes. Based on SIMS, the presence of NAD on the surface of "FeS on Au" was verified. The NAD degree of coverage was 47% while the degree of coverage of FeS on Au was 96%. The characteristic ions after introduction of NAD to Au-FeS were identified to be $(Ade\text{-}H)^-$, $(Ade\text{-}CNH)^-$, CN^-, $AuCN^-$, $AuSCN^-$, PO_2^-, PO_3^-., and $(PO_3)_2H^-$. The presence of deprotonated intact molecular ion of adenine, $(Ade\text{-}H)^-$ indicate that neither adenine nor nicotinamide participate in NAD binding to FeS via active NH_2 groups. However, nicotinamide has a carbonyl group, which can be a binding site – and

this was further verified via FTIR and confirmed using docking simulations. Anodic and cathodic peak currents of all the [Fe-S] electrodes linearly increased with increasing scan rates indicating that the electrode kinetics are controlled by diffusion. Inorganic [Fe-S] electrodes showed a notable enhancement in peak currents likely due to the simpler structures and conductive nature as opposed to the FDx-based electrodes. Among the inorganic [Fe-S], Fe_3S_4 had the highest surface coverage, lowest resistance, and highest desorption power requirement along with high binding affinities when used to wire the coenzymes onto the Au surface. Based on the findings, an approach to using inorganic iron-sulfur moieties to effectively anchor NAD/NADP, FAD, PQQ, and CoQ_{10} redox coenzymes to gold electrodes was established.

4. IDENTIFYING AND TESTING METHODS TO STUDY BIOSENSOR PERFORMANCE OF ENZYME ELECTRODES USING AN ESTABLISHED [FE-S]-COENZYME-ENZYME SYSTEM (I.E. AU-FES-NAD-GLYCEROL-DEHYDROGENASE ANODE)[*]

4.1. Introduction

An intensive interest in glycerol determination exists due to its extensive utility in the medical, food and biofuels industries. The conventional methods used for glycerol detection are expensive, complex, and often lack enough specificity. This issue has led to a quest for an accurate, rapid, and inexpensive method for glycerol quantification. One of the sought-after methods for analyte detection is biosensing. Enzymatic electrochemical biosensors especially have gathered considerable attention due to their simplicity, accuracy, high selectivity, and speediness in rendering results. Enzymatic electrochemical biosensors are analytical devices that integrate an enzyme as the active sensing element within an electrochemical transducing system (Ronkainen, Halsall, & Heineman, 2010). In enzymatic electrochemical biosensors, the electrical signal generated as a result of an electrochemical redox reaction that occurs at the active site is harnessed to produce inferences for the analyte concentrations. The dependency of the sensing system on the resultant electrical signals make electron-transfer between an

[*] Reprinted with permission from "An improved glycerol biosensor with an Au-FeS-NAD-glycerol-dehydrogenase anode." by Mahadevan, A. and Fernando, S., 2017. Biosensors and Bioelectronics, 92, pp.417-424, Copyright [2017] by Elsevier B.V.

active site of the immobilized enzyme and the electrode surface a key factor that decides the efficiency of the biosensor (Marcus & Sutin, 1985).

Enzymes that allow the electrochemical cell, i.e., the core of the sensing system, to operate must be "immobilized" near the anode and cathode in order to work properly. If not immobilized, these enzymes will diffuse into the cell's electrolyte, and most of the liberated electrons will not reach the electrodes, thus compromising its effectiveness. The overall effectiveness of all enzyme-based electrochemical devices is dependent on the ability of the molecules that attach enzymes to the electrode to successfully harvest and transport the charges from the outer oxidizing point (enzyme active-site) to the inner electrode surface.

When these enzymes are wired to electrodes (outside a living cell or ex vivo), their ability to harness these electrons (or electricity) diminishes significantly due to the thermodynamic limitations that are associated with the coenzymes (essential for proper functioning of the enzyme). The common coenzymes, nicotinamide-adenine-dinucleotide (NAD) and Flavin-adenine-dinucleotide (FAD), are resistant to cyclic oxidation and reduction ex vivo, and they require special molecules known as electron mediators to help extract electrons from the coenzyme to transfer to the final target. Since known electron mediators do not have the correct combination of prosthetic groups to anchor the coenzyme from/at one end and the base electrode from/at the other, molecules with appropriate functional groups need to be introduced to the wiring scheme to fulfill the anchoring function. Figure 4.1A(a) depicts a commonly used conventional wiring scheme that comprises cystamine, pyrroloquinoline quinone (PQQ), and boronic

acid, to attach the NAD coenzyme-based apoenzyme onto a metal electrode for sensing and biofuel cell applications.

The outcome of such a long wiring scheme is high ohmic resistance, which leads to constrained electron transport (Johnston et al., 2007; Park et al., 1999; Reed et al., 1997), resulting in sensors with low sensitivity (Minteer et al., 2007; Reed et al., 1997; Riklin et al., 1995).

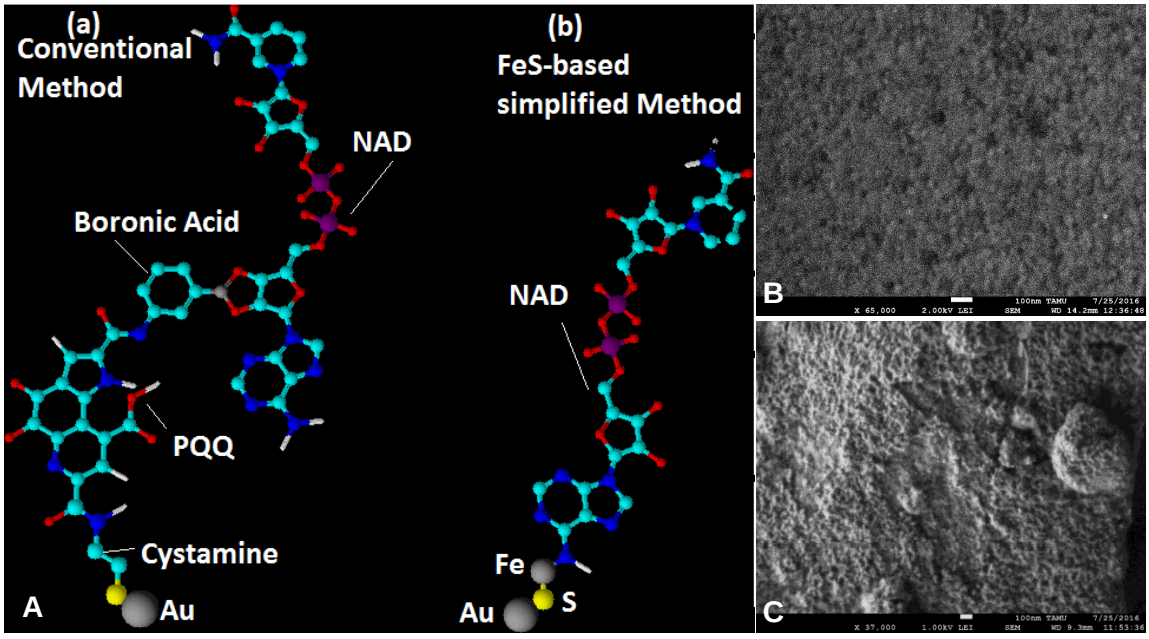

Figure 4.1 (A) A schematic of wiring systems. (a) Complex conventional wiring of the coenzyme NAD to a gold electrode using a series of molecules, including a cystamine linker, a PQQ mediator, and a phenyl boronic acid linker; (b) Simplified wiring of a NAD coenzyme directly onto the gold electrode by a multi-functional mediator, FeS; Surface morphology of (B) bare Au surface and (C) an enzyme immobilized Au surface examined via FE-SEM.

Interestingly, nature has found a way to circumvent overpotential (activation, transfer, and resistance overpotentials) and anchoring issues by using unique [Fe-S] clusters that have electron mediation properties (so as to cyclically reduce and oxidize between Fe^{2+}/Fe^{3+} while extracting electrons from the coenzyme molecule as soon as the

coenzyme is reduced and disposing of the electrons to the adjacent electron acceptor); a very short length to reduce the electron travel distance (thereby reducing the internal resistance of the conductor); and the correct prosthetic groups to anchor onto adjoining chemical moieties (sulfur that coordinates with metal centers (Graham & Dingman, 2006; Love et al., 2005; Mrksich et al., 1996; Tour et al., 1995; Zhong & Porter, 1994) and onto proteins with cysteinyl residues (Meyer, 2008) or iron that coordinates with the heterocyclic nitrogen atoms (Cline et al., 1985; Lavrenova et al., 1986; Marlin et al., 1999) such as those present in coenzymes and mitochondrial peptides).

The approach to improving electron transport in enzymatic electrodes ex vivo is to use iron-sulfur moieties (iron sulfides or [Fe-S] complexes) and directly attach the coenzyme-dependent redox enzyme systems onto the electrode, so that activation, transfer and resistance overpotentials are significantly reduced. The obstacle that prevents a replication of the core of the natural electron transport chain has been an inability to duplicate the functionality of iron-sulfur linker molecules ex vivo. Iron sulfides (and [Fe-S] complexes) are quite unstable in an aqueous environment, and all attempts to attach [Fe-S] complexes onto metal surfaces in an aqueous environment have thus far. This key knowledge gap was addressed through the breakthrough came as a result of performing an iron (II) sulfide (FeS) dissolution and attachment onto a gold electrode in a 100% ethanol environment (Figure 4.1A(b)) (Mahadevan et al., 2016).

The key objective of the current study was to develop a working glycerol biosensor fabricated via the novel iron-sulfur mediated molecular wiring scheme, then optimize it

and compare its sensing performance to those of a conventionally wired PQQ-based glycerol biosensor.

4.2. Materials and methods

4.2.1. Reagents and apparatus

NAD-dependent glycerol dehydrogenase from Cellulomonas sp. (EC.1.1.1.6), ß-nicotinamide adenine dinucleotide (NAD), glutaraldehyde, iron (II) sulfide (FeS), pyrroloquinoline quinone, cystamine dihydro chloride, 3-aminophenylboronic acid monohydrate, HEPES buffer, glycerol ≥99%, glucose and fructose were purchased from Sigma-Aldrich in the U.S. 1-Ethyl-3-(3-dimethylaminopropyl) carbodiimide (EDC) and N-Hydroxysuccinimide (NHS) were purchased form Thermo Fisher Scientific. A gold electrode polishing kit was purchased from CH Instruments, Inc. A 50 mM KOH solution made in 30 wt% H_2O_2 and 50mM KOH solution made in pure water were used in the gold cleaning procedure. FeS was suspended in ≥99.5% ethanol, and cystamine dihydro chloride was dissolved in pure water. ß-NAD, GlDH, and glutaraldehyde solutions were prepared in a 0.1 M phosphate buffer (pH = 7); PQQ and 3-aminophenylboronic acid solutions were prepared using 0.1 M HEPES buffer (pH 7.2) in the presence of 5 mM EDC and 2.5 mM NHS. Water containing the enzyme stimulants viz. $(NH_4)_2SO_4$ and $MnCl_2.4H_2O$ was used as the point of reference carrier electrolyte as described previously(Mahadevan et al., 2015). Molecular-biology-grade water (termed “pure water” in this paper) obtained from Sigma-Aldrich was used to

prepare all the aqueous-based solutions and for rinsing and cleaning throughout this study.

Two-millimeter size gold-disk working electrodes, Ag/AgCl reference electrodes, and Pt auxiliary electrodes were purchased from CH Instruments, Inc. All experiments were carried out in an electrochemical cell that was set up using a C3 cell stand from BASi. CHI8003D Potentiostat from CH Instruments, Inc. was used for electrochemical electrode cleaning and electrode testing methods.

4.2.2. Glycerol dehydrogenase electrode(s) fabrication

Two different glycerol oxidizing electrodes were fabricated, based on a FeS-based wiring system and a PQQ-based wiring system to tether the GlDH enzyme onto the gold electrode. A dip-coating method was used to fabricate the FeS-based and PQQ-based enzymatic biosensors applying the principle of layer-by-layer self-assembly. A gold (Álvarez-González et al.) working electrode cleaning procedure included – polishing Au electrodes using 1200 grit Carbimet disk (used occasionally to remove scratches); 1, 0.3, and 0.05 micron alumina in a sequence followed by sonication to remove alumina particles; dipping the Au electrodes in a 50 mM KOH solution made in 30 wt% H2O2 for 30 minutes, followed by rinsing with pure water; and finally, 5 cyclic voltammetry sweeps in the 50mM KOH solution made of pure water followed by thorough rinsing with pure water. For fabrication of FeS-based bioanode, the clean Au electrodes were first dipped into a 0.3 M FeS-in-ethanol solution for 2 Hrs. The FeS-tethered Au electrodes were immersed in 1 mM of ß-NAD for 2 Hrs after which, the

FeS-NAD-tethered Au electrodes were dipped in1 mg mL-1 of GlDH for 2 Hrs. The resulting FeS-NAD-GlDH functionalized electrodes were finally treated with 10% (v/v) glutaraldehyde for 20 min to crosslink and secure the protein (enzyme) layer. The PQQ-based bioanode was similarly fabricated by sequential dipping of the Au electrode in 0.1M cystamine dihydrochloride solution for 1 Hr, 3mM solution of PQQ for 2 Hrs, 1 mM 3-aminophenylboronic acid solution for 2 Hrs, 1 mM of ß-NAD solution for 2 Hrs, 1 mg.mL-1 GlDH for 2 Hrs and a final 20 Min treatment with 10% (v/v) glutaraldehyde. Note that, each sequential step was followed by a rinsing of the monolayer-tethered Au electrode with pure water. The surface morphology of the bare Au surface and the enzyme immobilized Au surface was examined using FE-SEM analysis (Figure 4.1 B&C).

4.2.3. Electrochemical measurements

Biosensor performance factors viz. sensitivity, detection limit, and response time were determined using dynamic constant potential amperometry (CPA). CPA for FeS, and PQQ- based electrodes was performed for glycerol detection under stirred conditions at 1.3 V vs. Ag/AgCl. After stabilization of the baseline current, 2 µL of 10 M glycerol was injected into the aqueous reaction solution containing enzyme stimulants – 0.03 M and 0.3 µM (hereinafter referred to as benchmark concentrations) of $(NH_4)_2SO_4$ and $MnCl_2.4H_2O$, respectively. Sensitivity was calculated from the slope of the linear portion in the calibration curves, using simple linear regression. The lower limit of detection (LOD) was calculated using the 3 sigma method (Vanegas et al., 2014). Response time

was obtained by taking the mean of the 95% steady state response time of 3 successive step changes over the linear range being tested.

Determination of optimal conditions under which the FeS-based biosensor generates maximum current response was electrochemically studied using cyclic voltammetry and constant potential amperometry. The effects of applied potential, scan rate, enzyme stimulants concentrations, buffer and pH on the FeS-based electrode were investigated. For all the studies, except for the study on enzyme stimulants, benchmark concentrations of enzyme stimulants were used. Further, recognizing that the potential application of this biosensor is in the beverage industry, the possible interference of glucose, fructose, ethanol, and acetic acid during glycerol detection was studied, using cyclic voltammetry at 0 – 1.5 V under non-buffered conditions with benchmark concentrations of enzyme stimulant concentrations as well as in Tris buffer/pH and optimized enzyme stimulant concentrations.

4.2.4. Statistical analysis

All the studies were conducted in three replications. Analysis was done using JMP pro 14 (Version 14.0.1, SAS Institute Inc., Cary, NC) with Analysis of Variance (ANOVA). Post Hoc test (Student's t test or Tukey-Kramer HSD) was used to compare treatments means. Significance levels were defined using $p < 0.05$.

4.3. Results and discussion

4.3.1. Glycerol biosensor performance

Glycerol biosensors that involve several glycerol-selective enzymes, glycerol oxidase, glycerol kinase, glycerol-3-phosphate dehydrogenase and glycerol dehydrogenase associated with different types of base electrodes and immobilization techniques have been reported on previously (Álvarez-González, Saidman, Lobo-Castañón, Miranda-Ordieres, & Tuñón-Blanco, 2000; Eftekhari, 2001; Katrlík et al., 2006; Niculescu, Sigina, & Csöregi, 2003). However, these biosensors were fabricated via traditional enzyme tethering methods (the majority of them utilize polymer-mediated enzyme immobilization). Glycerol biosensors based on immobilization of NAD-dependent glycerol dehydrogenase have previously been reported with very low detection limits (LOD): 0.005 mM in the presence of K^+ (Prodromidis, Stalikas, Tzouwara-Karayanni, & Karayannis, 1996), 4.3 x 10^{-4} mM (Álvarez-González et al., 2000), 1 x 10^{-3} mM (Eftekhari, 2001), 9 x 10^{-4} mM and 1 x 10^{-4} mM (Niculescu et al., 2003), and 2.2×10^{-3} mM (Radoi, Compagnone, Devic, & Palleschi, 2007).

In this study, dynamic constant potential amperometry (CPA) was performed for the FeS-based and PQQ-based biosensors to show their respective responses to the successive increments of 1 mM glycerol from 1 to 25 mM at an applied potential of 1.3 V (Figure 4.2 A).

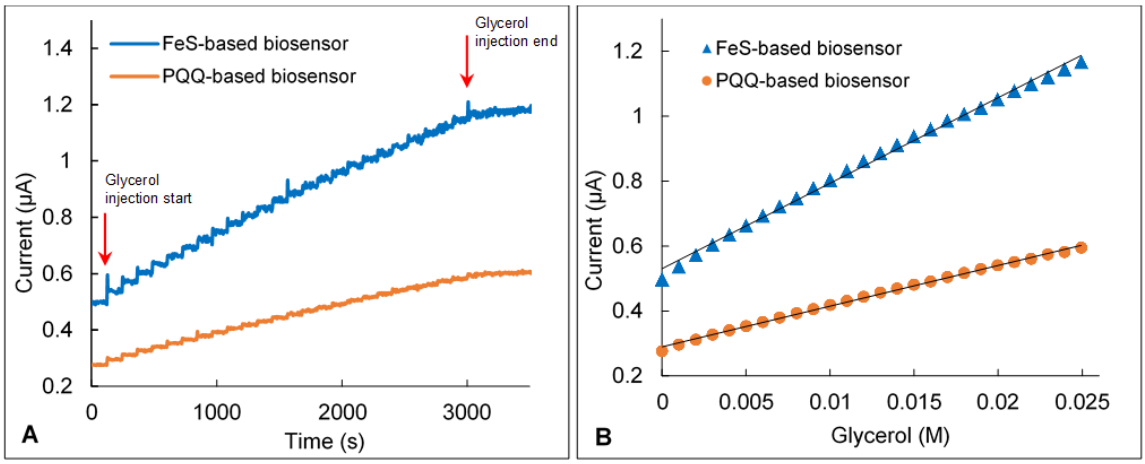

Wiring Type	Sensitivity (µA/M)		LOD (M)		Response Time (s)	
	Mean	Std.Dv	10^{-4} Mean	10^{-4} Std.Dv	Mean	Std.Dv
FeS-based	24.9	1.66	1.58	0.31	1.52	0.22
PQQ-based	14.1	1.73	3.36	0.4	0.57	0.07
% Change	+77 %		-53 %		+167 %	

C

Figure 4.2 (A) Amperometry responses to increments of 0.001 M glycerol at E = 1.3 V; (B) Calibration plots for current responses generated by the FeS-based biosensor and PQQ-based biosensor as a function of glycerol concentration; (C) Summary of the biosensor performance obtained from a dynamic CPA test.

Figure 4.2 B shows the calibration plot of current response to glycerol concentration derived from this study. The slope of the calibration plot represents the sensitivity of the biosensor (Bardeletti, Séchaud, & Coulet, 1991). The greater the slope, the higher is the sensitivity of biosensor. Both FeS-based and PQQ-based biosensors were found to respond linearly to glycerol concentrations with sensitivities 14 $\mu A.M^{-1}$ for PQQ-based biosensor and 25 $\mu A.M^{-1}$ for FeS-based biosensor obtained from the slopes of the calibration plots. LOD was calculated using 3 sigma method were found to be 0.34 mM for PQQ-based biosensor and 0.16 mM for FeS-based biosensor. These findings confirm that the PQQ-based and FeS-based bioanodes can be reliably used to

measure glycerol concentrations as low as 0.34 mM and 0.16 mM, respectively. Response times were calculated as 0.6 s for the PQQ-based biosensor and 1.5 s for the FeS-based biosensor. The performance factors for both types of biosensors obtained from the CPA test are summarized here in Figure 4.2 C.

These results indicate a 77% increase in sensitivity, a 53% decrease in LOD, and a 167% increase in response time for a FeS-based biosensor when compared to a PQQ-based biosensor for glycerol analysis. While the sensitivity and LOD of the FeS-based biosensor showed significant improvement, the increase in response time for the FeS-based biosensor was unanticipated, and is yet to be fully elucidated. The overall improvements are promising and support the premise of this study, namely, that the electron transfer characteristics of FeS-based bioanodes are favorable when compared to the PQQ-based conventional bioanodes. As reported in the previous communication (Mahadevan et al., 2016), the improved electron transfer characteristics of FeS-based bioanodes are due to an reduced internal resistance of the enzymatic electrode resulting from the shorter FeS single-molecular-wire, opposed to the conventional PQQ-based composite wiring system that requires a series of biomolecules to foster enzyme attachment and the ability of FeS to be a single-molecular anchoring agent to mediate electron shuttling between NAD and the supporting electrode.

4.3.2. Electrochemical behavior of a FeS-based biosensor

The electrochemical behavior of the FeS-based glycerol biosensor was characterized by cyclic voltammetry. Figure 4.3 A shows a typical cyclic voltammogram

(CV) obtained with the FeS-based biosensor in pure water containing enzyme stimulants with concentrations of glycerol ranging from 0.001 to 1 M. The CV labelled “a” shows the electrochemical behavior of the $(NH_4)_2SO_4$ enzyme stimulant, whereas b-e shows the current response under increasing glycerol concentrations. It should be noted that with increasing glycerol concentrations, an increase in the oxidation peak current at 1.3 V vs. Ag/AgCl was observed. This result indicates that glycerol oxidation takes place via the redox reaction of $(NH_4)_2SO_4$. The effect of applied potential that ranges from 0 to 1.5 V vs. Ag/AgCl on the current response of the FeS-based biosensor in the presence of 1 M glycerol is shown in Figure 4.3 B. Current remains nearly constant from 0 to 0.8 V, and from 1 V onwards current linearly increases with an increasingly applied potential and the highest current obtained at 1.5 V.

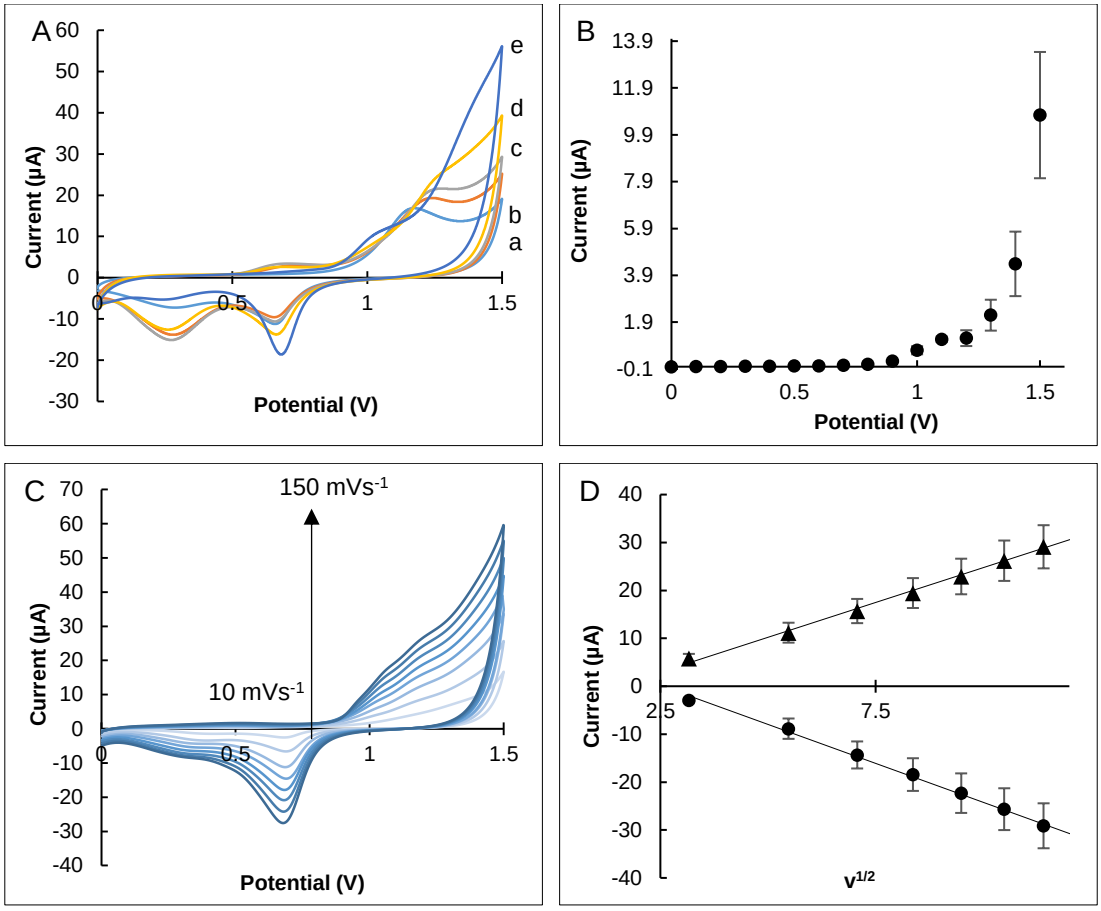

Figure 4.3 (A) Cyclic voltammograms for FeS-based biosensor in increasing concentrations of glycerol (a – 0 M, b – 0.001 M, c - 0.01 M, d - 0.1 M and e - 1 M) diluted with water containing enzyme stimulants at benchmark concentrations. Scan rate is 50 mV/s; (B) Effect of applied potential, ranging from 0 to 1.5 V on the current response of the FeS-based biosensor in the presence of 1 M glycerol; (C) Effect of scan rates (10, 30, 50, 70, 90, 110, 130, and 150) mVs^{-1} on the current response of the FeS-based biosensor in the presence of 1 M glycerol where the color intensity of the CV scan increases with an increasing scan rate in the figure; (D) Anodic and cathodic peak currents plotted with respect to the square root of the scan rate ($v^{1/2}$).

The type of controlled processes that occur during glycerol oxidation at the Au-FeS-NAD-GlDH electrode was elucidated by studying the effects of the scan rate (10 mVs^{-1} to 150 mVs^{-1}) on the peak current, as shown in Figure 4.3 C. Figure 4.3 D shows the changes of the anodic and cathodic peak currents under 1 M glycerol with the square root of the scan rate ($v^{1/2}$). The anodic and cathodic peak currents for glycerol increased linearly with the square root of the scan rate with a high correlation of ~ 0.996,

indicating that the electrode reaction of glycerol was diffusion-controlled. Reactions under diffusion-controlled (or diffusion-limited) conditions occur so quickly that the reaction rate is determined by the rate of transport of the reactants through the reaction solution (Atkins, 1998). This study thus further proves the redox mediation ability of the FeS to efficiently shuttle electrons between the enzyme active site and the gold electrode; and it proves that the layer of enzyme- immobilized molecular wires is permeable to glycerol for a redox reaction. Furthermore, with an increasing scan rate, the anodic and cathodic peak potentials shifted toward the positive and negative quadrants, respectively, indicating charge transfer kinetics limitations.

4.3.3. Effect of enzyme stimulants

Glycerol dehydrogenase catalyzes the oxidation of glycerol to form glycerone by using NAD as the coenzyme/coenzyme. The catalytic efficiency of the reaction is improved in the presence of $(NH_4)_2SO_4$ and $MnCl_2.4H_2O$ due to their stimulatory effects on the enzyme. Previously, it was found that the enzyme stimulants are indispensable for glycerol detection using the wired bioanodes under study. Substantial current responses generated by glycerol oxidation were achieved by using 0.03 M $(NH_4)_2SO_4$ and 0.3 µM $MnCl_2.4H_2O$. With the intention of further optimizing the detection conditions, the current responses of FeS-based biosensor generated in varying concentrations of the enzyme stimulants were studied between the ranges from 0 to 0.3 M for $(NH_4)_2SO_4$ and 0 to 0.001 M for $MnCl_2.4H_2O$ in a 1 M glycerol solution, using cyclic voltammetry and constant potential amperometry. Figure 4.4 indicates that the

highest current responses were obtained at 0.15 M $(NH_4)_2SO_4$ and 0.001 M $MnCl_2.4H_2O$, respectively, in non-buffered conditions.

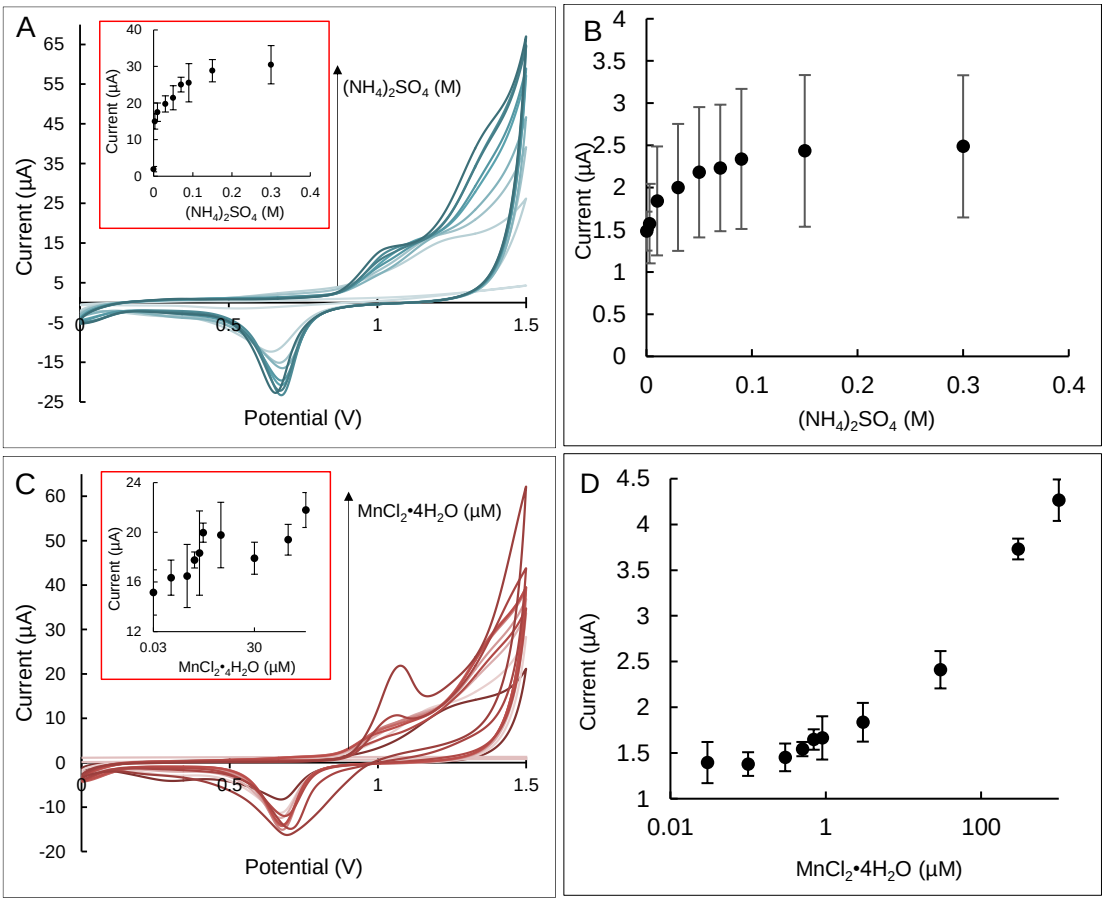

Figure 4.4 (A) Cyclic voltammograms of FeS-based biosensor in (0, 0.003, 0.01, 0.03, 0.05, 0.07, 0.09, 0.15 and 0.3) M of $(NH_4)_2SO_4$ diluted with water containing 1 M glycerol, scan rate is 50 mV/s. Color intensity of the CV scans increases with increasing concentrations of $(NH_4)_2SO_4$; (B) Equilibrated (60 s) constant potential amperometry measurements of anodic currents in increasing concentrations of $(NH_4)_2SO_4$ diluted with water containing 1 M glycerol, at E = 1.3 V; (C) Cyclic voltammograms of FeS-based biosensor in (0, 0.03, 0.1, 0.3, 0.5, 0.7, 0.9, 3, 30, 300 and 1000) µM of $MnCl_2.4H_2O$ diluted with water containing 1 M glycerol, scan rate is 50 mV/s. Color intensity of the CV scans increases with increasing concentrations of $MnCl_2.4H_2O$; (D) Equilibrated (60 s) constant potential amperometry measurements of anodic currents in increasing concentrations of $MnCl_2.4H_2O$ diluted with water containing 1 M glycerol, at E = 1.3 V.

4.3.4. The effects of buffers and the pH

NAD-dependent glycerol dehydrogenase is stable over the pH range of 7.5-10.5, exhibiting optimum activity at pH 10-10.5 (http://www.sigmaaldrich.com/catalog/product/sigma/g3512?lang=en&region=US; accessed May 23, 2016). However, the optimum activity of immobilized NAD-dependent glycerol dehydrogenase wired to the support electrode using FeS and in the presence of enzyme stimulants is not known. Therefore, the effects of buffers and pH on the current response of the FeS-based glycerol biosensor were studied. Current responses of the biosensor were obtained in potassium phosphate buffer (pH 6 – 8) and Tris buffer (pH 8 – 10), using cyclic voltammetry and constant potential amperometry. Benchmark concentrations of the enzyme stimulants and 5 mM glycerol were kept constant during this study. Figure 4.5 A (and Figure 4.S1 in Appendix B) shows current responses of the FeS-based glycerol biosensor to glycerol solution made in different buffers, using cyclic voltammetry. Clearly, the current response in the Tris buffer/pH 8-10 solutions was higher than that in the potassium phosphate buffer/pH 6-8. The striking difference is possibly due to the destructive effect of phosphate buffers on NADH, which results in a disruption of the electron transfer by causing irreversibility in the NAD/NADH redox cycle (Alivisatos, Ungar, & Abraham, 1965; Passonneau & Lowry, 1993). Also, as a result of the Tris buffer/pH 10 generating the maximum current and the optimum pH for glycerol dehydrogenase being between 10-10.5, Tris buffer/pH 10 was chosen as the optimum.

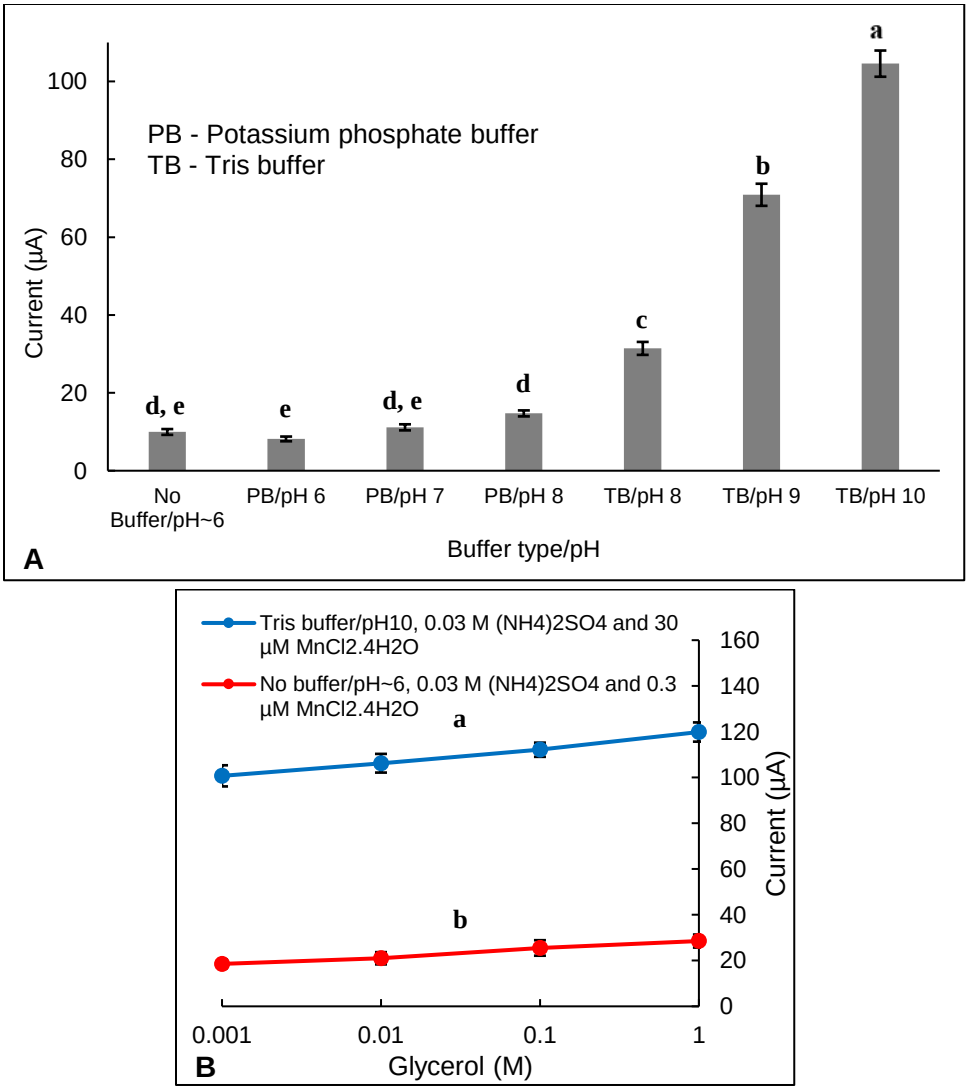

Figure 4.5 (A) Effect of pH/buffers on anodic currents at E=1.3 V, generated by FeS-based biosensor in 5 mM glycerol solution containing benchmark concentrations of enzyme stimulants; (B) Peak currents at 1.3 V vs. glycerol concentrations measured by FeS-based biosensor derived from CV scans between 0 and 1.5 V, scan rate 50 mV/s. A fitting equation for FeS-based biosensor @ 1.3 V under buffered conditions (Tris buffer/pH10, 0.03 M $(NH_4)_2SO_4$ and 30 µM $MnCl_2.4H_2O$) is y = 2.7ln(x) + 119.2, R^2 = 0.99, and non-buffered conditions (pH~6, 0.03 M $(NH_4)_2SO_4$ and 0.3 µM $MnCl_2.4H_2O$) is y = 1.5ln(x) + 28.6, R^2 = 0.99. Error bars depict ±1 standard deviation. Different letters indicate significant difference among the sample response means.

When the optimized enzyme stimulant concentrations (0.15 M $(NH_4)_2SO_4$ and 0.001 M $MnCl_2.4H_2O$) were combined with the optimal Tris buffer/pH 10, a dark brown precipitate (MnO_2) was formed in the absence and in the presence of glycerol. The

sensing performance of the FeS-based biosensor under these detection conditions (0.15 M $(NH_4)_2SO_4$ and 0.001 M $MnCl_2.4H_2O$ in the Tris buffer/pH10) was evaluated. However, the biosensor was not able to detect the glycerol satisfactorily. After screening different combinations of enzyme stimulant concentrations in the Tris buffer/pH10, it was found that in 0.03 M $(NH_4)_2SO_4$ and 30 µM $MnCl_2.4H_2O$ in the Tris buffer/pH10, the FeS-based glycerol biosensor generated a 422% higher current than the current generated in the non-buffered/benchmark enzyme stimulant concentration conditions (see Figure 4.5 B) when tested using cyclic voltammetry (non-stirring). Conversely, when tested for sensing performance using constant potential amperometry with stirring, the FeS-based enzyme electrode showed a decreasing current trend with each glycerol injection. The decreasing current trend possibly occurred due to a buffering effect during the glycerol injections.

Hence, it can be inferred that the optimum performance conditions under stirring remain 0.03 M $(NH_4)_2SO_4$ and 0.3 µM $MnCl_2.4H_2O$ in non-buffered aqueous electrolyte; whereas, under non-stirring conditions, the FeS-based electrode detects glycerol optimally in Tris buffer/pH10 containing 0.03 M $(NH_4)_2SO_4$ and 30 µM $MnCl_2.4H_2O$. Observations made from the cyclic voltammograms (non-stirring) of this study also showed that, at buffered conditions, the applied potential for glycerol detection was lowered from 1.3 V (non-buffered conditions) to 0.6 V, which is favorable considering that the oxidation of several interferents at 1.3 V can now be prevented.

4.3.5. Interference study

The effects of commonly considered interferents, typically present in fruit beverages and wine, on glycerol detection by the FeS-based glycerol biosensor was investigated. Considered compounds and their concentrations were 18 g/L glucose, 18 g/L fructose, 10% (v/v) ethanol, and 4 g/L acetic acid with 4 g/L glycerol, based on the normal concentration ranges of these components in wines and other fruit beverages. The peak currents at 1.3 V (non-buffered) and 0.6 V (buffered) as derived from cyclic voltammetry are illustrated in Figure 4.6.

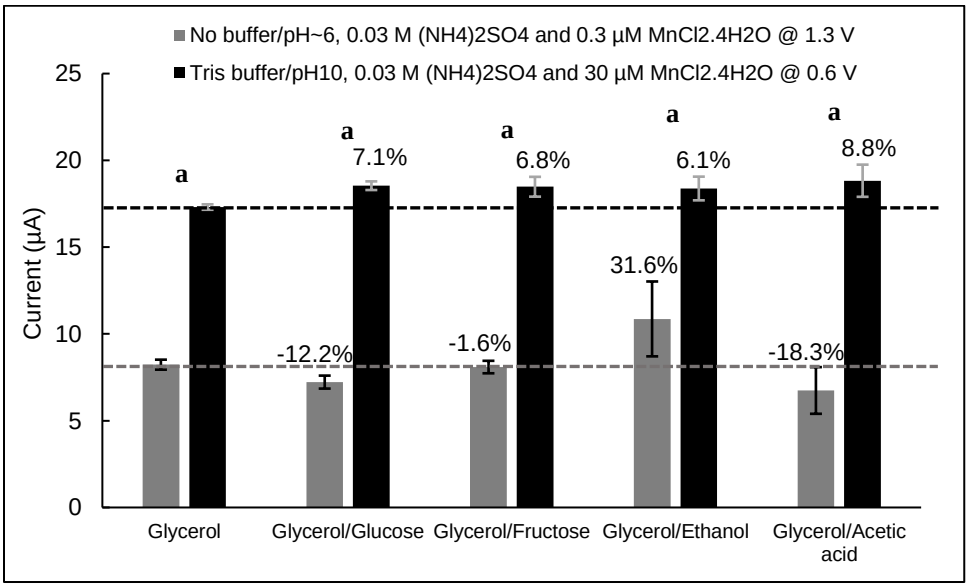

Figure 4.6 Effect of the interferents on the current responses generated by the FeS-based biosensor. Current responses were derived from cyclic voltammograms performed from 0 to 1.5 V. Grey color bars depict peak current derived at 1.3 V under No buffer/pH~6, 0.03 M $(NH_4)_2SO_4$ and 0.3 µM $MnCl_2.4H_2O$ conditions. Black color bars depict the peak current derived at 0.6 V under the Tris buffer/pH10, 0.03 M $(NH_4)_2SO_4$ and 30 µM $MnCl_2.4H_2O$ conditions. Different letters indicate significant difference among the sample response means.

It can be seen, therefore, that under the Tris buffer/pH10 with 0.03 M $(NH_4)_2SO_4$ and 30 µM $MnCl_2.4H_2O$, the presence of glucose, fructose, ethanol, or acetic acid was over-expressing currents, whereas under no buffer/pH~6, 0.03 M $(NH_4)_2SO_4$ and 0.3 µM

$MnCl_2.4H_2O$ conditions, ethanol was over-expressing, and glucose, fructose and acetic acid were under-expressing the currents. These results indicate that based on the presence/absence of such interferents, reading corrections still have to be made.

4.4. Conclusions

A glycerol-oxidizing biosensor was fabricated by direct attachment of NAD-glycerol dehydrogenase coenzyme-apoenzyme complex to supporting gold electrodes, using novel inorganic iron (II) sulfide (FeS)-based single molecular wire. The performance factors of the FeS-based biosensor were compared with those of the PQQ-based biosensor for glycerol detection. Both the biosensors responded linearly to glycerol concentrations as low as 0.34 mM and 0.16 mM with experimentally determined sensitivities of 14 $\mu A.M^{-1}$ for PQQ-based glycerol biosensor and 25 $\mu A.M^{-1}$ for FeS-based glycerol biosensor. The response time was calculated to be 0.6 s for a PQQ-based glycerol biosensor and 1.5 s for a FeS-based glycerol biosensor. A 77% increase in sensitivity, a 53% decrease in detection limit, and a 167% increase in response time were observed for the FeS-based biosensor when compared to the PQQ-based biosensor for glycerol detection. Such a remarkable improvement in the sensitivity and LOD of the novel FeS-based biosensor compared to the conventional PQQ-based counterpart indicates that FeS-based molecular wires have significant promise as tethers in enzymatic electrodes. However, further optimization studies are required to achieve detection limits comparable to the already existing glycerol biosensors. Considering all of these points, it is clear that both conventionally wired PQQ-based bioanode and the

uniquely wired FeS-based bioanode can be successfully used as biosensors for glycerol detection. Excitingly, the performance of the FeS-based glycerol biosensor was found to be far more superior when compared to the conventional PQQ-based one. For further optimization, the electrochemical performance of the FeS-based glycerol biosensor was studied under different concentrations of glycerol, along with the effects of applied potential and scan rate on the current response. Linearly increasing anodic and cathodic peak currents with increasing scan rates indicated that the electrode kinetics are controlled by diffusion. The optimum performance conditions were 0.03 M $(NH_4)_2SO_4$ and 0.3 µM $MnCl_2.4H_2O$ in non-buffered aqueous electrolyte under stirring, whereas under non-stirring, the optimal conditions were in Tris buffer at pH 10 with 0.03 M $(NH_4)_2SO_4$ and 30 µM $MnCl_2.4H_2O$. Further analysis indicated that the FeS-based wiring system in unstirred conditions was staying intact and performing the electron transport unfettered even under relatively extreme pH conditions, i.e., 10, at which point the GlDH enzyme performance becomes optimal. An interference study showed acceptable interference from glucose, fructose, ethanol, and acetic acid under buffered conditions and relatively higher interference from glucose, ethanol, and acetic acid under non-buffered conditions. Additional studies are needed to elucidate the reason(s) for the increased response time with the FeS-based electrode and also to limit interferences of commonly found analytes before these electrodes can be utilized for real world biosensing applications.

5. OPTIMIZATION OF IRON-SULFUR-BASED MOLECULAR WIRES AND COMPARISON OF THEIR PERFORMANCE WITH THE CONVENTIONAL PQQ-BASED MOLECULAR WIRE FOR BIOSENSING AND BIOFUEL CELL APPLICATIONS

5.1. Introduction

Diabetes is the seventh-leading cause of death in the U.S. (Murphy, Xu, Kochanek, & Arias, 2018) About 23.1 million people with diabetes are diagnosed and 7.2 million people with diabetes are undiagnosed. (Control & Prevention, 2017)There is need for a device that can entirely automate blood glucose regulation, provide continuous glucose monitoring and therapeutic delivery without any intervention from the diabetic patient. An automated glucose control device at a minimum requires a glucose sensing element, an actuation system (to release insulin for example), and a power supply to run the actuation module. If realized, such a system can simultaneously generate power to regulate glucose in diabetic patients. This can contribute to better diabetes management by helping to minimize the presumption that comes with making treatment decisions based solely on random blood glucose meter readings.

Redox enzymes such as glucose oxidase glucose dehydrogenase have the capability to act as glucose-selective sensing elements and a power supply since the catalytic oxidation of their substrate (i.e. glucose) results in an electron stream that is proportional to substrate concentration.

However, power generated by the existing enzymatic electrode systems (see Table 5.1) needs to be increased several orders of magnitude to be able to generate enough power for self-powering applications. Consequently, the inherent ability of enzymes to act as sensors and power generation devices has not been capitalized, especially due to the lack of an efficient direct electrical communication between the electrode surface and the enzyme.

Table 5.1 Recent glucose biofuel cells based on direct electron transfer

Electrode/ Molecular wire	Enzyme @ anode/ cathode	Power Density (μWcm^{-2})	Membrane	Reference
Graphite rod/AuNP/RGO	GOx/Air breathing cathode	138	Nafion Membrane	(Mazar, Alijanianzadeh, Molaeirad, & Heydari, 2017)
Graphite rod/AuNP/RGO/NR	GOx/Air breathing cathode	176	Nafion Membrane	(Mazar et al., 2017)
Au wire/AuNP	CDH/BOx	2	Membraneless	(Andoralov et al., 2013)
Buckypaper/MWCNT	(PQQf)-GDHg/laccase	5	-	(Castorena-Gonzalez et al., 2013)
Glassy carbon/SWCNT	GOx/laccase	57.1	-	(Castorena-Gonzalez et al., 2013)
Buckypaper/CNT	(PQQ)-GDH/laccase	30	Membraneless	(Halámková et al., 2012)
Buckypaper/CNT	(PQQ)-GDH/laccase	40	Membraneless	(Szczupak et al., 2012)
Silicon/SWCNT	GOx/laccase	1.38	Membraneless	(S. C. Wang et al., 2009)

AuNP: Au nanoparticles; SWCNT: single-walled carbon nanotubes; MWCNT: multi-walled carbon nanotubes; CNT: carbon nanotubes; RGO: reduced graphene oxide; GOx: glucose oxidase.

Direct electron transfer between the electrode surface and the enzyme is often difficult due to the insulation of enzyme active site from the electrode support by the protein matrix (Heller, 1992). Several methods to electrically connect enzymes with electrode supports were developed, including inventive approaches to align and orient the enzymes on the electrode surface to facilitate direct electrical communication. (Katz et al., 2004; Patolsky et al., 2004; I. Willner et al., 1996; Xiao et al., 2003) Despite the impressive advances in facilitating an electrical connection between enzymes and electrodes, thermodynamic and kinetic limitations that hamper effective direct electrical communication between the enzymes and electrode surfaces still exist. (Akkerman et al., 2006; Holmlin et al., 2001; Mahadevan et al., 2014) Moreover, the coenzymes at the redox enzyme active site(s) display a natural resistance to switching between oxidation and reduction reactions (generally referred to as activation overpotential) further hindering the use of enzymes for self-powered bioelectronics applications like biosensors and biofuel cells.

The lack of an effective method that allows unconstrained electron transport between enzymes and electrodes is a significant problem that deters the ability to harness the full potential of enzyme-based bioelectrodes to be used for self-powered applications such as biosensors and fuel cells. (Göpel & Heiduschka, 1995; Schuhmann, 1995; I. Willner et al., 1997)

Recently, a method to prove the ability of inorganic iron-sulfur clusters for direct and robust wiring of the coenzyme-enzyme system to an electrode base while eliminating the issue of constrained charge transport endemic to bioelectronic systems

was described.(Mahadevan & Fernando, 2018) Thus far, the ability of an array of inorganic iron-sulfur clusters (FeS, FeS_2, Fe_2S_3, and Fe_3S_4) to wire a NAD-glucose dehydrogenase (NAD-GDH) onto an electrode surface directly while maintaining excellent charge transport properties has been established (Section 2). The ability of inorganic iron-sulfur clusters to wire redox coenzymes (NAD/NADP, FAD, PQQ, and CoQ_{10}) and the interaction between iron-sulfur clusters and select coenzymes were also studied (Section 3). It has been discovered that the inorganic iron-sulfur moieties effectively anchor NAD/NADP, FAD, PQQ, and CoQ_{10} redox coenzymes to electrode bases. These studies showed FeS and Fe_3S_4 to be able to circumvent the kinetic limitations of the existing wiring systems optimally.

Hence, in this study it was attempted to further improve the FeS and Fe_3S_4 based molecular wires by using conductive linkers to construct NAD-GDH based glucose bioanodes. The optimal glucose bioanodes were used to develop a sensor and a biological fuel cell (that can be combined to create a self-power generation module) and evaluated how the electron transfer kinetics in sensing mode and fuel cell mode compare with existing wiring systems.

5.2. Materials and methods

5.2.1. Reagents and apparatus

NAD-GDH from Bacillus sp. (EC.1.1.1. 47) was purchased from Sekisui Diagnostics. ß-NAD, glutaraldehyde, iron(II) sulfide (FeS), pyrroloquinoline quinone (PQQ), cystamine dihydrochloride, 3-aminophenyl boronic acid monohydrate (APB), 4-

aminothiophenol (4ATP), and benzene-1,4-dithiol (BDT) were purchased from Sigma-Aldrich, USA (www.sigmaaldrich.com). Greigite (Fe_3S_4) was obtained from 1717 CheMall Corporation (www.1717chem.com). 1-Ethyl-3-(3-dimethylaminopropyl) carbodiimide (EDC) and N-Hydroxysuccinimide (NHS) were purchased from Thermo Fisher Scientific (www.thermofisher.com/us). β-D-glucose (hereafter mentioned as glucose) was purchased from Cayman Chemical (www.caymanchem.com).

Fe-S were suspended in ≥99.5% ethanol, and cystamine dihydrochloride was dissolved in pure water; ß-NAD, GDH, and glutaraldehyde solutions were prepared in a 0.1 M phosphate buffer (pH = 7); PQQ and 3-aminophenylboronic acid solutions were prepared using a 0.1 M HEPES buffer (pH 7.2) in the presence of 5 mM EDC and 2.5 mM NHS. (Mahadevan & Fernando, 2017) glucose solutions of different concentrations were prepared in 0.1 M Tris-HCl buffer (pH 8) and stored at 4°C for 36±1 hrs to allow mutarotation. Tris-HCl buffer (pH 8) was selected to enable optimal performance of the NAD-GDH without affecting the pH stability of the other components.

Molecular-biology-grade water obtained from Sigma-Aldrich was used to prepare all the aqueous-based solutions and for rinsing/cleaning purposes throughout this study. Two-millimeter gold-disk working electrodes (0.031 cm^2), Ag/AgCl (1M KCl) reference electrodes, platinum auxiliary electrodes and a gold electrode polishing kit (purchased from CH Instruments Inc.) were used for electrochemical studies. 1 cm x 1 cm 100 nm Au-coated silicon wafer chips, obtained from Platypus Technologies, were used for fuel cell analysis.

All experiments were carried out in an electrochemical cell set up using a C3 cell stand from BASi (www.basinc.com). A CHI8003D potentiostat from CH Instruments, Inc (www.chinstruments.com) was used for electrochemical studies. All the studies were conducted at room temperature.

5.2.2. Electrode preparation

Seven different glucose bioanodes were fabricated, based on Fe-S-based and PQQ-based molecular wiring systems used to tether the GDH enzyme system onto the gold electrode. Electrodes were fabricated via layer-by-layer self-assembly dip-coating method. Polishing of gold working electrode, fabrication of FeS, Fe_3S_4, and PQQ glucose bioanodes was done by using methods previously described (Mahadevan & Fernando, 2018). For fabrication of 4ATP and BDT based FeS and Fe_3S_4 glucose bioanodes, the clean gold electrodes were first dipped into 10 mM 4ATP/BDT-in-ethanol solution for 24 hrs, followed by dipping in 0.3 M FeS/Fe_3S_4-in-ethanol solution for 2 hrs. The modified electrodes were immersed in 1 mM of ß-NAD for 2 hrs after which the electrodes were dipped in 1mg mL^{-1} of GDH for 2 hrs. The resulting electrodes were lastly treated with 10% (v/v) glutaraldehyde for 20 min to crosslink and secure the GDH enzyme layer as described in the previous work (Mahadevan & Fernando, 2018).

The same method was used as described above to prepare the glucose biofuel cell, but 1 cm x 1 cm 100 nm gold-coated silicon wafer chips were used in the place of 2mm gold-disk working electrodes.

5.2.3. Glucose biosensor analysis

The electrochemical studies for the glucose biosensors were performed using the conventional three-electrode system (i.e., an enzymatic working electrode, a platinum counter electrode, and an Ag/AgCl reference electrode) placed in an electrochemical cell containing 10 mL of the corresponding substrates.

The glucose biosensors were tested for sensitivity and detection limits using cyclic voltammetry with glucose concentrations ranging between 0-100 mM. The glucose anodes were scanned from −1 V to +1 V, at a scan rate of 0.05 V/s, to obtain the anodic peak current densities at 0.5 V resulting from glucose oxidation.

For studying the storage stability of the glucose biosensor, the enzyme electrodes were washed thoroughly with 0.1 M THB8 and stored at 4°C in a dry state after the cyclic voltammetry measurements on select days.

The effect of interferents – ascorbic acid (AS, 10 mg/dL), acetaminophen (AC, 15 mg/dL), dopamine (DO, 10 mg/dL), uric acid (UR 10 mg/dL), caffeine (CF, 10 mg/dL), and other monosaccharides [mannose (MA, 10 mg/dL), xylose (XY, 10 mg/dL), and fructose (FR, 30 mg/dL)] were tested using cyclic voltammetry in the presence of 5 mM glucose (i.e., 90 mg/dL).

5.2.4. Glucose fuel cell analysis

For development of characteristic curves (i.e., the polarization and power curves), the voltages of the glucose biofuel cells were recorded using multimeters with external resistors attached between the glucose bioanode and a platinum cathode in an

electrochemical cell containing 10 mL of 10 mM glucose. Under different load conditions (1 –1M Ω) the voltage generated was recorded at room temperature with an interval of 10 minutes between each pair of measurements. The current density and the power density were calculated based on the geometric area (1 cm^{-2}) and of the gold chips.

5.2.5. Statistical analysis

All the studies were conducted in three replications. Analysis was done using JMP pro 14 (Version 14.0.1, SAS Institute Inc., Cary, NC) with Analysis of Variance (ANOVA). Post Hoc test (Student's t test or Tukey-Kramer HSD) was used to compare treatments means. Significance levels were defined using $p < 0.05$.

5.3. Results and discussion

5.3.1. Optimization studies of glucose biosensor

Two factors that largely determine the performance of biosensors are – the conductivity of the electrode which may further depend on the nature of modifiers used for fabrication and the enzyme loading on the electrode surface. Based on these factors, an optimization study was performed to improve the performance of the biosensors. Two aromatic thiol linkers, 4ATP and BDT reported to have high electrical conductivity (Chao et al., 2007), were selected based on the hypothesis that their inclusion (between gold electrode base and iron-sulfur molecules), and their affinity for gold, FeS and Fe_3S_4

(due to the presence of thiol groups in aromatic thiols) will improve the enzyme loading on the electrode surface.

Cyclic voltammetry (CV) was conducted for glucose concentrations ranging from 0.1 – 100 mM. Figure 5.1 A depicts how different electrodes responded to a given concentration of the analyte (100 mM) in a cyclic voltammogram (CV). anodic peak currents at 0.5 V plotted against the glucose concentration. When calibrated for a range of glucose concentration, 0.1 – 100 mM (see Figure 5.1 B), it was noted that Fe_3S_4 followed by FeS resulted in the highest anodic peak currents (I_p) followed by other electrodes in the order of ATP-FeS>PQQ>ATP-Fe_3S_4>BDT-FeS>BDT-Fe_3S_4.

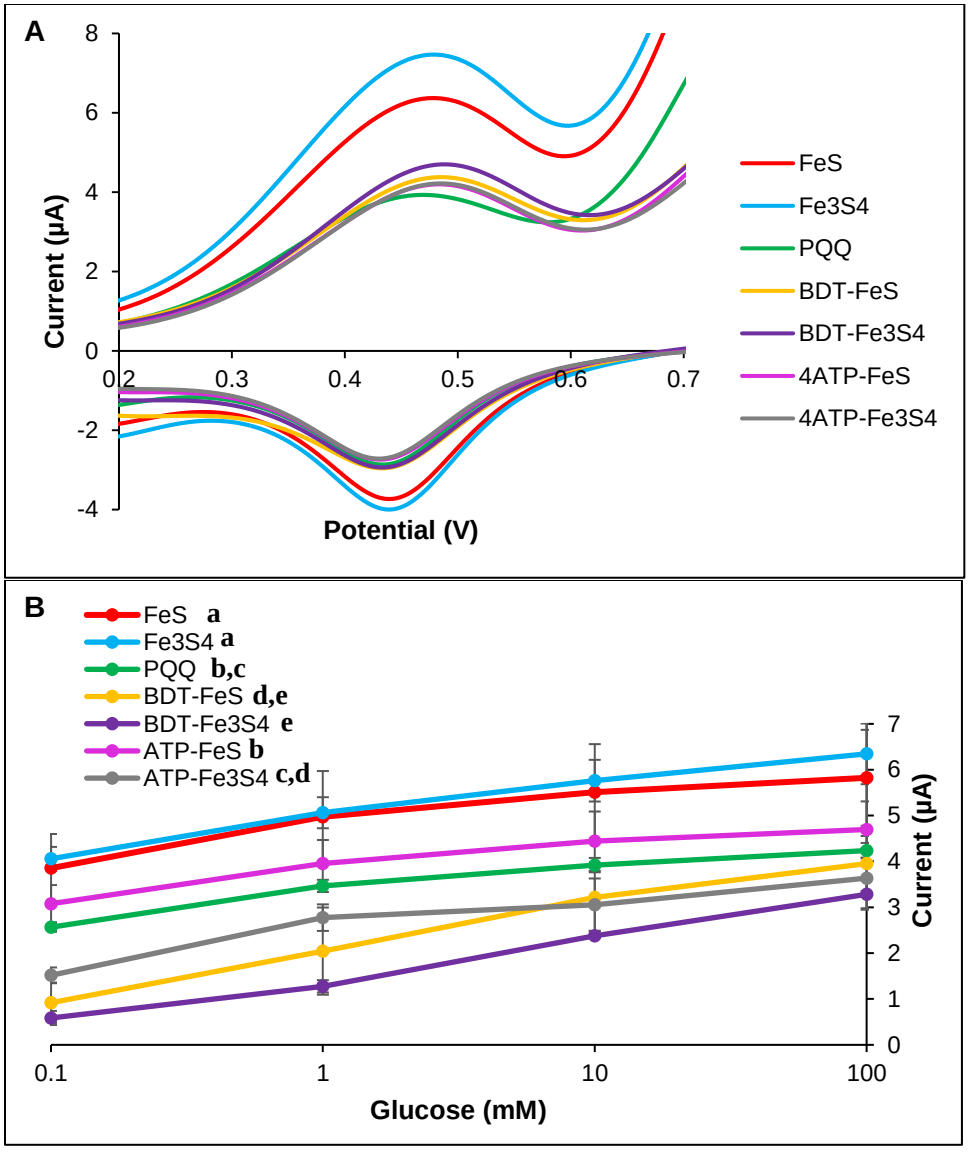

Figure 5.1 (A) Voltammetry analysis of anodes: Excerpts of cyclic voltammograms scanned at a sweep rate of 0.05 V/s vs. Ag/AgCl reference electrode within potential window −1 V and + 1 V display anodic and cathodic peaks of BDT-FeS, BDT-Fe_3S_4, ATP-FeS, ATP-Fe_3S_4, FeS, Fe_3S_4, and PQQ based glucose anodes in 100 mM glucose prepared with 100 mM Tris-HCl buffer (pH 8); (B) Calibration plot: Logarithmic calibration plots for the glucose concentration 0.1 – 100 mM using the voltammetry analysis at 0.5 V. Different letters indicate significant difference among the sample response means.

To measure the biosensor performance factors viz. sensitivity and detection limit, cyclic voltammetry was conducted in the presence of 0 – 0.1 mM glucose concentrations. Anodic peak currents at 0.5 V (glucose oxidation potential) increased as

a function of the concentration of the analyte. A calibration plot was developed between the anodic peak currents at 0.5 V and glucose concentrations of which the slopes gave the sensitivity of the biosensors (Figure 5.2 A). The detection limits of the biosensors (Figure 5.2 B) were calculated using the 3-sigma method. Figure 5.1A&B shows that sensitivity (from CV Scan 1) was achieved in the order of BDT-FeS (14.4 $\mu A/mM/cm^2$)>BDT-Fe_3S_4 (12.9 $\mu A/mM/cm^2$)>Fe_3S_4 (10.6 $\mu A/mM/cm^2$)>ATP-Fe_3S_4 (9.3 $\mu A/mM/cm^2$)> FeS (9 $\mu A/mM/cm^2$)> PQQ (7.7 $\mu A/mM/cm^2$) > ATP-FeS (7.5 $\mu A/mM/cm^2$). Similarly, detection limits varied in the order of 4-ATP-FeS (2.7 mM)>Fe_3S_4 (2 mM)> FeS (1.3 mM) > BDT-Fe_3S_4 (1.2 mM)>4ATP-Fe_3S_4 (0.9 mM)> PQQ (0.7 mM)>BDT-FeS (0.4 mM). The higher performance of BDT linker when compared with 4ATP linker can be attributed to the presence of two S atoms in BDT as opposed to one S atom in 4-ATP. One S atom of BDT may link with the gold surface while the other links with Fe of the FeS and Fe_3S_4 molecules. It is possible that this arrangement enables relatively higher loading of FeS/Fe_3S_4 on gold surface, further increasing the NAD and enzyme loading. Since BDT-FeS and BDT-Fe_3S_4 clearly performed well overall compared to other wiring types, BDT based glucose bioanodes were selected for further studies along with controls – FeS, Fe_3S_4, and PQQ based glucose bioanodes.

The sensitivities of the select glucose bioanodes were calculated from scan 1 and scan 2 anodic peak currents of the cyclic voltammograms as displayed in Figure 5.2 A to distinguish the performance of bioanodes on a continuous basis. For instance, although the Fe_3S_4 (Control) electrode which consists of only Fe_3S_4-modified gold electrode with

no NAD-glucose dehydrogenase attached shows a sensitivity of 8.4 µA/mM/cm^2 for scan 1, it is unable to sense glucose in scan 2 due to the absence of the glucose selective enzyme. Similarly, BDT-FeS had the highest sensitivity (from scan 1), BDT-Fe_3S_4 was found to perform consistently well with high sensitivities based on both scans 1 and 2.

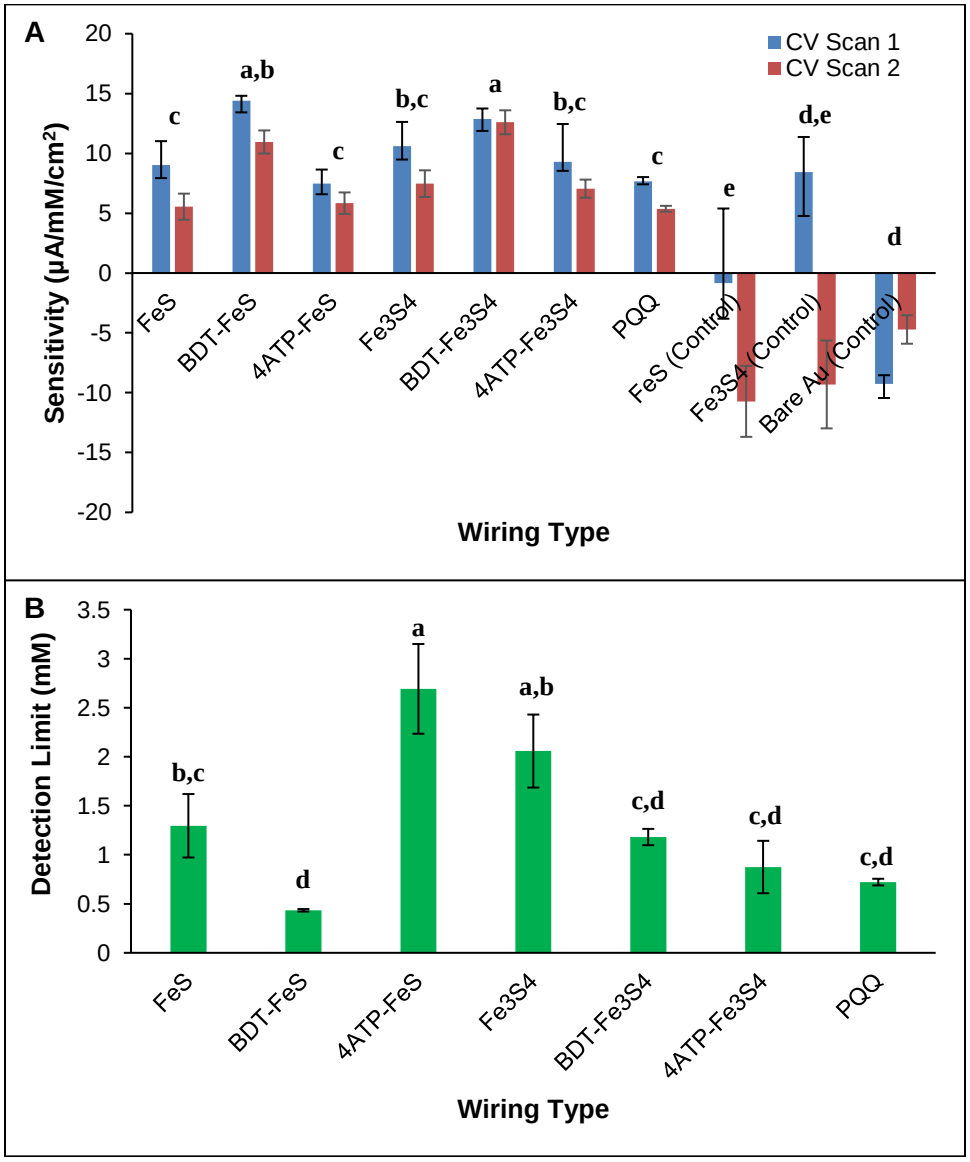

Figure 5.2 Sensitivity and lower detection limits: Sensitivity (A) and detection limits (B) of the glucose biosensors based on different wiring types obtained through cyclic voltammetry indicate BDT-FeS-based glucose anode being more suitable for sensing applications with the highest sensitivity (14.4 µA mM^{-1} cm^{-2}) and lowest detection limits (0.4 mM). Different letters indicate significant difference among the sample response means.

5.3.2. Storage stability

Storage stability of the glucose biosensors was studied by observing the sensitivity (calculated using the same method as described in "glucose biosensor optimization") variations over a period of 30 days. Figure 5.3 illustrates the storage stability of the glucose bioanodes using a scatter plot of their sensitivities versus days of measurements over the 30 days. In all cases, a decrease in sensitivity was observed as the storage time progressed. This can be illustrated by the logarithmic trendlines for the different biosensors on the scatter plot, which shows slopes trending downward (in the order PQQ>BDT-Fe_3S_4> Fe_3S_4>BDT-FeS>FeS) as storage time increases. Although PQQ based glucose biosensor has the lowest slope the sensitivity values were much lower compared to the other iron-sulfur based electrodes. BDT-Fe_3S_4 and Fe_3S_4 based glucose biosensors showed the second and third lowest slope along with higher sensitivities than other wiring types. Hence, BDT-Fe_3S_4 and Fe_3S_4 based glucose biosensors displayed the optimal performance based on storage stability. The results indicate Fe3S4 may play a role in stabilizing enzymatic electrodes, likely due to Fe_3S_4 having more binding points to allow secure binding of the enzyme system to the gold support.

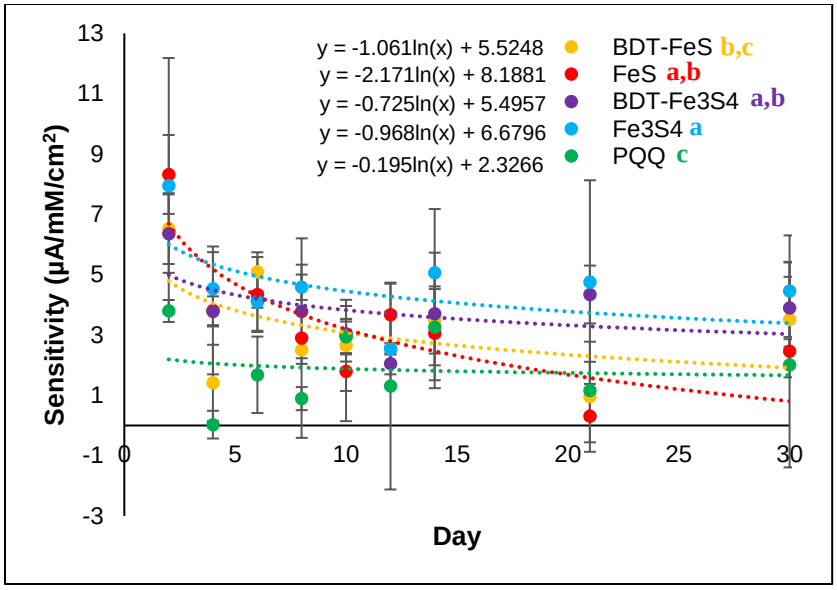

Figure 5.3 Storage stability – Sensitivity of the electrodes measured by cyclic voltammetry for 30 days indicate BDT-Fe_3S_4 and Fe_3S_4 based electrodes to be more stable as biosensors compared to other wiring types. Different letters indicate significant difference among the sample response means.

5.3.3. Interference study

The effect of interferents (see Figure 5.4) was tested using cyclic voltammetry in the presence of 5 mM glucose. The interferents were chosen considering the application of the glucose biosensor for blood glucose analyses. Ascorbic acid (AS, 10 mg/dL), acetaminophen (AC, 15 mg/dL), dopamine (DO, 10 mg/dL), uric acid (UR 10 mg/dL), caffeine (CF, 10 mg/dL), and other monosaccharides [mannose (MA, 10 mg/dL), xylose (XY, 10 mg/dL), and fructose (FR, 30 mg/dL)] were tested because these are common naturally occurring interfering species in blood. Serious interferences were observed for DO>AC>UR>AS, as the oxidation potentials of these compounds are similar to that of glucose. FR, MA, XY, and CF did not significantly interfere with glucose selectivity of the biosensors.

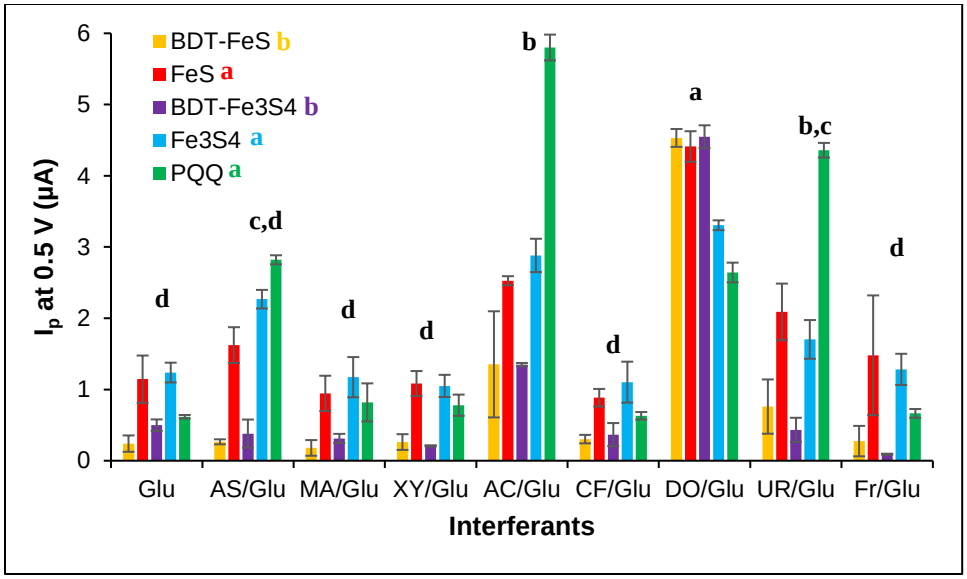

Figure 5.4 The effect of interference on biosensor response at 0.5 V in the presence of 5mM glucose. Different letters indicate significant difference among the sample response means (black letters – response means of interferants; colored letters – response means of glucose biosensors with different wiring types).

It should be noted that Nafion polymer as an effectively permselective barrier can circumvent the entry of interferants. (Emr & Yacynych, 1995; X. Liu, Shi, Niu, Li, & Xu, 2008) So coating a thin film of Nafion polymer on the outside of glucose bioanode could further eliminate the interferences and enhance selectivity of the biosensor.

5.3.4. Glucose biofuel cell

A series of studies were conducted to evaluate if the glucose bioanodes could be used as a self-powered electrochemical cell, i.e., biological fuel cell. A schematic of the glucose biofuel cell tested is shown in Figure 5.5 A. The open circuit voltage (OCV) of the glucose biofuel cell represents the potential generated between the enzymatic anode and platinum cathode placed in glucose (fuel) solution with no load in the circuit. The

effect of different wiring systems on the OCV generated in 10 mM glucose is shown in Figure 5.5 B. All the glucose biosensors generated an OCV of 0.5 ± 0.02 V. Fe_3S_4 based glucose biosensor generated the highest OCV of 0.521 V, whereas BDT-Fe_3S_4 generated the lowest OCV of 0.497 V. It should be noted that all the electrodes displayed acceptable OCV as compared to theoretical cell voltage (1.3 V) (Aurélien, Karine, Sophie, & Boniface, 2011) suggesting no significant overpotential losses.

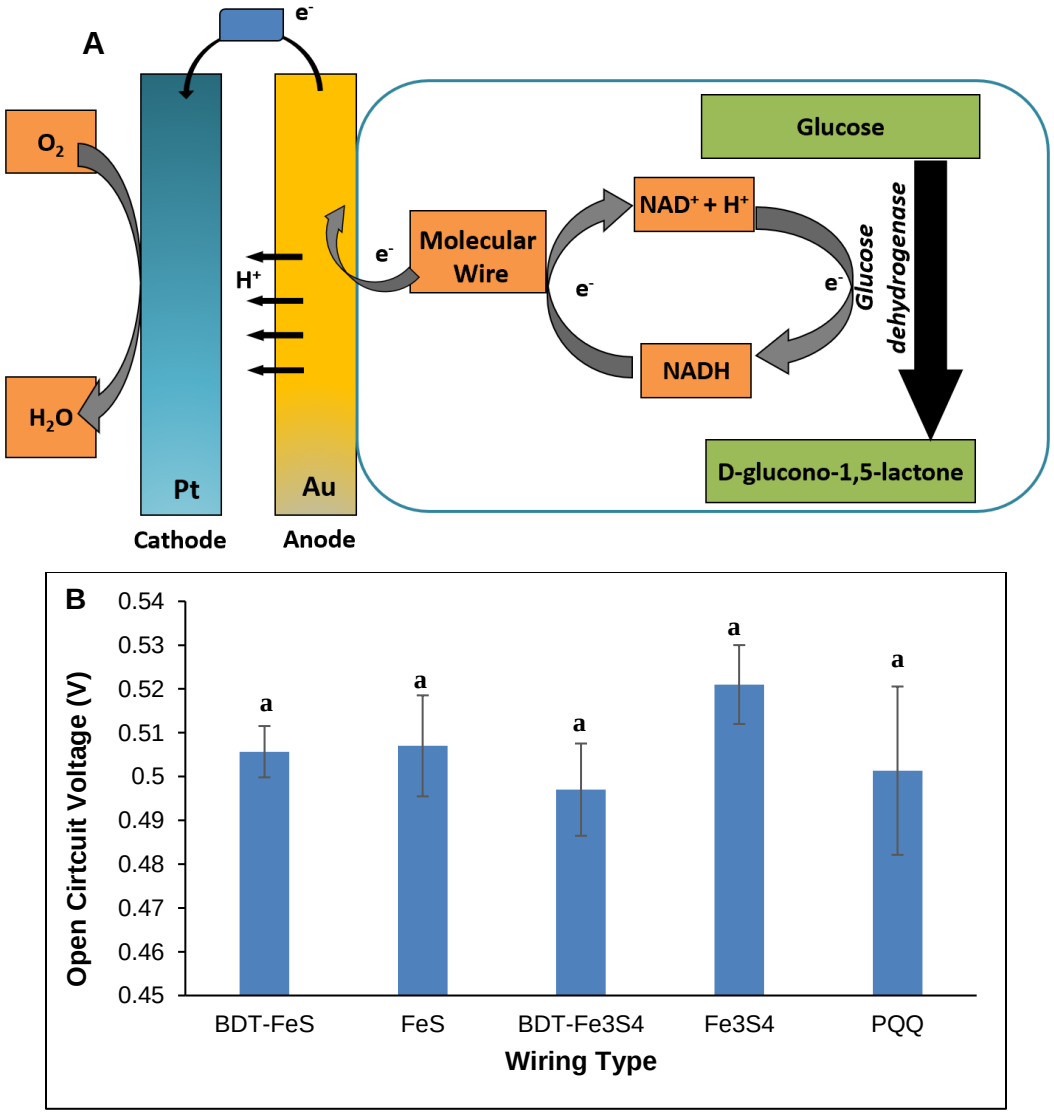

Figure 5.5 (A) Schematic of a membraneless enzymatic glucose biofuel cell; (B) Open circuit voltages generated by glucose biofuel cells based on different wiring types vs. platinum cathode. Different letters indicate significant difference among the sample response means.

The voltage output of the cells was recorded using multimeters as the electron stream generated by glucose oxidation on the anode surface was routed via appropriate loads. The polarization curve (voltage vs. current density; power density vs. current density) was developed using this data and compared for the five electrode systems, see

Figure 5.6 A&B. BDT-FeS and FeS based glucose biofuel cells generated significantly higher power densities compared to the BDT-Fe_3S_4, Fe_3S_4 and PQQ based glucose biofuel cells. The maximum power densities of 2.3 µW/cm^2 (BDT-FeS) and 2 µW/cm^2 (FeS) are comparable with the power densities of similar membraneless enzyme-based glucose biofuel cell recently reported. It was also noted that PQQ resulted in the lowest power density indicating the disadvantages of using conventional wiring systems for power generation or self-powering applications. It should be noted that the fuel cell study was designed for comparing the effectiveness of wiring systems for power generation alone and there is scope for significant improvement to attain higher power densities to facilitate practical applications via increasing electrode surface area and compartmentalizing the half cells.

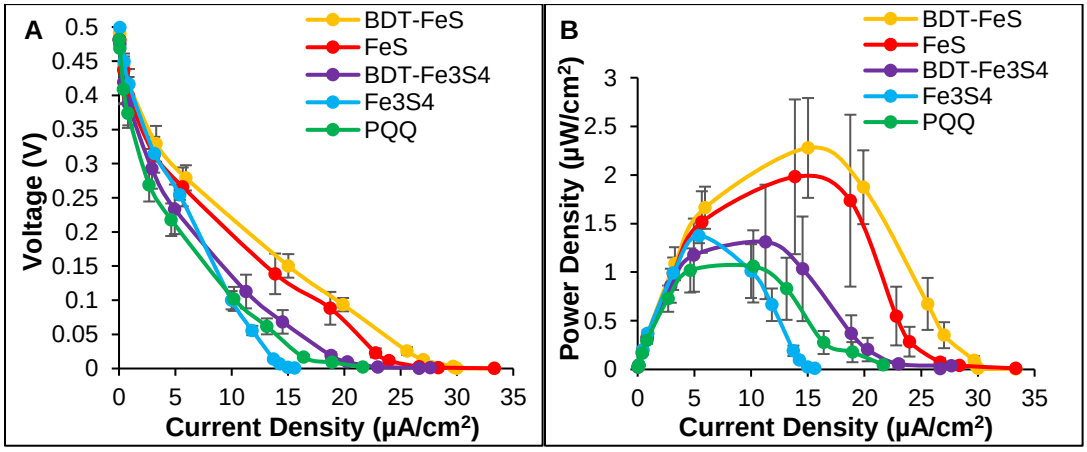

Figure 5.6 (A) Polarization curves and (B) power density curves of membraneless glucose biofuel cells based on different wiring types at room temperature under steady-state conditions. Note that power values pertinent to very low resistance values for select electrodes were excluded due to practical insignificance.

5.4. Conclusions

Glucose bioanodes were developed using iron-sulfur (FeS and Fe_3S_4) based molecular wires to immobilize NAD-GDH on gold electrode base for direct electron transfer. Aromatic thiols, BDT and 4ATP, with high electrical conductance and binding points for iron-sulfur molecules were used linkers to improve enzyme loading on the electrode bases. The biosensor performance (sensitivity and detection limit) of the resulting glucose bioanodes were tested using cyclic voltammetry. Although generating low currents, BDT-FeS and BDT-Fe_3S_4 had the highest sensitivities among 4ATP-FeS, 4ATP-Fe_3S_4, FeS, Fe_3S_4, and PQQ based glucose biosensors. In a 30-day stability study, Fe_3S_4 was found to stabilize the glucose bioanodes when compared with FeS based ones. Although PQQ based glucose biosensor was the most stable biosensor, it generated the lowest currents. BDT-FeS based glucose biosensor was the least affected by common interferents, whereas PQQ based one was the most affected. The glucose bioanodes were also tested for biofuel cell performance with a platinum cathode, where highest power densities were achieved by BDT-FeS and FeS based glucose fuel cells, and PQQ generated the lowest power density. From these studies, it can be concluded that a combination of FeS and Fe_3S_4 combined with BDT linker are promising materials for developing enzymatic glucose sensor and fuel cell.

6. CONCLUSIONS

The ability of an array of inorganic [Fe-S] to wire a redox enzyme onto an electrode surface directly while maintaining charge transport properties was demonstrated. Although many linker molecules have been attempted thus far to anchor redox enzymes to supporting electrode surfaces, none have been effective enough to emulate the functionality of biological electron transport chains. This is because there are no known entities (other than iron-sulfur complexes) that have the required (multi-functional) capabilities embedded in a single molecule, i.e., the ability to anchor the enzyme from one end and to the electrode support from the other, facilitate electron mediation, and enhance charge transport. It was discovered in this study that the [Fe-S]-based enzyme electrodes could amplify current signals as compared to electrodes fabricated using conventional wiring schemes. This was possible due to the reduced internal resistance of the [Fe-S]-based electrodes resulting from the simpler/shorter [Fe-S]-based single-molecular-wires; the ability of [Fe-S] to not only be a single-molecular anchoring agent but also being able to shuttle electrons between the enzyme and the supporting electrode; and their ability to bind the enzyme system to the supporting electrode with high affinity. The inorganic [Fe-S] were also effectively able to anchor NAD/NADP, FAD, PQQ, and CoQ_{10} redox coenzymes to gold electrodes, indicating that they can be used for wiring several redox enzymes. When used in constructing enzymatic biosensors, a 77% increase in sensitivity and a 53% improvement in detection limit was observed for a FeS-based glycerol biosensor when compared to the conventional PQQ-based counterpart, for glycerol concentrations ranging from 1–25

mM. When tested to construct glucose-selective bioanode, a combination of FeS and Fe_3S_4 combined with BDT (an aromatic thiol linker) gave promising performances when used as glucose sensor and fuel cell. From these studies, it can be concluded that a practical analog of the biological electron transport chain was developed using iron-sulfur molecular wires that is robust enough to be used for ex vivo bioelectronics applications demanding low resistance such as highly sensitive biosensors and high-power-density biofuel cells.

7. RECOMMENDATIONS FOR FUTURE WORK

1. Determine methods to improve iron-sulfur wire stability, coverage, and performance of electrodes specially for self-powering sensing applications
2. Investigate the possibility of coupling iron-sulfur clusters with high surface area materials
3. To study the applicability of the iron-sulfur based wiring schemes for use in biological control systems

REFERENCES

Akkerman, H. B., Blom, P. W., De Leeuw, D. M., & De Boer, B. (2006). Towards molecular electronics with large-area molecular junctions. Nature, 441(7089), 69-72.

Alivisatos, S. G., Ungar, F., & Abraham, G. J. (1965). Spontaneous Reactions of 1, 3-Substituted 1, 4-Dihydropyridines with Acids in Water at Neutrality. I. Kinetic Analysis and Mechanism of the Reactions of Dihydronicotinamide-Adenine Dinucleotide with Orthophosphates*. Biochemistry, 4(12), 2616-2630.

Álvarez-González, M. I., Saidman, S. B., Lobo-Castañón, M. J., Miranda-Ordieres, A. J., & Tuñón-Blanco, P. (2000). Electrocatalytic detection of NADH and glycerol by NAD+-modified carbon electrodes. Analytical Chemistry, 72(3), 520-527.

Andoralov, V., Falk, M., Suyatin, D. B., Granmo, M., Sotres, J., Ludwig, R., . . . Shleev, S. (2013). Biofuel cell based on microscale nanostructured electrodes with inductive coupling to rat brain neurons. Scientific reports, 3, 3270.

Andrade, S. L., Adams, M. W., Bonomi, F., Booker, S., Boyd, E. S., Broderick, J. B., . . . Dos Santos, P. (2014). Iron-Sulfur Clusters in Chemistry and Biology: Walter de Gruyter GmbH & Co KG.

Andreini, C., Rosato, A., & Banci, L. (2017). The Relationship between Environmental Dioxygen and Iron-Sulfur Proteins Explored at the Genome Level. PloS one, 12(1), e0171279.

Arihara, K., Ariga, T., Takashima, N., Arihara, K., Okajima, T., Kitamura, F., . . . Ohsaka, T. (2003). Multiple voltammetric waves for reductive desorption of

cysteine and 4-mercaptobenzoic acid monolayers self-assembled on gold substrates. Physical Chemistry Chemical Physics, 5(17), 3758-3761.

Atkins, P. (1998). Physical Chemistry. 6th. In: Oxford University Press.

Aurélien, H., Karine, S., Sophie, T., & Boniface, K. (2011). Performances of enzymatic glucose/O2 biofuel cells. In Biofuel's Engineering Process Technology: IntechOpen.

Ayala-Castro, C., Saini, A., & Outten, F. W. (2008). Fe-S cluster assembly pathways in bacteria. Microbiology and Molecular Biology Reviews, 72(1), 110-125.

Bagotsky, V. S. (2005). Fundamentals of electrochemistry (Vol. 44): John Wiley & Sons.

Bardeletti, G., Séchaud, F., & Coulet, P. R. (1991). Amperometric enzyme electrodes for substrate and enzyme activity determinations. Biosensor principles and applications, 7-45.

Bedford, R. B., Bruce, D. W., Frost, R. M., & Hird, M. (2005). Simple iron-amine catalysts for the cross-coupling of aryl Grignards with alkyl halides bearing [small beta]-hydrogens. Chemical Communications(33), 4161-4163. doi:10.1039/b507133j

Beinert, H., Holm, R. H., & Münck, E. (1997). Iron-Sulfur Clusters: Nature's Modular, Multipurpose Structures. Science, 277(5326), 653-659. doi:10.1126/science.277.5326.653

Beinert, H., & Kiley, P. J. (1999). Fe-S proteins in sensing and regulatory functions. Current Opinion in Chemical Biology, 3(2), 152-157. doi:http://dx.doi.org/10.1016/S1367-5931(99)80027-1

Berk, A., Zipursky, S., & Lodish, H. (2000). Molecular Cell Biology 4th edition.

Braun, E., Eichen, Y., Sivan, U., & Ben-Yoseph, G. (1998). DNA-templated assembly and electrode attachment of a conducting silver wire. Nature, 391(6669), 775-778.

Campaner, V. P., Luiz-Silva, W., & Machado, W. (2014). Geochemistry of acid mine drainage from a coal mining area and processes controlling metal attenuation in stream waters, southern Brazil. Anais da Academia Brasileira de Ciências, 86(2), 539-554.

Castorena-Gonzalez, J. A., Foote, C., MacVittie, K., Halámek, J., Halámková, L., Martinez-Lemus, L. A., & Katz, E. (2013). Biofuel cell operating in vivo in rat. Electroanalysis, 25(7), 1579-1584.

Chao, Y., Zhou, Q., Li, Y., Yan, Y., Wu, Y., & Zheng, J. (2007). Potential dependent surface-enhanced Raman scattering of 4-mercaptopyridine on electrochemically roughened silver electrodes. The Journal of Physical Chemistry C, 111(45), 16990-16995.

Chenault, H. K., & Whitesides, G. M. (1987). Regeneration of nicotinamide cofactors for use in organic synthesis. Applied biochemistry and biotechnology, 14(2), 147-197.

Chiriţă, P. (2009). Iron monosulfide (FeS) oxidation by dissolved oxygen: characteristics of the product layer. Surface and Interface Analysis, 41(5), 405-411.

Chiriță, P. (2016). Aqueous Oxidation of Iron Monosulfide (FeS) by Molecular Oxygen. Mineral Processing and Extractive Metallurgy Review, 37(5), 305-310.

Chu, B. C., Garcia-Herrero, A., Johanson, T. H., Krewulak, K. D., Lau, C. K., Peacock, R. S., . . . Vogel, H. J. (2010). Siderophore uptake in bacteria and the battle for iron with the host; a bird's eye view. Biometals, 23(4), 601-611.

Cline, J. F., Hoffman, B. M., Mims, W. B., LaHaie, E., Ballou, D. P., & Fee, J. A. (1985). Evidence for N coordination to Fe in the [2Fe-2S] clusters of Thermus Rieske protein and phthalate dioxygenase from Pseudomonas. Journal of Biological Chemistry, 260(6), 3251-3254.

Control, C. f. D., & Prevention. (2017). National diabetes statistics report, 2017. In: Atlanta, GA: Centers for Disease Control and Prevention.

Dowdy, C. E., & Leopold, M. C. (2010). Enhanced electrochemistry of nanoparticle-embedded polyelectrolyte films: Interfacial electronic coupling and distance dependence. Thin Solid Films, 519(2), 790-796.

Eftekhari, A. (2001). Glycerol biosensor based on glycerol dehydrogenase incorporated into polyaniline modified aluminum electrode using hexacyanoferrate as mediator. Sensors and Actuators B: Chemical, 80(3), 283-289. doi:http://dx.doi.org/10.1016/S0925-4005(01)00916-9

Eller, M., Verkhoturov, S., Della-Negra, S., & Schweikert, E. (2013). SIMS instrumentation and methodology for mapping of co-localized molecules. Review of Scientific Instruments, 84(10), 103706.

Emr, S. A., & Yacynych, A. M. (1995). Use of polymer films in amperometric biosensors. Electroanalysis, 7(10), 913-923.

Ertek, B., Akgül, C., & Dilgin, Y. (2016). Photoelectrochemical glucose biosensor based on a dehydrogenase enzyme and NAD+/NADH redox couple using a quantum dot modified pencil graphite electrode. RSC Advances, 6(24), 20058-20066.

Fischer, W. W., Hemp, J., & Valentine, J. S. (2016). How did life survive Earth's great oxygenation? Current opinion in chemical biology, 31, 166-178.

Fontecave, M. (2006). Iron-sulfur clusters: ever-expanding roles. Nat Chem Biol, 2(4), 171-174.

Göpel, W., & Heiduschka, P. (1995). Interface analysis in biosensor design. Biosensors and bioelectronics, 10(9), 853-883.

Graham, D., & Dingman, S. (2006). Material Matters (Vol. 2): Sigma Aldrich.

Gray, H. B., & Ellis Jr, W. R. (1994). Electron transfer. Bioinorganic Chemistry. Sausalito, CA: University Science Books, 315-363.

Gray, H. B., & Winkler, J. R. (1996). Electron transfer in proteins. Annual review of biochemistry, 65(1), 537-561.

Gray, H. B., & Winkler, J. R. (2005). Long-range electron transfer. Proceedings of the National Academy of Sciences of the United States of America, 102(10), 3534-3539.

Gray, H. B., & Winkler, J. R. (2010). Electron flow through metalloproteins. Biochimica et Biophysica Acta (BBA)-Bioenergetics, 1797(9), 1563-1572.

Guo, M., Sulc, F., Ribbe, M. W., Farmer, P. J., & Burgess, B. K. (2002). Direct Assessment of the Reduction Potential of the [4Fe− 4S] 1+/0 Couple of the Fe Protein from Azotobacter v inelandii. Journal of the American Chemical Society, 124(41), 12100-12101.

Halámková, L., Halámek, J., Bocharova, V., Szczupak, A., Alfonta, L., & Katz, E. (2012). Implanted biofuel cell operating in a living snail. Journal of the American Chemical Society, 134(11), 5040-5043.

Hans, M., Buckel, W., & Bill, E. (2008). Spectroscopic evidence for an all-ferrous [4Fe–4S] 0 cluster in the superreduced activator of 2-hydroxyglutaryl-CoA dehydratase from Acidaminococcus fermentans. JBIC Journal of Biological Inorganic Chemistry, 13(4), 563-574.

Heller, A. (1992). Electrical connection of enzyme redox centers to electrodes. The Journal of physical chemistry, 96(9), 3579-3587.

Holmlin, R. E., Haag, R., Chabinyc, M. L., Ismagilov, R. F., Cohen, A. E., Terfort, A., . . . Whitesides, G. M. (2001). Electron transport through thin organic films in metal− insulator− metal junctions based on self-assembled monolayers. Journal of the American Chemical Society, 123(21), 5075-5085.

Imlay, J. A. (2006). Iron-sulphur clusters and the problem with oxygen. Molecular microbiology, 59(4), 1073-1082.

Ito, E., Noh, J., & Hara, M. (2008). Steric effects on adsorption and desorption behaviors of alkanethiol self-assembled monolayers on Au (111). Chemical Physics Letters, 462(4), 209-212.

Johnston, D. E., Strachan, D. R., & Johnson, A. T. C. (2007). Parallel fabrication of nanogap electrodes. Nano letters, 7, 2474-2477.

Kakiuchi, T., Usui, H., Hobara, D., & Yamamoto, M. (2002). Voltammetric properties of the reductive desorption of alkanethiol self-assembled monolayers from a metal surface. Langmuir, 18(13), 5231-5238.

Katrlík, J., Mastihuba, V., Voštiar, I., Šefčovičová, J., Štefuca, V., & Gemeiner, P. (2006). Amperometric biosensors based on two different enzyme systems and their use for glycerol determination in samples from biotechnological fermentation process. Analytica Chimica Acta, 566(1), 11-18. doi:http://dx.doi.org/10.1016/j.aca.2006.02.063

Katz, E., Heleg-Shabtai, V., Willner, B., Willner, I., & Bückmann, A. F. (1997). Electrical contact of redox enzymes with electrodes: novel approaches for amperometric biosensors. Bioelectrochemistry and Bioenergetics, 42(1), 95-104. doi:http://dx.doi.org/10.1016/S0302-4598(96)05142-2

Katz, E., Sheeney-Haj-Ichia, L., & Willner, I. (2004). Electrical Contacting of Glucose Oxidase in a Redox-Active Rotaxane Configuration. Angewandte Chemie International Edition, 43(25), 3292-3300.

Kim, D.-M., Kim, M.-y., Reddy, S. S., Cho, J., Cho, C.-h., Jung, S., & Shim, Y.-B. (2013). Electron-transfer mediator for a NAD-glucose dehydrogenase-based glucose sensor. Analytical Chemistry, 85(23), 11643-11649.

Kondo, K., Okamoto, A., Hashimoto, K., & Nakamura, R. (2015). Sulfur-mediated electron shuttling sustains microbial long-distance extracellular electron transfer with the aid of metallic iron sulfides. Langmuir, 31(26), 7427-7434.

Kondoh, H., Kodama, C., & Nozoye, H. (1998). Structure-Dependent Change of Desorption Species from n-Alkanethiol Monolayers Adsorbed on Au(111): Desorption of Thiolate Radicals from Low-Density Structures. The Journal of Physical Chemistry B, 102(13), 2310-2312. doi:10.1021/jp980175j

Kowalewska, B., & Jakubow, K. (2017). The impact of immobilization process on the electrochemical performance, bioactivity and conformation of glucose oxidase enzyme. Sensors and Actuators B: Chemical, 238, 852-861.

Lavrenova, L. G., Ikorskii, V. N., Varnek, V. A., Oglezneva, I. M., & Larionov, S. V. (1986). High-temperature spin transition in coordination compounds of iron(II) with triazoles. Journal Name: Sov. J. Coordinat. Chem.; (United States); Journal Volume: 12:2; Other Information: Translated from Koordinatsionnaya Khimiya, 12: No. 2, 207-215(Feb 1986), Medium: X; Size: Pages: 119-127.

Lavrich, D. J., Wetterer, S. M., Bernasek, S. L., & Scoles, G. (1998). Physisorption and chemisorption of alkanethiols and alkyl sulfides on Au (111). The Journal of Physical Chemistry B, 102(18), 3456-3465.

Léger, C., & Bertrand, P. (2008). Direct electrochemistry of redox enzymes as a tool for mechanistic studies. Chemical reviews, 108(7), 2379-2438.

Lill, R. (2009). Function and biogenesis of iron–sulphur proteins. Nature, 460(7257), 831-838.

Lill, R., Diekert, K., Kaut, A., Lange, H., Pelzer, W., Prohl, C., & Kispal, G. (1999). The essential role of mitochondria in the biogenesis of cellular iron-sulfur proteins. Biological chemistry, 380(10), 1157-1166.

Lin-Vien, D., Colthup, N. B., Fateley, W. G., & Grasselli, J. G. (1991). The handbook of infrared and Raman characteristic frequencies of organic molecules: Elsevier.

Lippard, S. J., & Berg, J. M. (1994). Principles of bioinorganic chemistry: University Science Books.

Liu, T., DuBois, D. L., & Bullock, R. M. (2013). An iron complex with pendent amines as a molecular electrocatalyst for oxidation of hydrogen. Nat Chem, 5(3), 228-233. doi:http://www.nature.com/nchem/journal/v5/n3/abs/nchem.1571.html#supplementary-information

Liu, X., Shi, L., Niu, W., Li, H., & Xu, G. (2008). Amperometric glucose biosensor based on single-walled carbon nanohorns. Biosensors and Bioelectronics, 23(12), 1887-1890.

Love, J. C., Estroff, L. A., Kriebel, J. K., Nuzzo, R. G., & Whitesides, G. M. (2005). Self-Assembled Monolayers of Thiolates on Metals as a Form of Nanotechnology. Chemical Reviews, 105(4), 1103-1170. doi:10.1021/cr0300789

Luong, J. H., Glennon, J. D., Gedanken, A., & Vashist, S. K. (2017). Achievement and assessment of direct electron transfer of glucose oxidase in electrochemical biosensing using carbon nanotubes, graphene, and their nanocomposites. Microchimica Acta, 184(2), 369-388.

Madoz-Gurpide, J., Abad, J. M., Fernandez-Recio, J., Velez, M., Vazquez, L., Gomez-Moreno, C., & Fernandez, V. M. (2000). Modulation of electroenzymatic NADPH oxidation through oriented immobilization of ferredoxin: NADP+ reductase onto modified gold electrodes. Journal of the American Chemical Society, 122(40), 9808-9817.

Mahadevan, A., & Fernando, S. (2017). An improved glycerol biosensor with an Au-FeS-NAD-glycerol-dehydrogenase anode. Biosensors and Bioelectronics, 92, 417-424. doi:https://doi.org/10.1016/j.bios.2016.10.085

Mahadevan, A., & Fernando, S. (2018). Inorganic iron-sulfur clusters enhance electron transport when used for wiring the NAD-glucose dehydrogenase based redox system. Microchimica Acta, 185(7), 337.

Mahadevan, A., Fernando, T., & Fernando, S. (2016). Iron–sulfur-based single molecular wires for enhancing charge transport in enzyme-based bioelectronic systems. Biosensors and Bioelectronics, 78, 477-482.

Mahadevan, A., Gunawardena, D. A., & Fernando, S. (2014). Biochemical and electrochemical perspectives of the anode of a microbial fuel cell. In Technology and Application of Microbial Fuel Cells: InTech.

Mahadevan, A., Gunawardena, D. A., Karthikeyan, R., & Fernando, S. (2015). Potentiometric vs amperometric sensing of glycerol using glycerol dehydrogenase immobilized via layer-by-layer self-assembly. Microchimica Acta, 182(3-4), 831-839.

Marcus, R. A., & Sutin, N. (1985). Electron transfers in chemistry and biology. Biochimica et Biophysica Acta (BBA)-Reviews on Bioenergetics, 811(3), 265-322.

Marlin, D. S., Olmstead, M. M., & Mascharak, P. K. (1999). Carboxamido Nitrogens Are Good Donors for Fe(III): Syntheses, Structures, and Properties of Two Low-Spin Nonmacrocyclic Iron(III) Complexes with Tetracarboxamido-N Coordination. Inorganic chemistry, 38(13), 3258-3260. doi:10.1021/ic981461c

Mazar, F. M., Alijanianzadeh, M., Molaeirad, A., & Heydari, P. (2017). Development of Novel Glucose oxidase Immobilization on Graphene/Gold nanoparticles/Poly Neutral red modified electrode. Process Biochemistry, 56, 71-80.

Mehmeti, E., Stanković, D. M., Chaiyo, S., Zavasnik, J., Žagar, K., & Kalcher, K. (2017). Wiring of glucose oxidase with graphene nanoribbons: an electrochemical third generation glucose biosensor. Microchimica Acta, 184(4), 1127-1134.

Meyer, J. (2008). Iron–sulfur protein folds, iron–sulfur chemistry, and evolution. JBIC Journal of Biological Inorganic Chemistry, 13(2), 157-170. doi:10.1007/s00775-007-0318-7

Minteer, S. D., Liaw, B. Y., & Cooney, M. J. (2007). Enzyme-based biofuel cells. Current Opinion in Biotechnology 18(3), 228-234

Mrksich, M., Chen, C. S., Xia, Y., Dike, L. E., Ingber, D. E., & Whitesides, G. M. (1996). Controlling cell attachment on contoured surfaces with self-assembled monolayers of alkanethiolates on gold. Proceedings of the National Academy of Sciences, 93(20), 10775-10778.

Munro, A. W., & McLean, K. J. (2013). Electron Transfer Cofactors. Encyclopedia of Biophysics, 601-606.

Murphy, S. L., Xu, J., Kochanek, K. D., & Arias, E. (2018). Mortality in the United States, 2017.

Niculescu, M., Sigina, S., & Csöregi, E. (2003). Glycerol dehydrogenase based amperometric biosensor for monitoring of glycerol in alcoholic beverages. Analytical letters, 36(9), 1721-1737.

Outten, F. W. (2015). Recent advances in the Suf Fe–S cluster biogenesis pathway: Beyond the Proteobacteria. Biochimica et Biophysica Acta (BBA)-Molecular Cell Research, 1853(6), 1464-1469.

Pakapongpan, S., & Poo-Arporn, R. P. (2017). Self-assembly of glucose oxidase on reduced graphene oxide-magnetic nanoparticles nanocomposite-based direct electrochemistry for reagentless glucose biosensor. Materials Science and Engineering: C, 76, 398-405.

Park, H., Lim, A. K. L., Alivisatos, A. P., Park, J., & McEuen, P. L. (1999). Fabrication of metallic electrodes with nanometer separation by electromigration. Appl. Phys. Lett., 75, 303-304.

Passonneau, J. V., & Lowry, O. H. (1993). Enzymatic analysis: a practical guide: Springer Science & Business Media.

Patolsky, F., Weizmann, Y., & Willner, I. (2004). Long-range electrical contacting of redox enzymes by SWCNT connectors. Angewandte Chemie International Edition, 43(16), 2113-2117.

Prodromidis, M., Stalikas, C., Tzouwara-Karayanni, S., & Karayannis, M. (1996). Determination of glycerol in alcoholic beverages using packed bed reactors with immobilized glycerol dehydrogenase and an amperometric FIA system. Talanta, 43(1), 27-33.

Qi, W., & Cowan, J. A. (2011). Structural, mechanistic and coordination chemistry of relevance to the biosynthesis of iron–sulfur and related iron cofactors. Coordination chemistry reviews, 255(7-8), 688-699.

Radoi, A., Compagnone, D., Devic, E., & Palleschi, G. (2007). Low potential detection of NADH with Prussian Blue bulk modified screen-printed electrodes and recombinant NADH oxidase from Thermus thermophilus. Sensors and Actuators B: Chemical, 121(2), 501-506.

Reed, M. A., Zhou, C., Muller, C. J., Burgin, T. P., & Tour, J. M. (1997). Conductance of a molecular junction. Science, 278, 252-254.

Rees, D. C., & Howard, J. B. (2003). The interface between the biological and inorganic worlds: iron-sulfur metalloclusters. Science, 300(5621), 929-931.

Rickman, R., Verkhoturov, S., Parilis, E., & Schweikert, E. (2004). Simultaneous ejection of two molecular ions from keV gold atomic and polyatomic projectile impacts. Physical review letters, 92(4), 047601.

Riklin, A., Katz, E., Willner, I., Stocker, A., & Buckmann, A. F. (1995). Improving enzyme-electrode contact redox modifications cofactors. Nature (376,), 672-675.

Roling, P. V., Parker, W. L., Goliaszewski, A. E., Williams, T. S., Groce, B. C., & Sintim, Q. K. (2001). Inhibition of pyrophoric iron sulfide activity. In: Google Patents.

Ronkainen, N. J., Halsall, H. B., & Heineman, W. R. (2010). Electrochemical biosensors. Chemical Society Reviews, 39(5), 1747-1763.

Rouault, T. A., & Klausner, R. D. (1996). Iron-sulfur clusters as biosensors of oxidants and iron. Trends in Biochemical Sciences, 21(5), 174-177.

Sagiv, J. (1980). Organized monolayers by adsorption. 1. Formation and structure of oleophobic mixed monolayers on solid surfaces. Journal of the American Chemical Society, 102(1), 92-98.

Scheibel, T., Parthasarathy, R., Sawicki, G., Lin, X.-M., Jaeger, H., & Lindquist, S. L. (2003). Conducting nanowires built by controlled self-assembly of amyloid fibers and selective metal deposition. Proceedings of the National Academy of Sciences, 100(8), 4527-4532.

Schuhmann, W. (1995). Electron-transfer pathways in amperometric biosensors. Ferrocene-modified enzymes entrapped in conducting-polymer layers. Biosensors and bioelectronics, 10(1), 181-193.

Sessions, A. L., Doughty, D. M., Welander, P. V., Summons, R. E., & Newman, D. K. (2009). The continuing puzzle of the great oxidation event. Current Biology, 19(14), R567-R574.

Szczupak, A., Halámek, J., Halámková, L., Bocharova, V., Alfonta, L., & Katz, E. (2012). Living battery–biofuel cells operating in vivo in clams. Energy & Environmental Science, 5(10), 8891-8895.

Touati, D. (2000). Iron and oxidative stress in bacteria. Archives of biochemistry and biophysics, 373(1), 1-6.

Tour, J. M., Jones, L., Pearson, D. L., Lamba, J. J. S., Burgin, T. P., Whitesides, G. M., . . . Atre, S. (1995). Self-Assembled Monolayers and Multilayers of Conjugated Thiols, .alpha.,.omega.-Dithiols, and Thioacetyl-Containing Adsorbates. Understanding Attachments between Potential Molecular Wires and Gold Surfaces. Journal of the American Chemical Society, 117(37), 9529-9534. doi:10.1021/ja00142a021

Tudos, A. J., & Johnson, D. C. (1995). Dissolution of gold electrodes in alkaline media containing cysteine. Analytical Chemistry, 67(3), 557-560.

Updike, S., & Hicks, G. (1967). The enzyme electrode. Nature, 214, 986-988.

van Zundert, G. C., Jaeqx, S., Berden, G., Bakker, J. M., Kleinermanns, K., Oomens, J., & Rijs, A. M. (2011). IR Spectroscopy of Isolated Neutral and Protonated Adenine and 9-Methyladenine. ChemPhysChem, 12(10), 1921-1927.

Vanegas, D. C., Taguchi, M., Chaturvedi, P., Burrs, S., Tan, M., Yamaguchi, H., & McLamore, E. S. (2014). A comparative study of carbon–platinum hybrid nanostructure architecture for amperometric biosensing. Analyst, 139(3), 660-667.

Verkhoturov, D. S., Geng, S., Verkhoturov, S. V., Kim, H., & Schweikert, E. A. (2016). SIMS of transfer ribonucleic acid molecules encapsulated between free-standing graphene sheets. Biointerphases, 11(2), 02A324.

Verkhoturov, S., Eller, M., Rickman, R., Della-Negra, S., & Schweikert, E. (2009). Single impacts of C60 on solids: emission of electrons, ions and prospects for surface mapping. The Journal of Physical Chemistry C, 114(12), 5637-5644.

Verkhoturov, S., Schweikert, E., Chechik, V., Sabapathy, R. C., Crooks, R. M., & Parilis, E. (2001). Auger stimulated ion desorption of negative ions via K-capture radioactive decay. Physical review letters, 87(3), 037601.

Verkhoturov, S. V., Geng, S., Czerwinski, B., Young, A. E., Delcorte, A., & Schweikert, E. A. (2015). Single impacts of keV fullerene ions on free standing graphene: Emission of ions and electrons from confined volume. The Journal of Chemical Physics, 143(16), 164302.

Wang, J. (2008). Electrochemical glucose biosensors. Chemical reviews, 108(2), 814-825.

Wang, S. C., Yang, F., Silva, M., Zarow, A., Wang, Y., & Iqbal, Z. (2009). Membrane-less and mediator-free enzymatic biofuel cell using carbon nanotube/porous silicon electrodes. Electrochemistry Communications, 11(1), 34-37.

Willner, B., Katz, E., & Willner, I. (2006). Electrical contacting of redox proteins by nanotechnological means. Current opinion in biotechnology, 17(6), 589-596.

Willner, I., Heleg-Shabtai, V., Blonder, R., Katz, E., Tao, G., Bückmann, A. F., & Heller, A. (1996). Electrical wiring of glucose oxidase by reconstitution of FAD-modified monolayers assembled onto Au-electrodes. Journal of the American Chemical Society, 118(42), 10321-10322.

Willner, I., Katz, E., & Willner, B. (1997). Electrical contact of redox enzyme layers associated with electrodes: routes to amperometric biosensors. Electroanalysis, 9(13), 965-977.

Xiao, Y., Patolsky, F., Katz, E., Hainfeld, J. F., & Willner, I. (2003). " Plugging into enzymes": Nanowiring of redox enzymes by a gold nanoparticle. Science, 299(5614), 1877-1881.

Yu, Y., Chen, Z., He, S., Zhang, B., Li, X., & Yao, M. (2014). Direct electron transfer of glucose oxidase and biosensing for glucose based on PDDA-capped gold nanoparticle modified graphene/multi-walled carbon nanotubes electrode. Biosensors and Bioelectronics, 52, 147-152.

Zhong, C.-J., & Porter, M. D. (1994). Evidence for Carbon-Sulfur Bond Cleavage in Spontaneously Adsorbed Organosulfide-Based Monolayers at Gold. Journal of

the American Chemical Society, 116(25), 11616-11617. doi:10.1021/ja00104a071

Zhou, H., Zhang, Z., Yu, P., Su, L., Ohsaka, T., & Mao, L. (2010). Noncovalent attachment of NAD+ cofactor onto carbon nanotubes for preparation of integrated dehydrogenase-based electrochemical biosensors. Langmuir, 26(8), 6028-6032.

Zuo, W., Lough, A. J., Li, Y. F., & Morris, R. H. (2013). Amine(imine)diphosphine Iron Catalysts for Asymmetric Transfer Hydrogenation of Ketones and Imines. Science, 342(6162), 1080-1083. doi:10.1126/science.1244466

APPENDIX A

SECTION 3 SUPPLEMENTARY INFORMATION

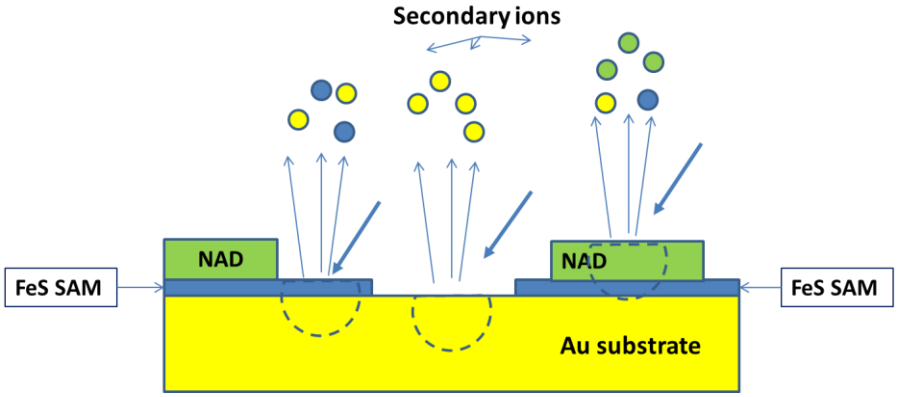

Figure S3.1. Sketch of 50 keV C_{60}^{2+} impacts on "NAD+FeS on Au" sample. If the coverage by FeS and NAD is not complete, there are three types of projectile impacts: 1) Impacts on bare Au, when the emitted ions are Au atomic ions and Au cluster ions, 2) Impacts on surface of FeS, when the emitted from the emission volume (approximately semispherical of Ø 5nm) ions belong to Au substrate and FeS layer,3) Impacts on the surface of NAD, when all types of emitted ions detected as individual mass spectra)

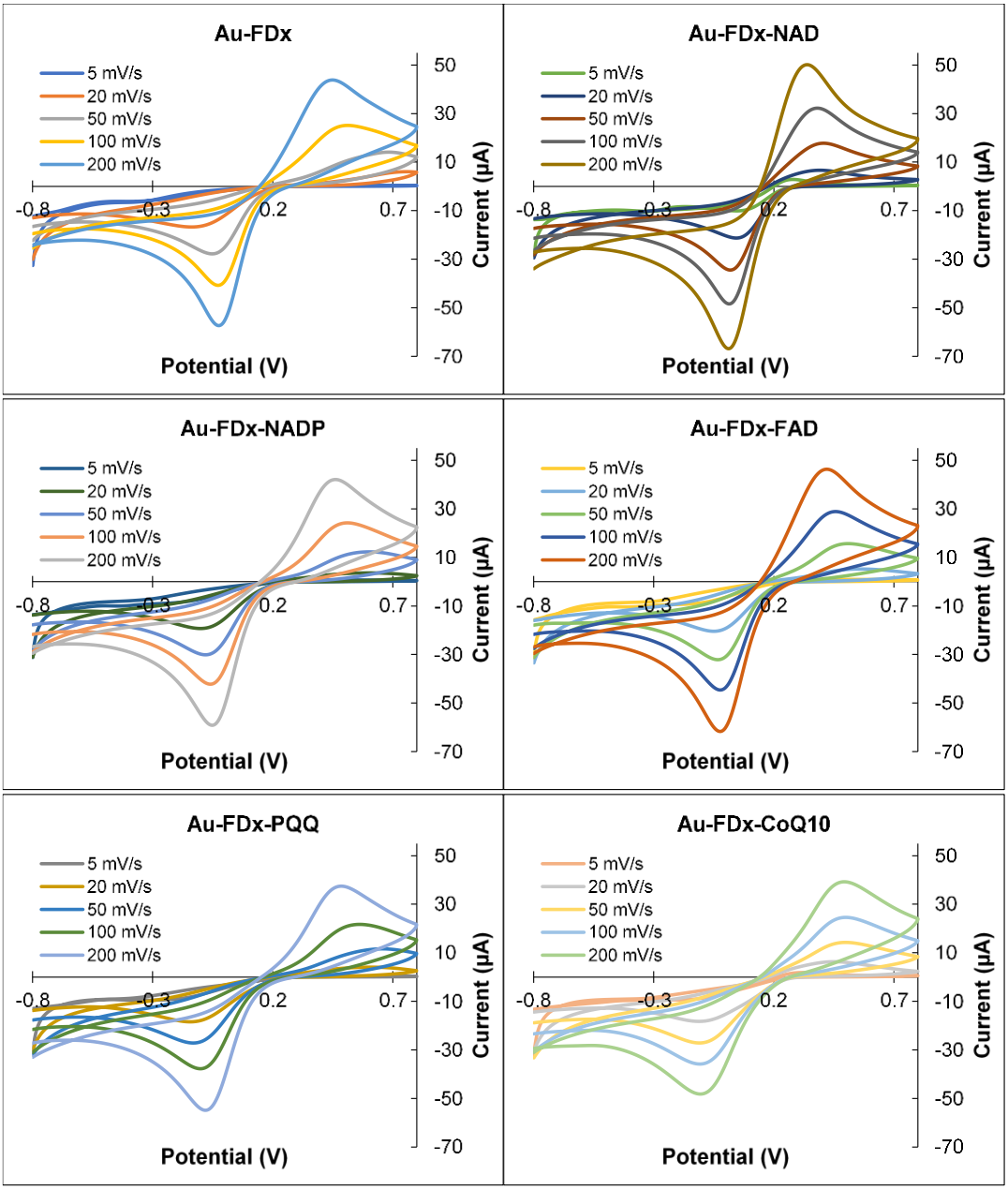
Au-FDx
5 mV/s
20 mV/s
50 mV/s
100 mV/s
200 mV/s
-0.8
-0.3
0.2
0.7
50
30
10
-10
-30
-50
-70
Current (µA)
Potential (V)
Au-FDx-NAD
5 mV/s
20 mV/s
50 mV/s
100 mV/s
200 mV/s
Potential (V)
Au-FDx-NADP
5 mV/s
20 mV/s
50 mV/s
100 mV/s
200 mV/s
Potential (V)
Au-FDx-FAD
5 mV/s
20 mV/s
50 mV/s
100 mV/s
200 mV/s
Potential (V)
Au-FDx-PQQ
5 mV/s
20 mV/s
50 mV/s
100 mV/s
200 mV/s
Potential (V)
Au-FDx-CoQ10
5 mV/s
20 mV/s
50 mV/s
100 mV/s
200 mV/s
Potential (V)

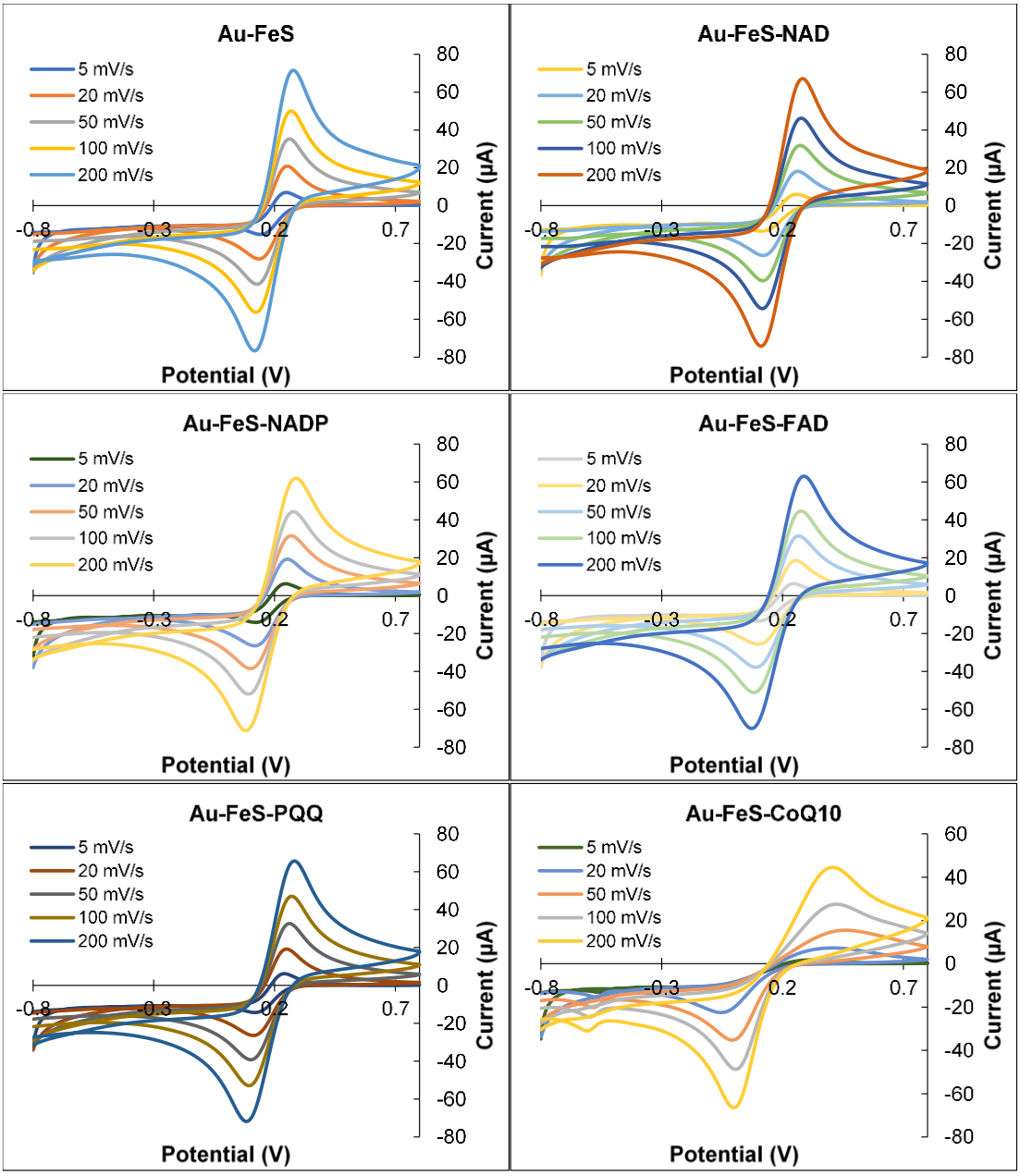
Au-FeS
5 mV/s
20 mV/s
50 mV/s
100 mV/s
200 mV/s
Current (µA)
Potential (V)
Au-FeS-NAD
Au-FeS-NADP
Au-FeS-FAD
Au-FeS-PQQ
Au-FeS-CoQ10

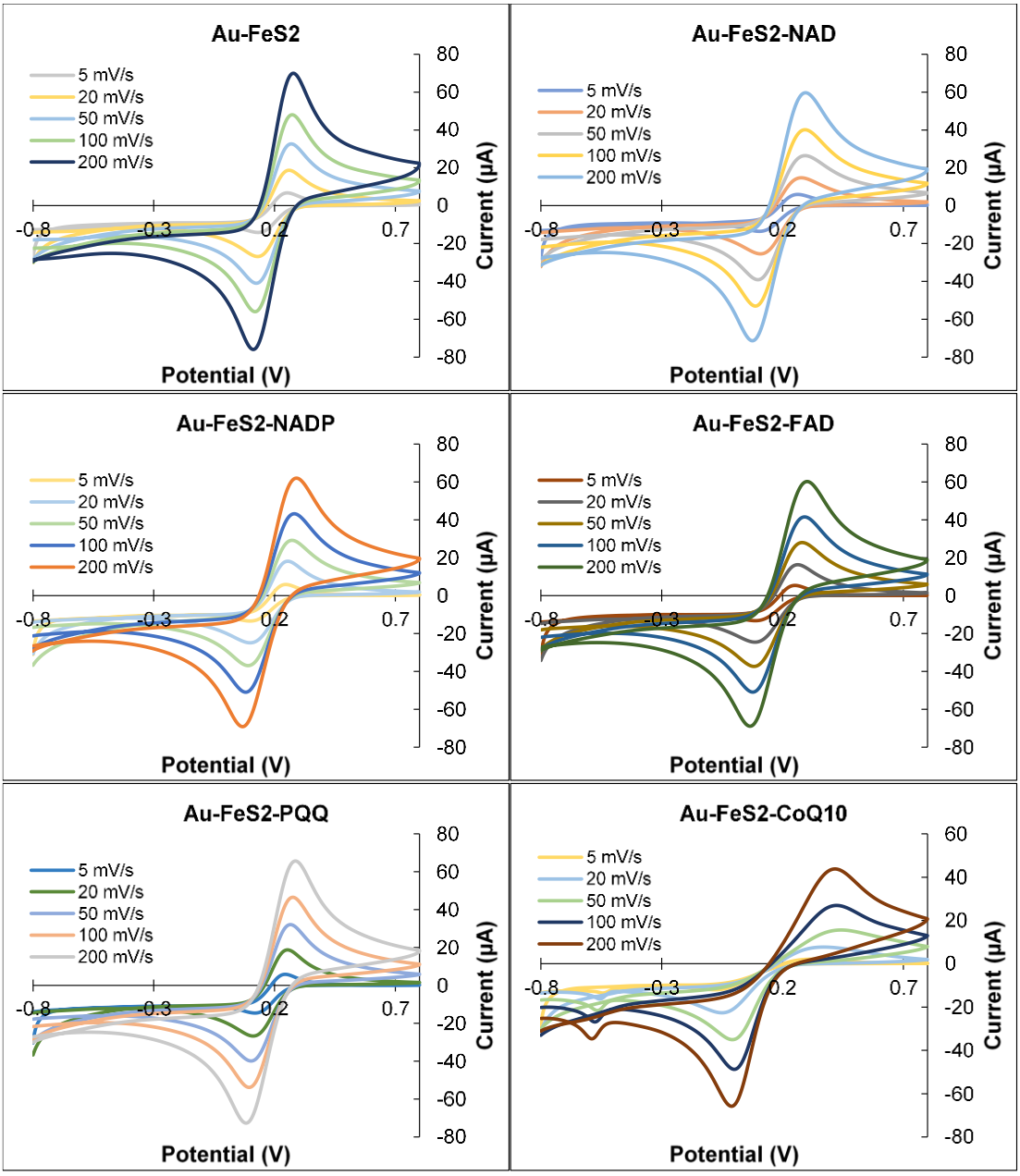
Au-FeS2
5 mV/s
20 mV/s
50 mV/s
100 mV/s
200 mV/s
Current (µA)
Potential (V)
Au-FeS2-NAD
Au-FeS2-NADP
Au-FeS2-FAD
Au-FeS2-PQQ
Au-FeS2-CoQ10

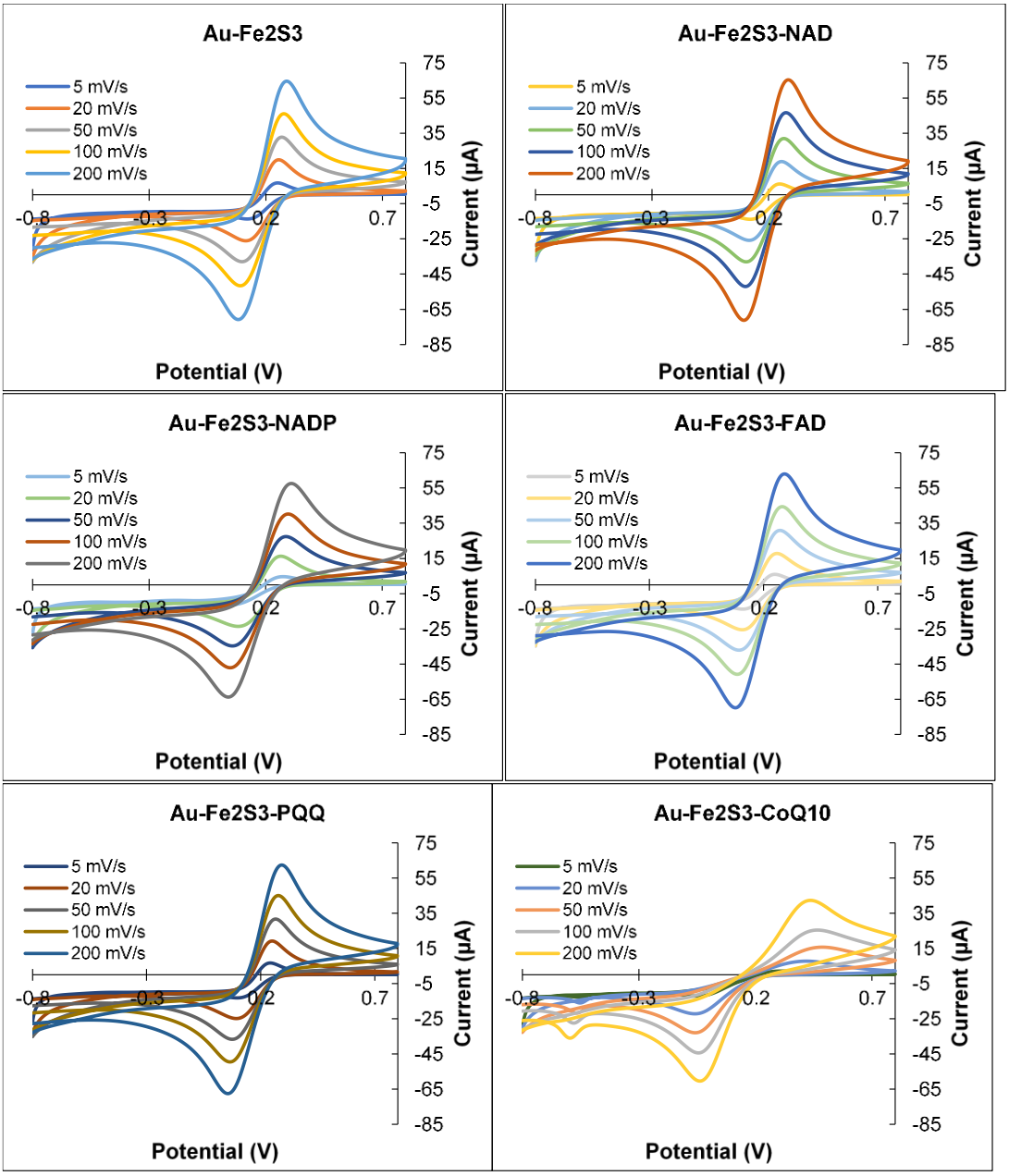
Au-Fe2S3
5 mV/s
20 mV/s
50 mV/s
100 mV/s
200 mV/s
-0.8
-0.3
0.2
0.7
75
55
35
15
-5
-25
-45
-65
-85
Current (µA)
Potential (V)
Au-Fe2S3-NAD
5 mV/s
20 mV/s
50 mV/s
100 mV/s
200 mV/s
-0.8
-0.3
0.2
0.7
75
55
35
15
-5
-25
-45
-65
-85
Current (µA)
Potential (V)
Au-Fe2S3-NADP
5 mV/s
20 mV/s
50 mV/s
100 mV/s
200 mV/s
-0.8
-0.3
0.2
0.7
75
55
35
15
-5
-25
-45
-65
-85
Current (µA)
Potential (V)
Au-Fe2S3-FAD
5 mV/s
20 mV/s
50 mV/s
100 mV/s
200 mV/s
-0.8
-0.3
0.2
0.7
75
55
35
15
-5
-25
-45
-65
-85
Current (µA)
Potential (V)
Au-Fe2S3-PQQ
5 mV/s
20 mV/s
50 mV/s
100 mV/s
200 mV/s
-0.8
-0.3
0.2
0.7
75
55
35
15
-5
-25
-45
-65
-85
Current (µA)
Potential (V)
Au-Fe2S3-CoQ10
5 mV/s
20 mV/s
50 mV/s
100 mV/s
200 mV/s
-0.8
-0.3
0.2
0.7
75
55
35
15
-5
-25
-45
-65
-85
Current (µA)
Potential (V)

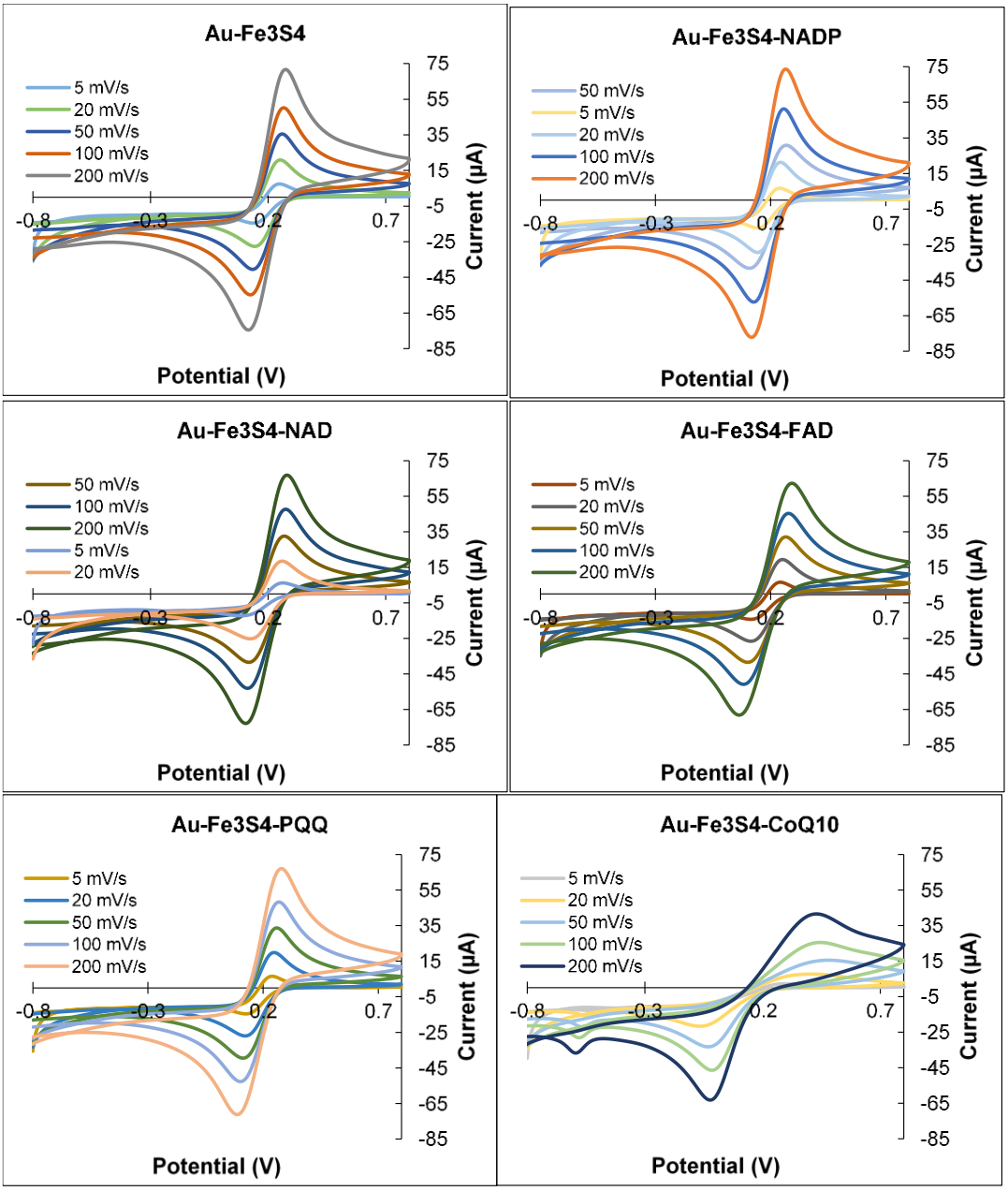

Figure S3.2. Effects of scan rates (10 mVs^{-1} to 150 mVs^{-1}) on peak currents of Au-[Fe-S] / Au-[Fe-S]-[cofactor] electrodes studied by cyclic voltammetry conducted in 0.01 M potassium ferricyanide with 0.1 M KNO_3 to confirm reversibility of the modified electrodes.

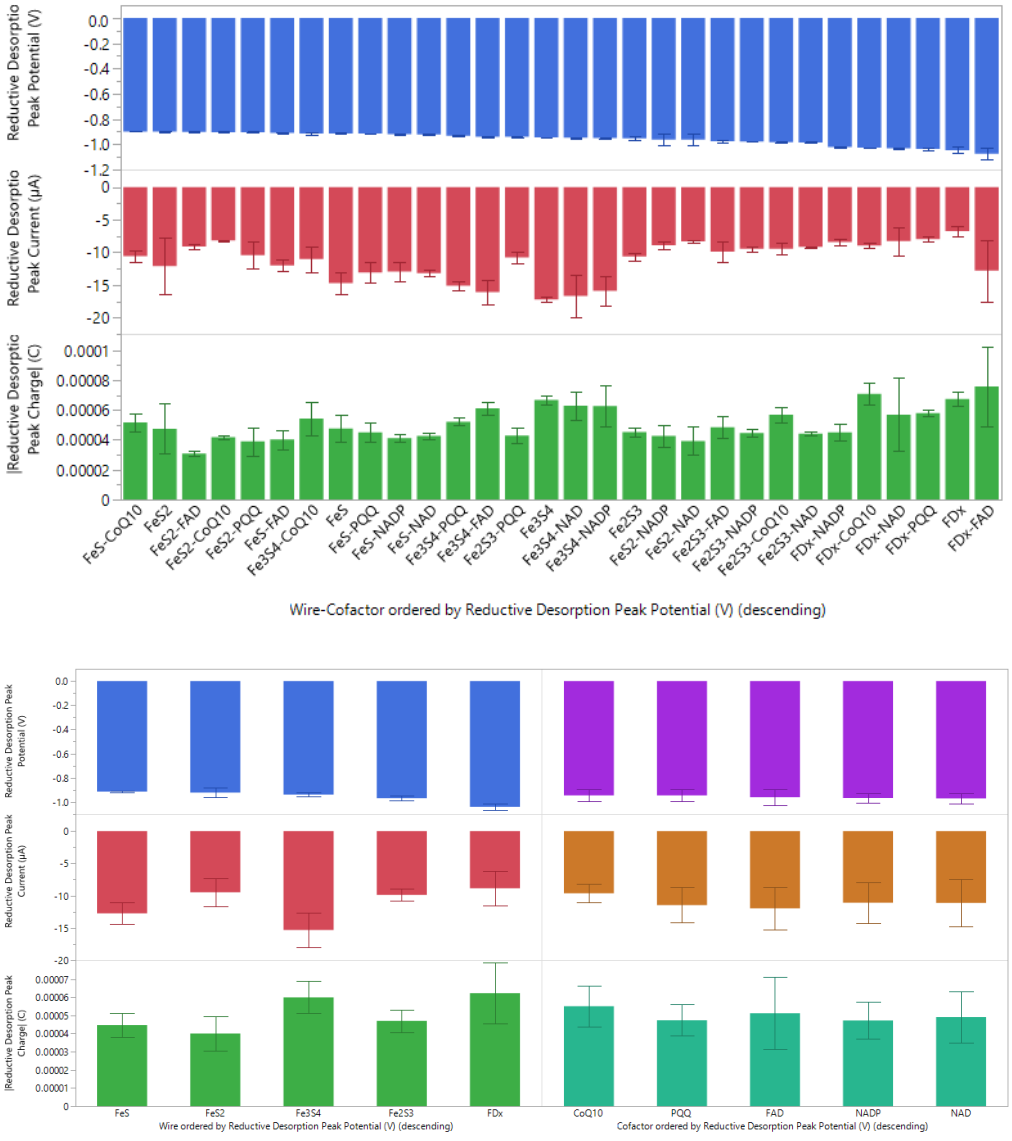

Figure S3.3. Reductive desorption using linear sweep voltammetry: Desorption potential (V_p)/ Desorption current (I_p)/ Desorption charge of the [Fe-S] and [Fe-S]-[cofactors] modified Au electrodes (Q)

FeS-NADP

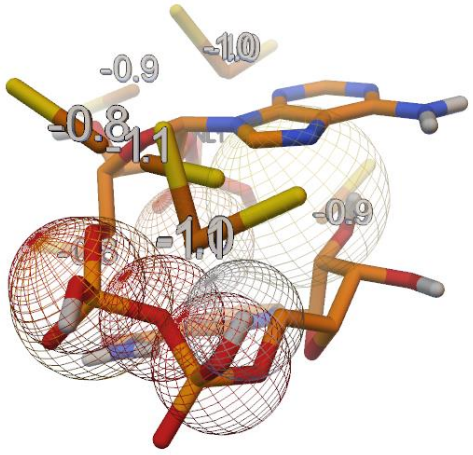

FeS-FAD

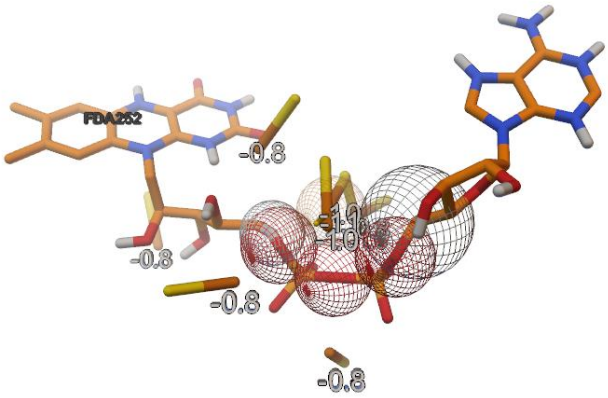

FeS-PQQ

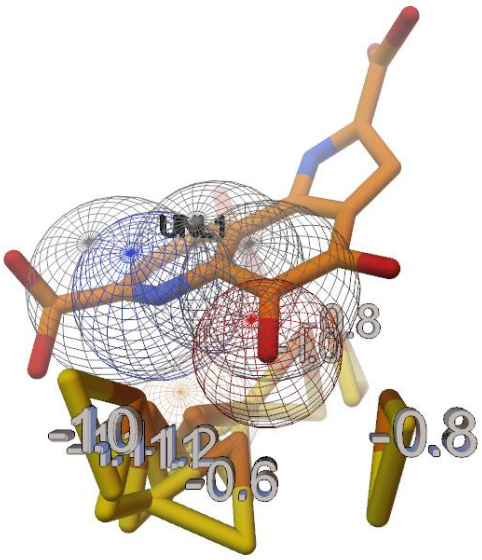

FeS-CoQ_{10}

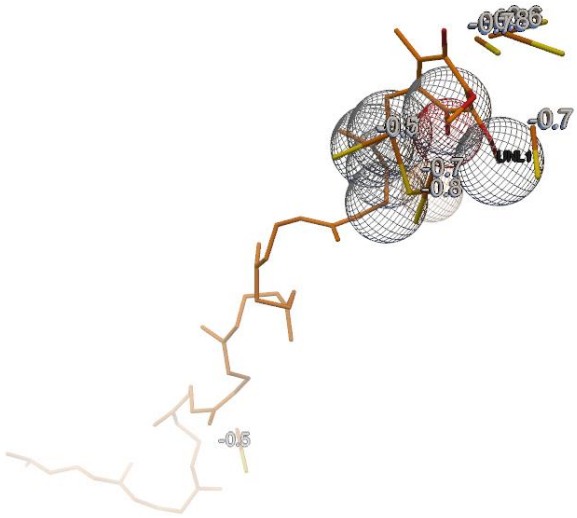

FeS_2-NAD

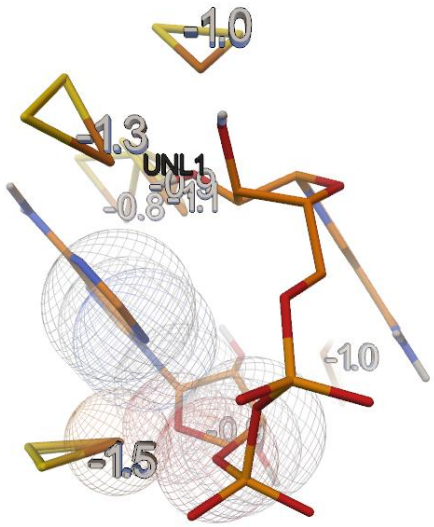

FeS_2-NADP

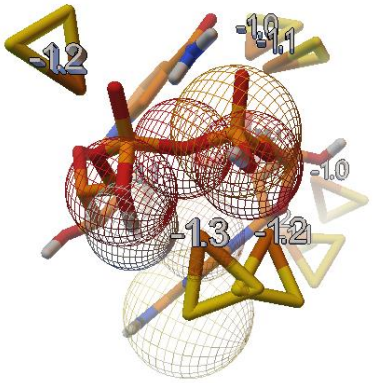

FeS_2-FAD

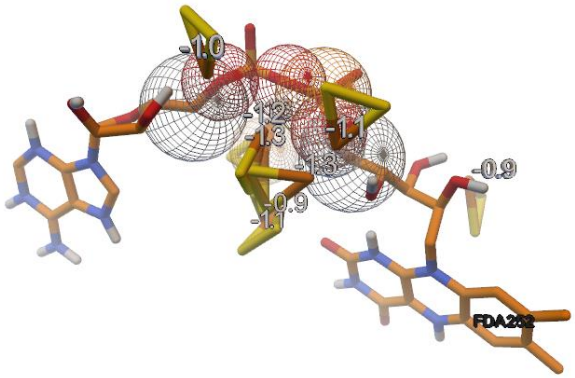

FeS_2-PQQ

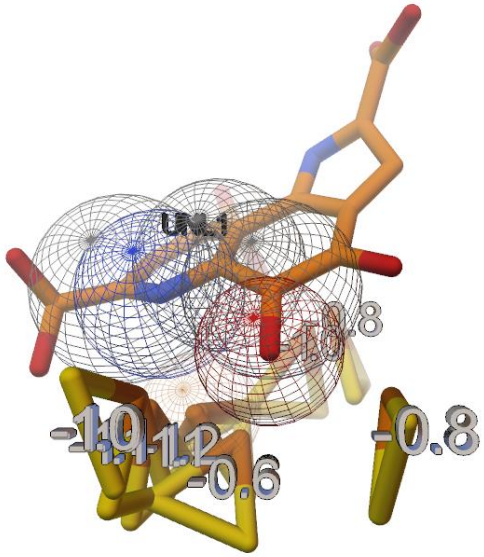

FeS_2-CoQ_{10}

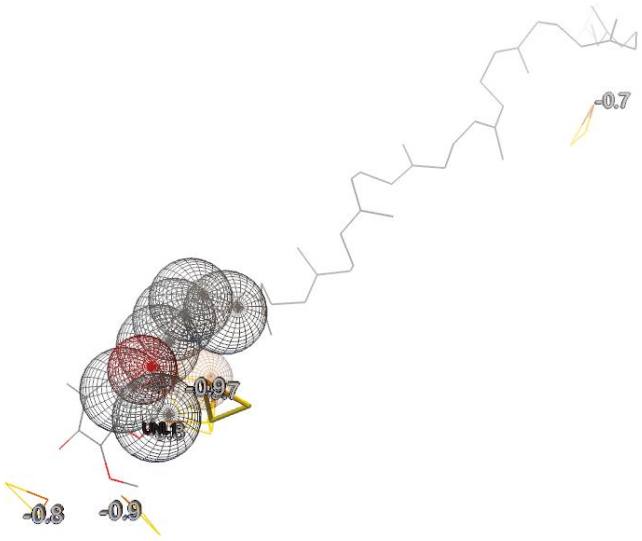

Fe_2S_3-NAD

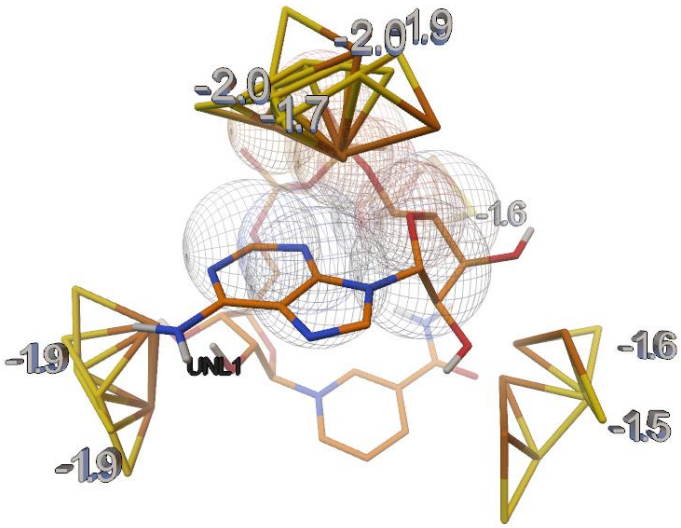

Fe_2S_3-NADP

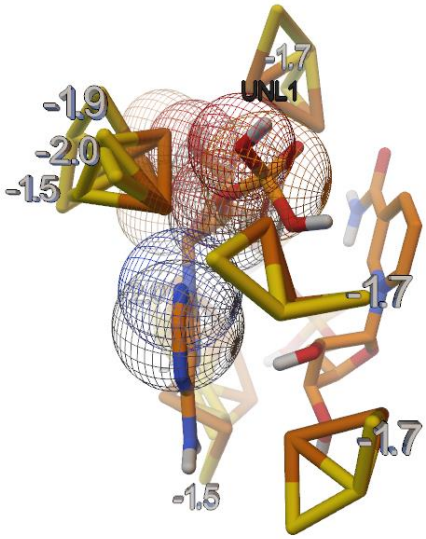

Fe_2S_3-FAD

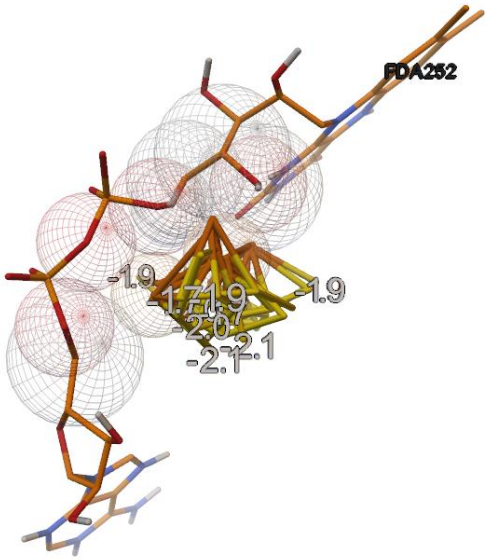

Fe_2S_3-PQQ

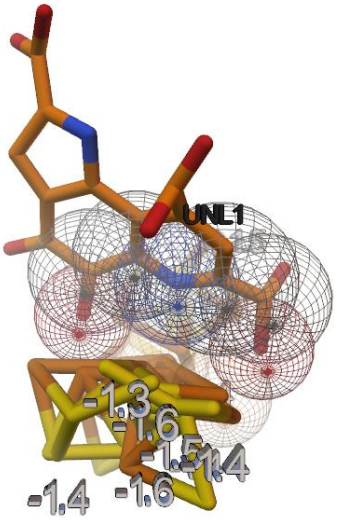

Fe_2S_3-CoQ_{10}

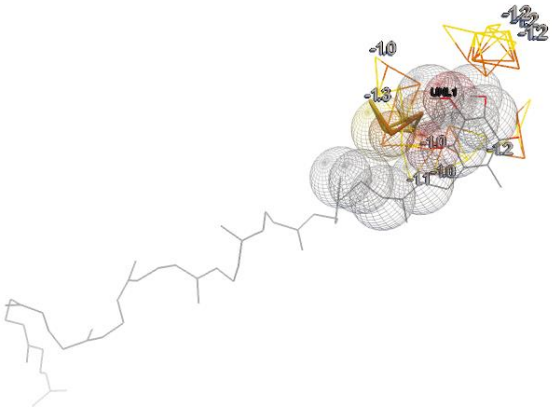

Fe_3S_4-NAD

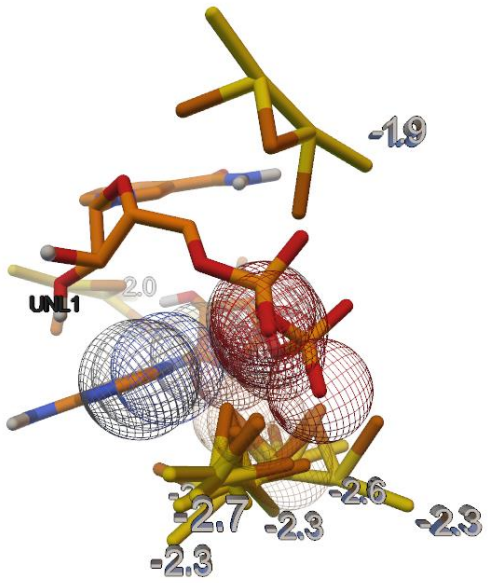

Fe_3S_4-NADP

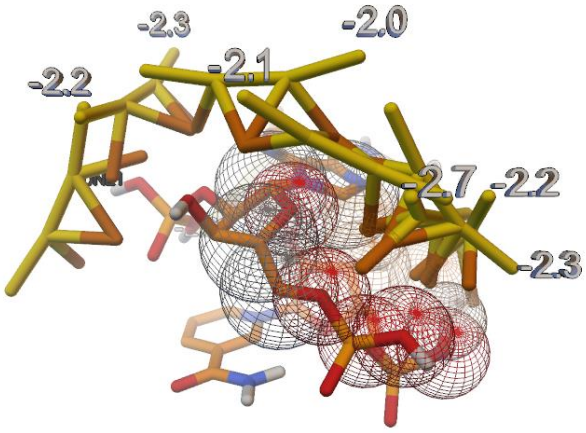

Fe_3S_4-FAD

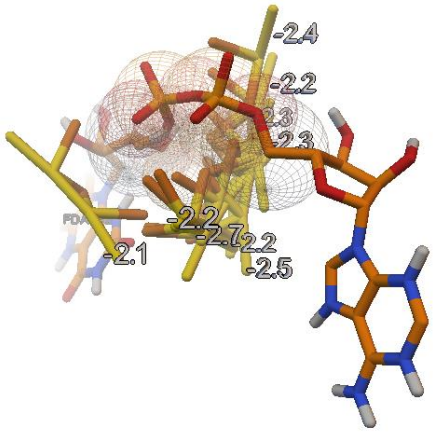

Fe_3S_4-PQQ

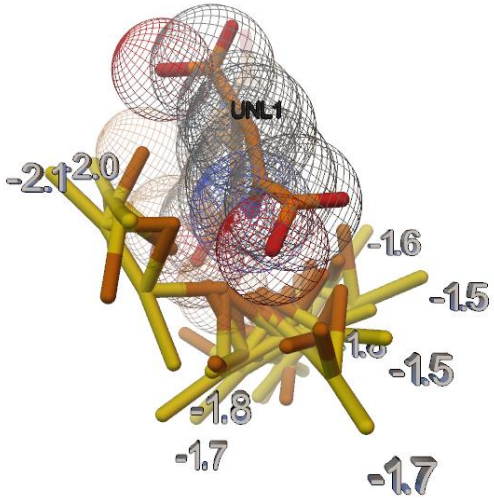

Fe_3S_4-CoQ_{10}

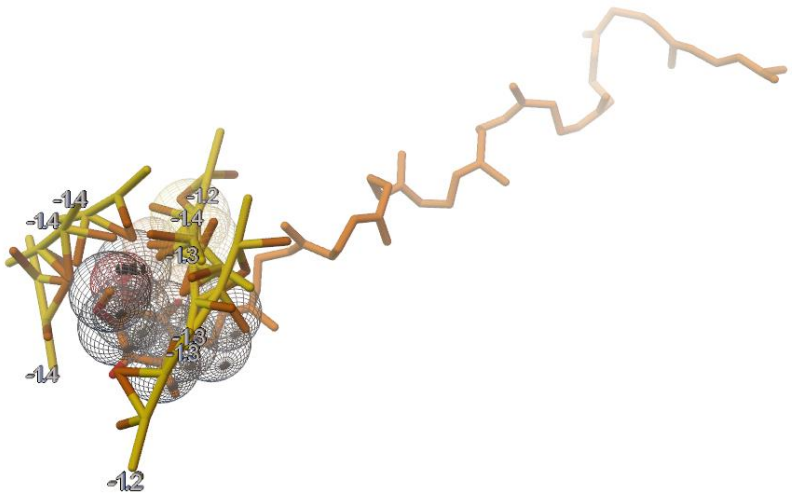

Figure S3.4. Three-dimensional interactions between [Fe-S] and cofactors using Autodock Vina.

APPENDIX B

SECTION 4 SUPPLEMENTARY INFORMATION

In Figure S4.1 the anodic and cathodic peaks of the cyclic voltammograms were observed to shift towards the negative quadrant (or cathodically) with increasing pH conditions. This observation indicates that 1) glycerol oxidation is enabled; 2) at higher pH, glycerol oxidation is energetically; and 3) protons were involved in the electrode reaction. Anodic peak potentials are listed in Table. S4.1. In order to recognize if the peaks are characteristic of $(NH_4)_2SO_4$ or glycerol redox reaction, a cyclic voltammetry study was performed. From Figure S4.2A, one anodic peak was recognizable; that appeared that appeared ~1V being that of the $(NH_4)_2SO_4$ enzyme stimulant. Figure S4.2B shows the comparison of current response generated by the bioelectrode in buffer only (without glycerol) and buffer containing glycerol.

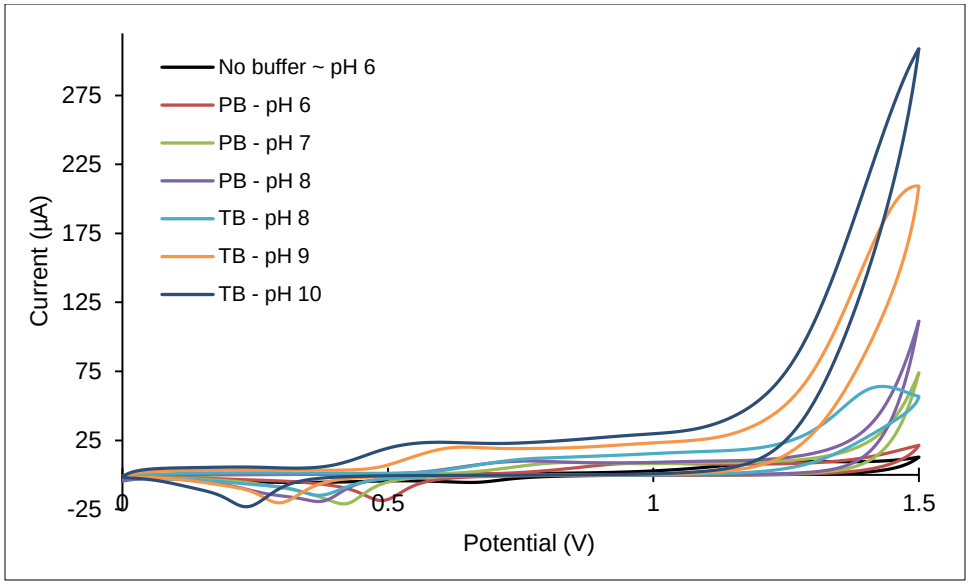

Figure S4.1. Cyclic voltammograms showing the effect of buffers and pH on the current responses generated by FeS-based bioelectrode in 5 mM glycerol solution containing benchmark concentrations of enzyme stimulants.

Table. S4.1. Anodic peak potentials derived from the cyclic voltammograms of the buffers/pH study

Buffer	pH	Anodic peak potential (V)
No buffer	~6	1.28
Potassium phosphate buffer	6	0.971
Potassium phosphate buffer	7	0.85
Potassium phosphate buffer	8	0.761
Tris buffer	8	0.768
Tris buffer	9	0.64
Tris buffer	10	0.6

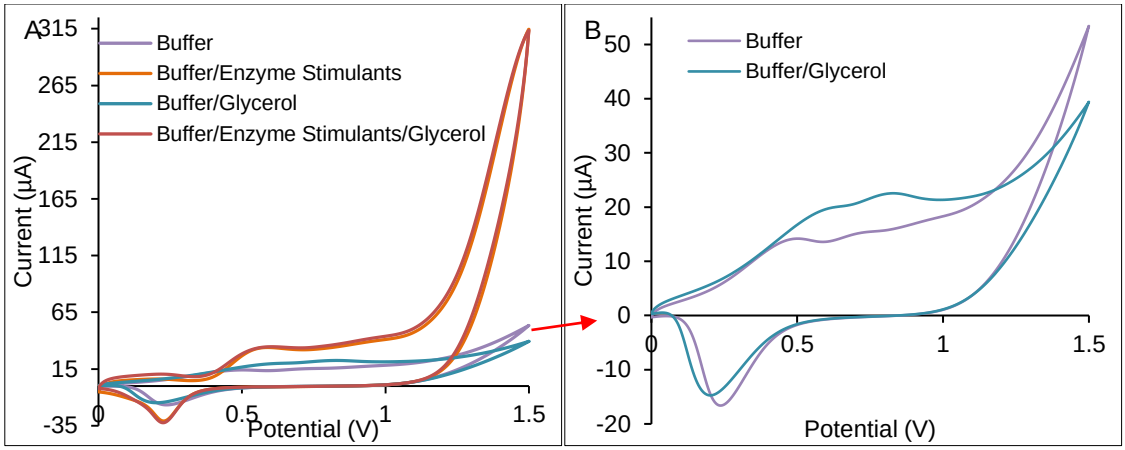

Figure S4.2. (A) Cyclic voltammograms of FeS-based bioelectrode in buffer, buffer/enzyme stimulants, buffer/glycerol and buffer/enzyme stimulants/glycerol; (B) Cyclic voltammograms of FeS-based bioelectrode in buffer and buffer/glycerol.

Figure S4.3 depicts the current and pH response to varying glycerol concentrations. It is clear that higher concentrations of glycerol reduce system pH and has an inverse relation to the current response.

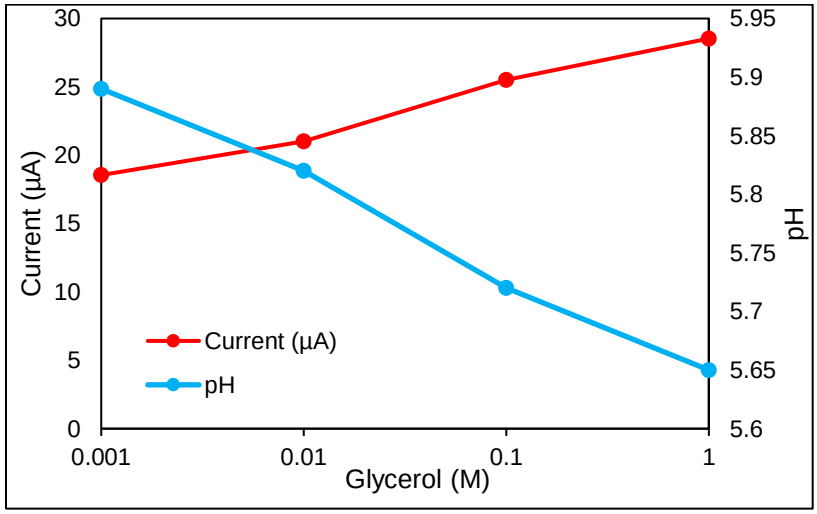

Figure S4.3. The current and pH response to varying glycerol concentrations in non-buffered carrier electrolyte.